FREE-STREAM CHARACTERISTICS OF A FAMILY OF LOW-ASPECT-RATIO, ALL-MOVABLE CONTROL SURFACES FOR APPLICATION TO SHIP DESIGN

L. Bolger Whicker, et al

David Taylor Model Basin
Washington, D. C.

December 1958

HYDROMECHANICS

AERODYNAMICS

STRUCTURAL MECHANICS

APPLIED MATHEMATICS

FREE-STREAM CHARACTERISTICS OF A FAMILY OF LOW-ASPECT-RATIO, ALL-MOVABLE CONTROL SURFACES FOR APPLICATION TO SHIP DESIGN

by

L. Folger Whicker, D.Eng., and Leo F. Fehlner

Revised Edition

HYDROMECHANICS LABORATORY
RESEARCH AND DEVELOPMENT REPORT

NATIONAL TECHNICAL INFORMATION SERVICE

December 1963 Report 933

FREE-STREAM CHARACTERISTICS OF A FAMILY OF LOW-ASPECT-RATIO, ALL-MOVABLE CONTROL SURFACES FOR APPLICATION TO SHIP DESIGN

by

L. Folger Whicker, D. Eng., and Leo F. Fehlner

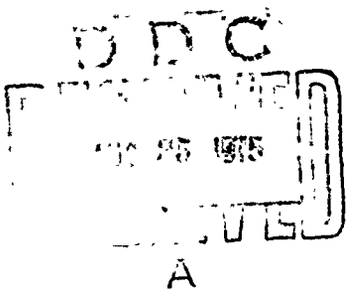

Revised Edition

December 1958

Report 933

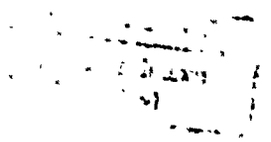

TABLE OF CONTENTS

LIST OF ILLUSTRATIONS

Page

NOTATION

The data are presented in the form of nondimensional force and moment coefficients which are referred to the 25-percent mean-geometric-chord point projected on the plane of the root section. The positive direction of the forces, moments, and angular displacements is shown in Figure 1. The coefficients and symbols are defined as follows:

a_e	Effective aspect ratio, b^2/S
a_0	Section-lift-curve slope, $\left(\frac{\partial C_l}{\partial \alpha}\right)_{\alpha=0} = C_{l_\alpha}$
$b/2$	Semi-span, measured perpendicular to plane of root section
c	Chord, measured parallel to plane of root section
$\bar{c}$	Mean geometric chord, $\frac{c_t + c_r}{2}$
C_D	Drag coefficient, $\frac{\text{Drag}}{qS}$
C_{D_c}	Crossflow drag coefficient
C_χ	Root bending-moment coefficient, $\frac{\text{bending moment}}{qS\ b/2}$
C_L	Lift coefficient, $\frac{\text{Lift}}{qS}$
C_l	Section lift coefficient
C_{L_α}	Lift-curve slope, $\left(\frac{\partial C_L}{\partial \alpha}\right)_{\alpha=0}$
$C_{m_{C_L}}$	$\left(\frac{\partial C_m}{\partial C_L}\right)_{C_L=0}$
$C_{m_{\bar{c}/4}}$	Torque or pitching moment coefficient about quarter-chord point of mean geometric chord, $\frac{\text{pitching moment}}{qS\bar{c}}$
C_N	Axial bending or yawing-moment coefficient, $\frac{\text{yawing moment}}{qS\ b/2}$
$(CP)_{\bar{c}}$	Chordwise center of pressure measured from leading edge at mean geometric chord in percent of the mean geometric chord, $(CP)_c = 0.25 - \frac{C_{m_{\bar{c}/4}}}{C_L \cos\alpha + C_D \sin\alpha}$

$(CP)_s$ Spanwise center of pressure measured from plane of root section in percent of semispan, $(CP)_s = \dfrac{C_x \cos\alpha - C_N \sin\alpha}{C_L \cos\alpha + C_D \sin\alpha}$

q Dynamic pressure, $\dfrac{\rho U^2}{2}$

Subscript r Root

R Reynolds number, $\dfrac{U\bar{c}}{\nu}$

S Planform area

Subscript t Tip

U Free-stream velocity

x Chordwise distance, measured parallel to plane of root section

α Angle of attack

λ Taper ratio, c_t/c_r

ν Kinematic viscosity

Λ Angle of sweep of quarter chord line

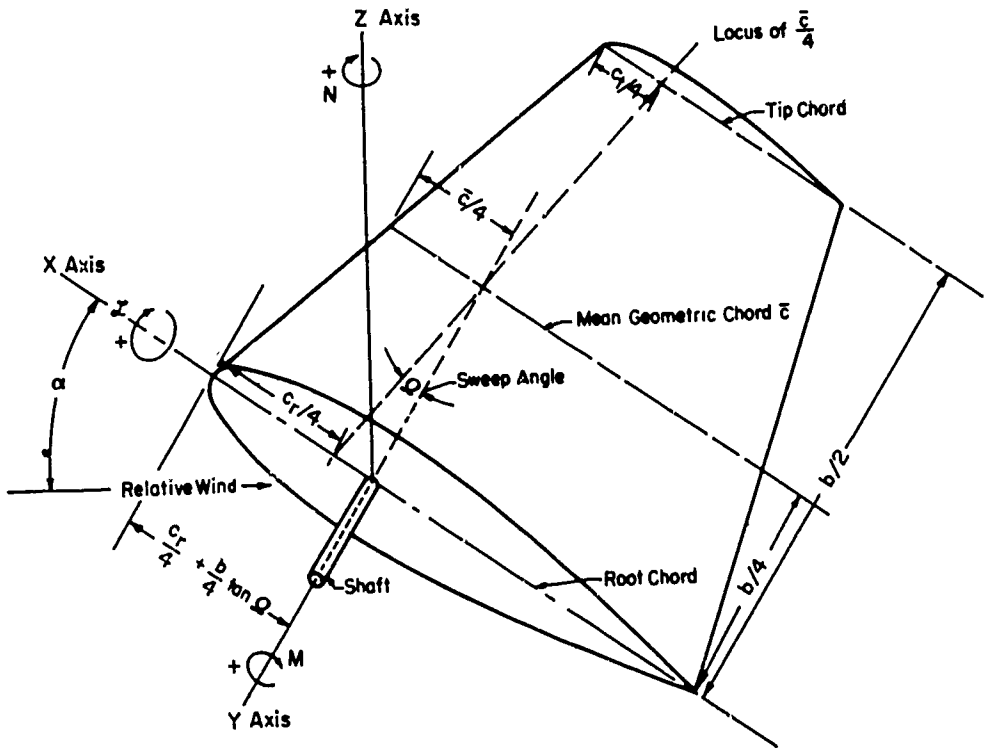

Figure 1 - Coodinate System Showing Positive Direction of Forces, Moments, and Angle of Attack

ABSTRACT

The free-stream characteristics of a family of low-aspect-ratio, all-movable control surfaces are presented. These characteristics—i.e., force and moment coefficients, and chordwise and spanwise center of pressure locations—are plotted as functions of the angle of attack for each surface at various Reynolds numbers in both the ahead and the astern conditions. Investigations were made of the following: three aspect ratios 1, 2, and 3; five section shapes (NACA 0015, Navy Standard Strut, TMB-EPH, TMB Fairing No. 7, and TMB-No. 07507515); two tip shapes, faired and square; and three sweep angles (−8, 0, 11). Cross-plots were made to assess the effects of these parameters, and semi-empirical equations for the force and moment coefficients suitable for design applications are presented. Also included is a design technique for computing the control surface shaft torque.

INTRODUCTION

An investigation of a family of all-movable, low-aspect-ratio control surfaces was made to determine the free-stream characteristics. The purpose of this report is to present design information and procedures based on the results obtained from these tests.

The tremendous growth of the field of aerodynamics has been of great benefit to the ship and submarine designer as well as the designer of aircraft. However, there are significant differences between aerodynamics and hydrodynamics, and many times the data derived from one are not *directly* applicable to the other. An example of this is control surface design, where the hydrodynamicist or naval architect is, in general, concerned with control surfaces of low-aspect ratio (effective aspect ratio of 3 or less) as well as problems of cavitation and effects of free surface.

Recognizing the need for additional information for use of the ship and submarine designer, the David Taylor Model Basin undertook a program of research on control surface design. The first step in this program was to establish the direction in which research should proceed. This resulted in an extensive bibliography[1] and a report[2] which presents a general discussion of the design of control surfaces for hydrodynamic applications. The latter report points out the superiority of the all-movable control surface for such applications. The second step consisted of extensive wind-tunnel tests of a family of all-movable control surfaces of low-aspect ratio. The third step was evaluation of these data, preparation of design charts, and comparison with existing theory and semi-empirical design procedures. The fourth step is to extend the test program to include a series of all-movable, low-aspect-ratio, flapped-

---

[1] References are listed on page 30.

type control surfaces, with and without tabs. This phase is presently under way and will be the subject of a future report.

In this report the free-stream characteristics of a particular series of control surfaces are presented for various Reynolds numbers in both the ahead and astern conditions. Also, the effects of variations of the geometric parameters and Reynolds numbers are shown, and the results are compared with theory. Equations for computing the lift, drag, and moment coefficients which are satisfactory for design purposes are also presented.

BASIC CONSIDERATIONS

In an effort to obtain sufficient data for comparative purposes, a family of control surfaces was selected to cover a wide operating range. In the past hydrodynamic control surfaces and struts have been designed with various cross sections, such as the Navy Standard Strut and TMB-EPH section. Both of those sections were designed for low drag and anti-cavitating properties, under the assumption that they would always be operating at very low angles of attack. Control surfaces and even struts, however, are often subjected to large angles of attack. It is thus frequently necessary for the designer to select a control surface for low drag and anti-cavitating properties at high as well as low angles of attack.

Often, available space and operating conditions require low-aspect-ratio control surfaces to satisfy design conditions. Many planforms used on ships and submarines were determined on the basis of space available. A basic planform with zero sweep was selected for this investigation, and planforms with both sweep forward and sweepback were investigated. The control surfaces investigated are approximately 15 percent thick, which represents a reasonable compromise between the hydrodynamic and structural requirements.

SECTION SHAPE

Five section shapes (Navy Standard Strut, TMB-EPH, TMB-No. 07507515, TMB-Fairing No. 7, and NACA 0015) were selected as representing typical sections in use at the present time. Figure 2 compares these section shapes and shows that both the nose radius and the location of maximum thickness differ for the various sections.

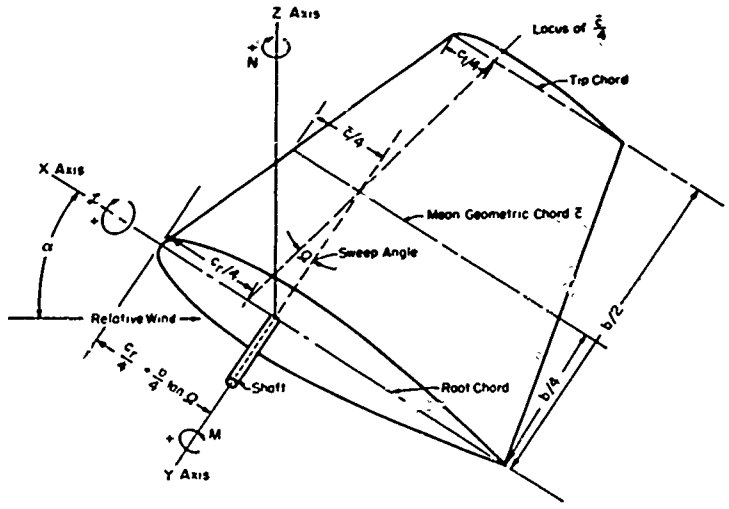

Figure 1 - Coordinate System Showing Positive Direction of Forces, Moments, and Angle of Attack

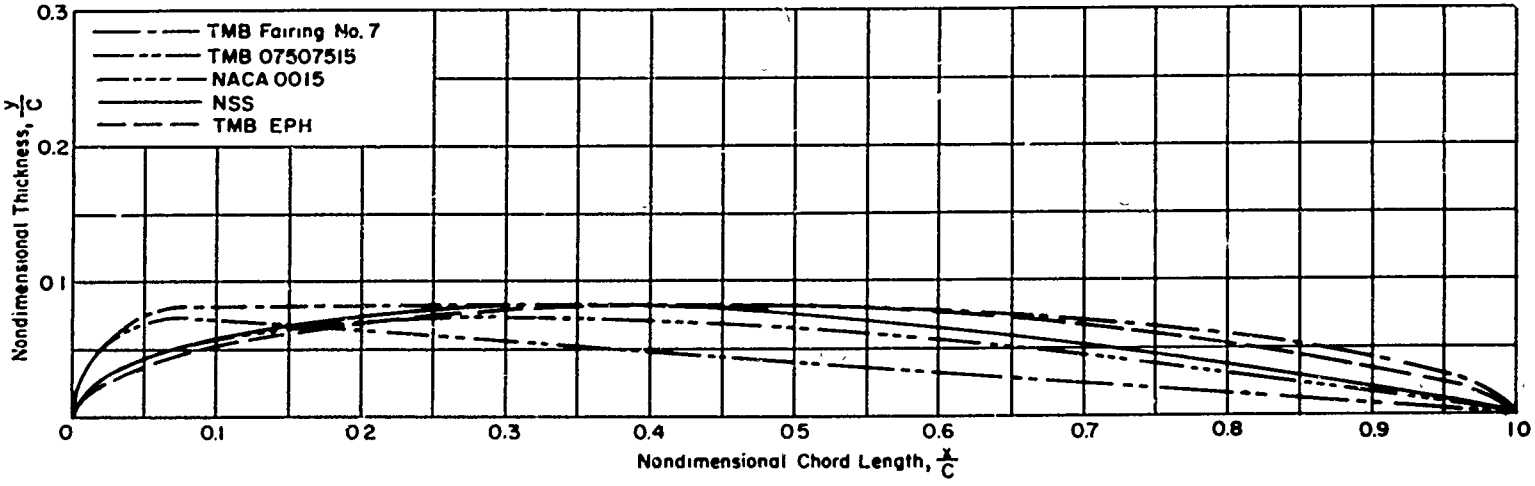

Figure 2 - Section Shape of Models Used in This Investigation

PLANFORM

There are many combinations of parameters which describe the geometry of a control surface. It was decided, therefore, to reduce the arbitrariness of planform selection by relating planforms through the concept of elliptical spanwise load distribution. Theoretically, such a distribution results in minimum drag and maximum lift-curve slope for a surface operating in a uniform stream. Reference 3 employs a simplified lifting surface theory to show that, for elliptic loading, the location of the spanwise center of pressure is independent of aspect ratio for a certain functional relation between taper ratio and sweep angle. This relationship between taper ratio and sweep angle is reproduced herein as Figure 3. From this curve a taper ratio of 0.45 was chosen for all models of the series, since theoretically, this value produces elliptic loading for a quarter-chord sweep-angle of zero. Further, in order to cover a range to each side of the curve for elliptic loading, models having sweep angle of 8 degrees forward and 11 degrees aft were also included in this series. The planforms of the models are shown in Figure 4.

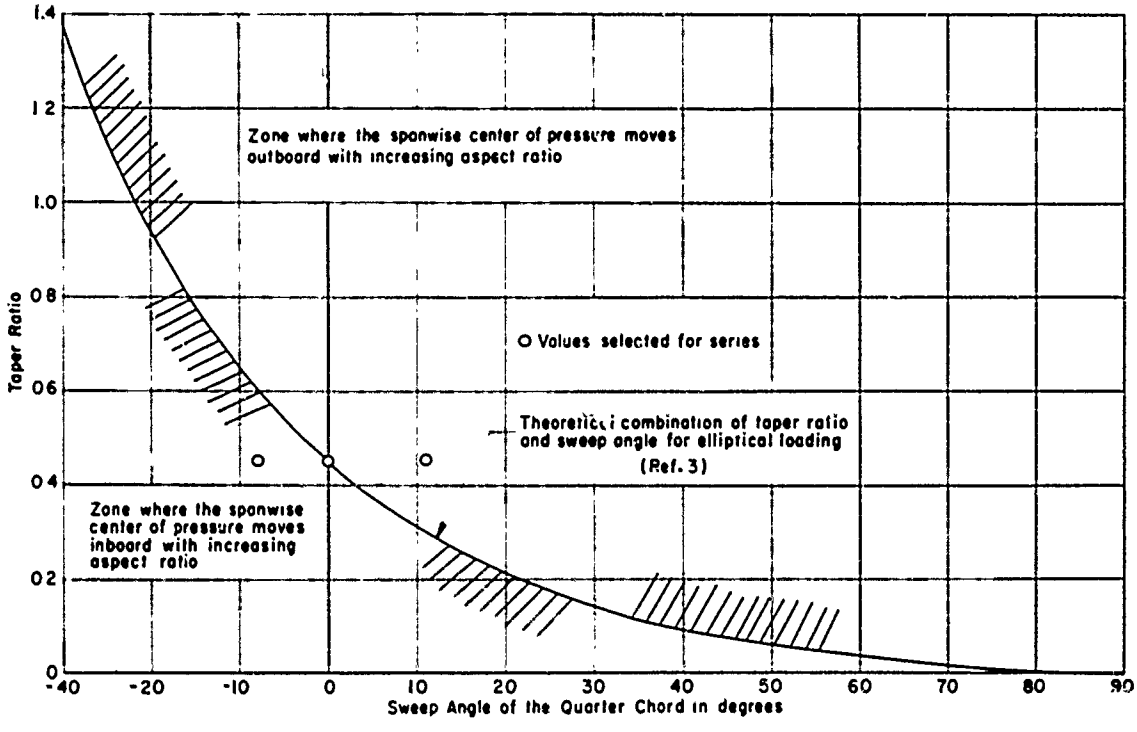

Figure 3 - Theoretical Relationship between Taper Ratio and Sweep Angle for Which the Location of the Spanwise Center of Pressure Is Independent of Aspect Ratio

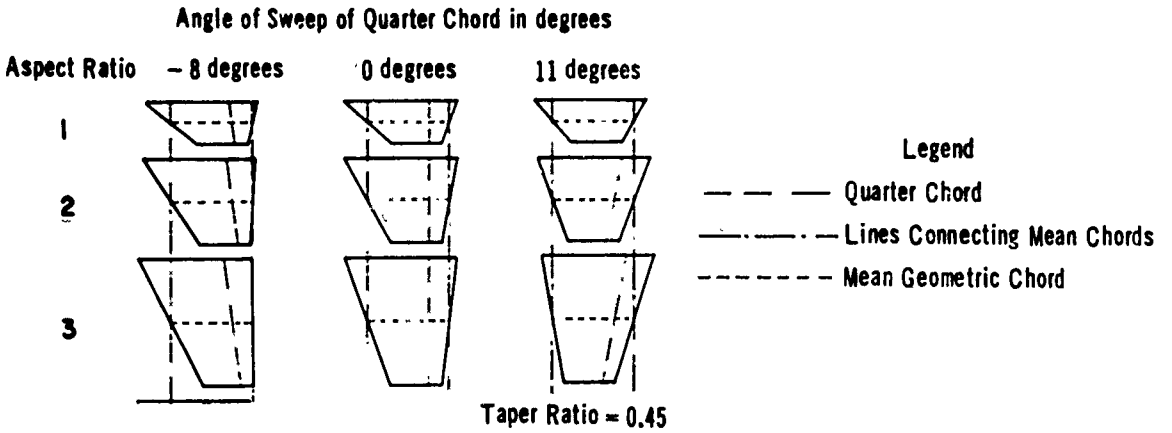

Figure 4 - Planforms of All-Movable Control Surfaces

TIP SHAPE

Two tip shapes, square and faired, were investigated for selected members of the series. The faired tips were generated, as shown in Figure 5, where for a particular planform and a given value of x along the root chord, a ray l is drawn which passes through the apex of the cone. The circle, tangent to the upper and lower surfaces of the control surface, is then constructed as shown in section A-A. This defines the shape of the tip fairing for all values of x.

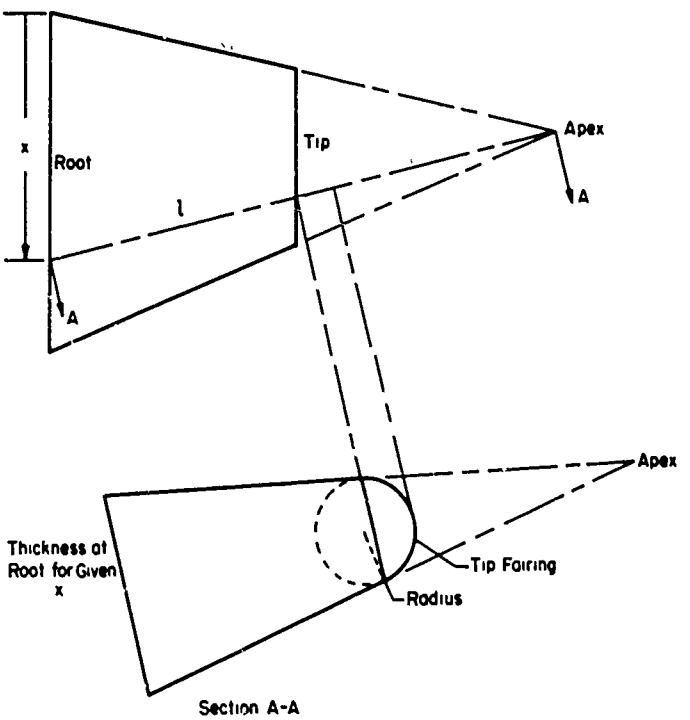

Figure 5 - Method Used to Design Tip Fairings

DESCRIPTION OF MODELS

All models were constructed of mahogany with a mean geometric chord ($\bar{c}$) of 2 feet. This value was selected as a maximum in order to minimize wall effects in the TMB 8- by 10-foot low-speed wind tunnel.

Control surfaces with geometric aspect ratios of 0.5, 1.0, and 1.5 were constructed by varying the semi-span from 1 to 3 feet. It should be noted that these values correspond to effective aspect ratios of 1.0, 2.0 and 3.0, since the models were mounted on a ground board in the wind tunnel. The geometric characteristics of the models are listed in Table 1, and the non-dimensional offsets are given in Table 2.

TABLE 1

Geometric Characteristics of Control Surface Models

All models have a mean geometric chord of 2 feet, a taper ratio of 0.45, and root chord of 33.110 inches.

TMB Model No.	Section Shape	Aspect Ratio a_e	Sweep Angle Λ deg	Semi-Span $b/2$ ft	Planform Area (Semi-Span) S sq ft	Thickness Ratio * t/c percent
AM 101	NACA 0015	1	− 8	1	2	15
102	↓	1	0	1	2	↓
103		1	11	1	2	
104		2	− 8	2	4	
105		2	0	2	4	
106		2	11	2	4	
107		3	− 8	3	6	
108	↓	3	0	3	6	
109		3	11	3	6	↓
110	TMB-EPH	2	0	2	4	16.67
111	Navy Std Strut	2	0	2	4	16.67
112	TMB-07507515	2	0	2	4	15.0
113	TMB-Fairing No. 7	2	0	2	4	16.67

* t is maximum thickness,
c is section chord length.

TABLE 2

Nondimensional Offsets for Control Surface Sections

NACA 0015 *		TMB-EPH-16.7**		Navy Std Strut †		TMB-0750715		TMB Fairing No. 7 ††	
x/c	$\pm y/c$	x/c	$\pm y/c$	x/c	$\pm y/c$	x/c	$\pm y/c$	x/c	$\pm y/c$
								Circular Nose	
0	0	0	0	0	0				
0.0125	0.02367	0.005	0.01258	0.001547	0.0082079				
0.0250	0.03267	0.010	0.01775	0.005882	0.0159418	Circular leading edge with straight taper from point of tangency to trailing edge.		0.08333	0.08333
0.0500	0.04442	0.020	0.02495	0.01752	0.02722			0.3333	0.08333
0.0750	0.05249	0.040	0.03487	0.05	0.044610			0.4000	0.08327
0.1000	0.05824	0.070	0.04529	0.10	0.060067			0.4667	0.08281
0.1500	0.06680	0.100	0.05311	0.15	0.069836			0.5333	0.08157
0.2000	0.07170	0.200	0.07008	0.20	0.076291			0.6000	0.07917
0.2500	0.07424	0.250	0.07538	0.25	0.080393	$R/c = 0.075$		0.6667	0.07519
0.3000	0.07500	0.300	0.07918	0.30	0.082643			0.7333	0.06927
0.4000	0.07252	0.400	0.08307	0.35	0.083351	Max. thickness at $x/c = 0.075$		0.8000	0.06100
0.5000	0.06615	0.43612	0.08335	0.40	0.082720	$t/c = 0.15$		0.8667	0.05000
0.6000	0.05703	0.450	0.08330	0.45	0.080897			0.9000	0.04330
0.7000	0.04579	0.550	0.08052	0.50	0.077983			0.9333	0.03536
0.8000	0.03278	0.600	0.07747	0.55	0.074062			0.9667	0.02500
0.9000	0.01809	0.650	0.07333	0.60	0.069183			0.9833	0.01768
0.9500	0.01008	0.700	0.06810	0.65	0.063425			1.0000	0
1.0000	0.00158	0.800	0.05434	0.70	0.056790				
		0.850	0.04583	0.75	0.049322				
		0.900	0.03617	0.80	0.041038				
		0.930	0.02962	0.85	0.031957				
		0.950	0.02467	0.90	0.022086				
		0.970	0.01882	0.95	0.011434				
		0.990	0.01070	1.00	0				
		1.000	0						

*Reference 16.

**Reference 4.

†These values of y/c have been revised from those given in Reference 5, which were not correct to the number of significant figures given. These tabulated offsets have been checked and are believed to be accurate.

††Reference 6.

APPARATUS AND TESTS

Tests were made in the 8-by 10-foot low-speed wind tunnel at the Taylor Model Basin. This tunnel is an atmospheric, closed-throat, return-flow type in which an air speed of about 160 mph ($q = 60$ psf) can be obtained. The Reynolds number range of the tests was approximately 1 to 3 million (Mach number range of 0.07 to 0.21).

The control surfaces were mounted on a ground board, as shown in Figure 6, and the gap between the control surface and the ground board was approximately 0.005 $\overline{c}$ (1/8 inch). The ground board was located 2 feet above the tunnel floor; hence the effective size of the test section was 6 by 10 feet. Tunnel wall corrections were applied, in accordance with Reference 7.

Force and moment measurements were made, using the wind-tunnel balance, which is is a motor-driven, null-type, mechanical system. The measuring accuracy was: lift, $\pm$ 0.2 pounds; drag, $\pm$ 0.1 pounds; and moment, $\pm$ 0.1 foot-pound.

Figure 6a - With Faired Tip

Figure 6b - Without Faired Tip

Figure 6 - Control Surface Model Mounted over Ground Board in Wind Tunnel

PRESENTATION OF DATA

The results of the wind-tunnel investigation[8, 9] are presented in nondimensional form in Appendixes A through D. These plots show force coefficients, moment coefficients, and spanwise and chordwise center of pressure versus angle of attack. Also, the theoretical spanwise center of pressure location, which is $4/3\pi\ b/2$ for elliptic loading, is indicated. The NACA 0015 section shape was used for the major portion of this investigation. The results for these surfaces in the ahead condition with square tips are in Appendix A, with faired tips in Appendix B, and in the astern condition (trailing edge forward) in Appendix C. Appendix D contains the results for the TMB-EPH, NSS, TMB-07507515, and TMB Fairing No. 7 in the ahead and astern conditions.

Cross plots (Figures 7 through 27) show the effect of varying the Reynolds number, sweep angle, and aspect ratio on the measured quantities.

(Text continued on page 17).

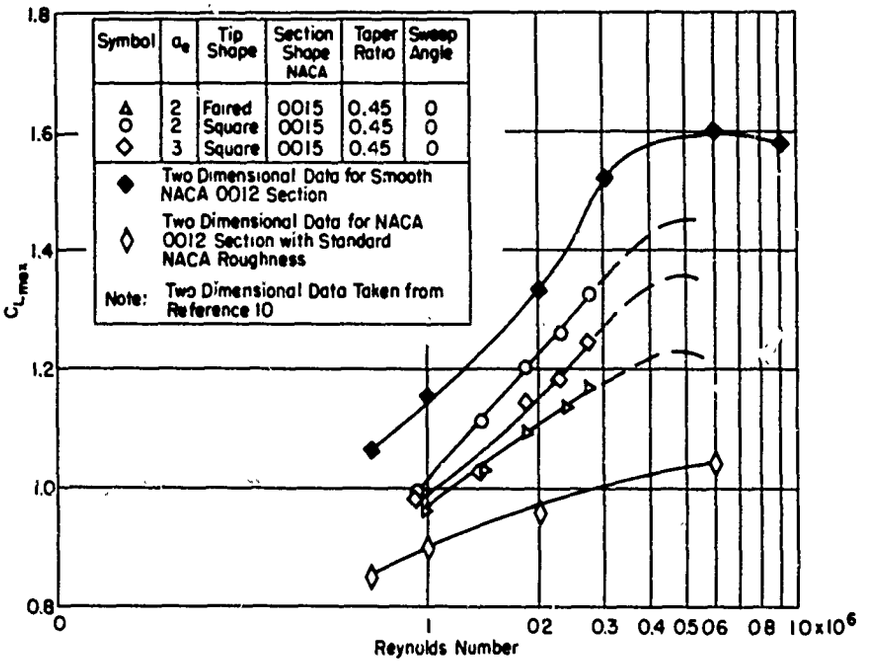

Figure 7 - Effect of Reynolds Number and Roughness on Maximum Lift Coefficient of Control Surfaces

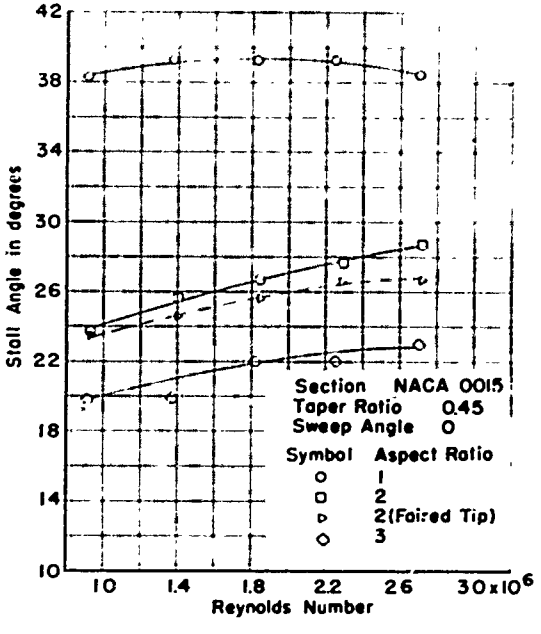

Figure 8 - Effect of Reynolds Number on Stall Angle of Control Surfaces with NACA 0015 Section

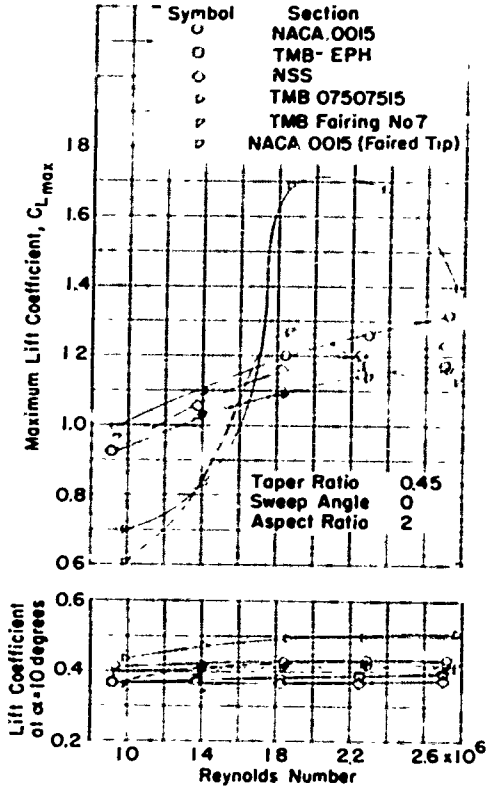

Figure 9 - Effect of Reynolds Number on Lift Coefficient of Several Control Surfaces of Different Section

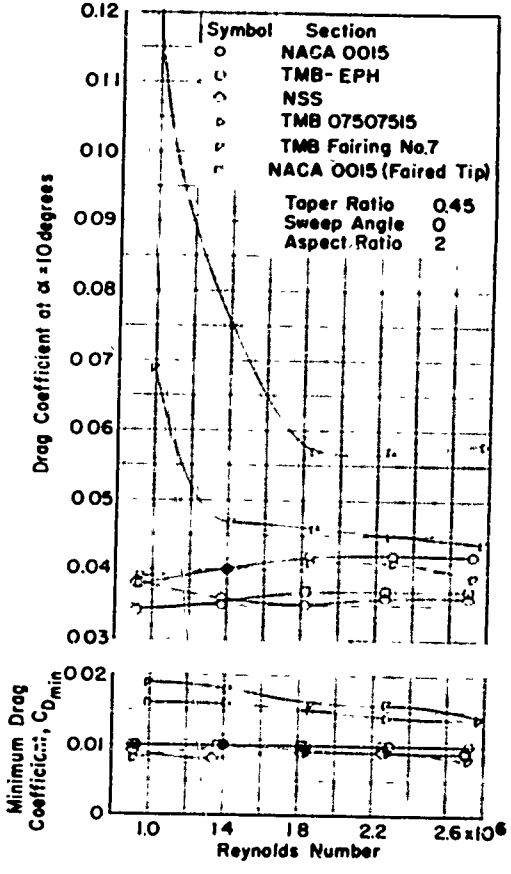

Figure 10 - Effect of Reynolds Number on Drag Coefficient of Several Control Surfaces of Different Section

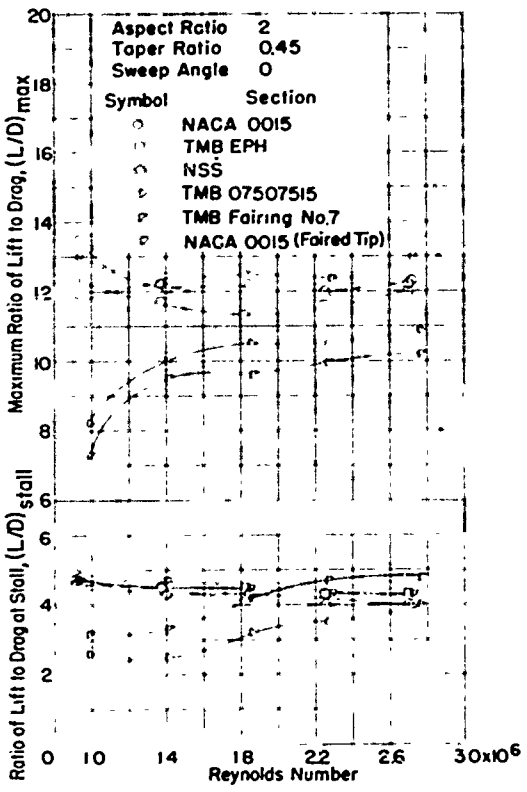

Figure 11 - Effect of Reynolds Number on Lift/Drag Ratio of Several Control Surfaces of Different Section

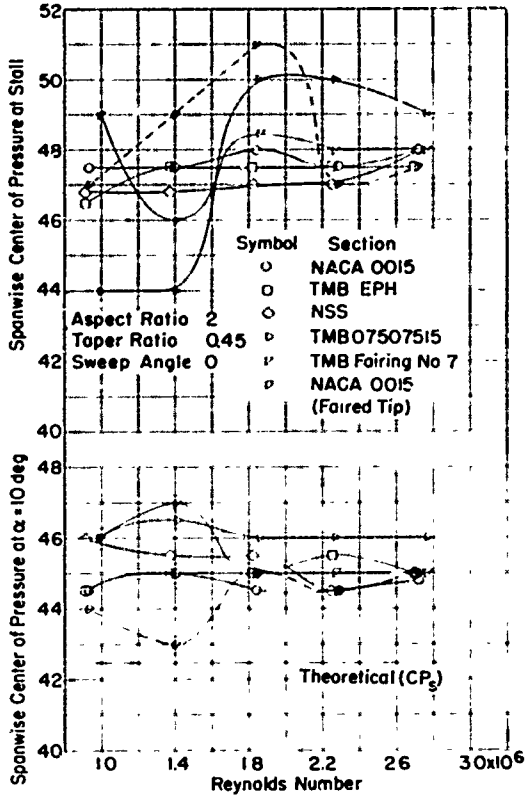

Figure 12 - Effect of Reynolds Number on Location of Spanwise Center of Pressure of Several Control Surfaces of Different Section

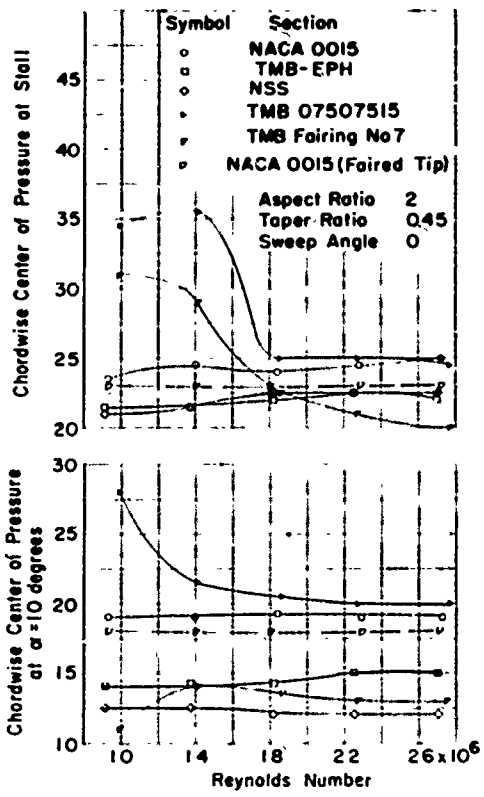

Figure 13 - Effect of Reynolds Number on Location of Chordwise Center of Pressure of Several Control Surfaces of Different Section

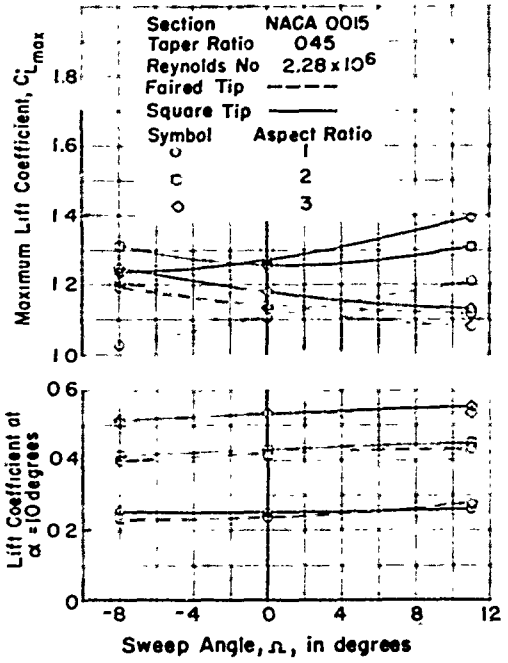

Figure 14 - Effect of Sweep Angle on Lift Coefficient of Control Surfaces with NACA 0015 Section

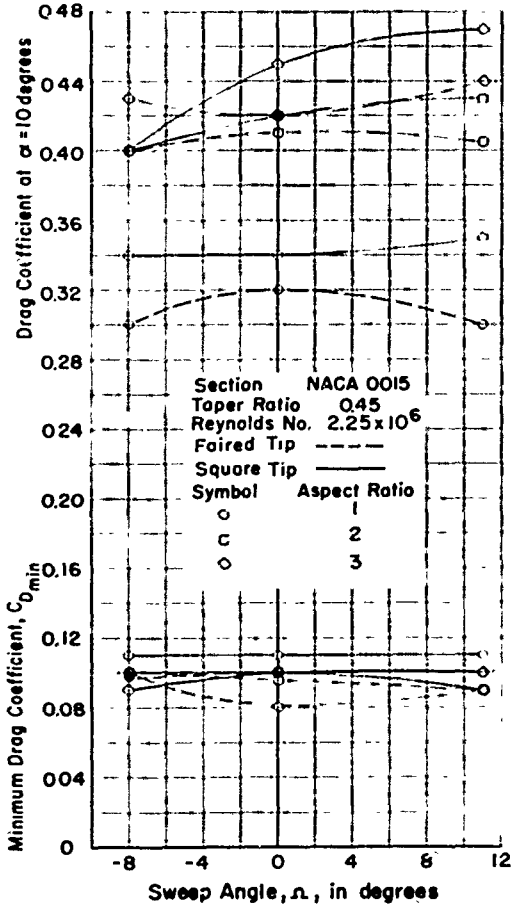

Figure 15 - Effect of Sweep Angle on Drag Coefficient of Control Surfaces with NACA 0015 Section

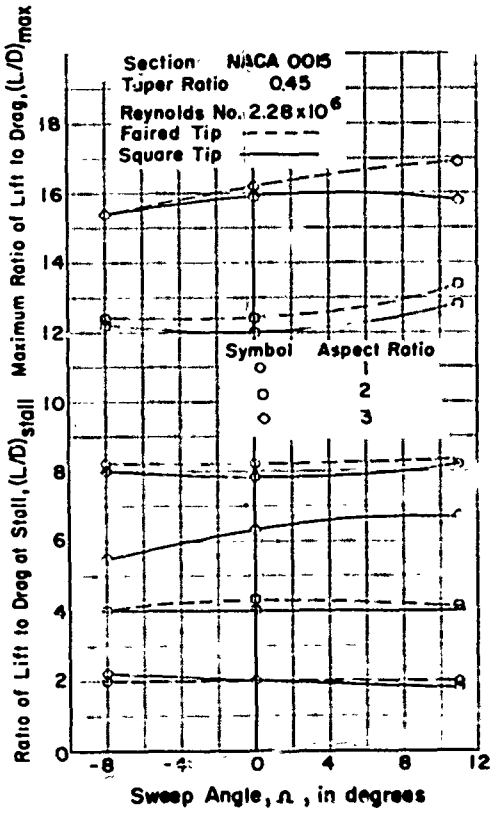

Figure 16 - Effect of Sweep Angle on Lift/Drag Ratio of Control Surfaces with NACA 0015 Section

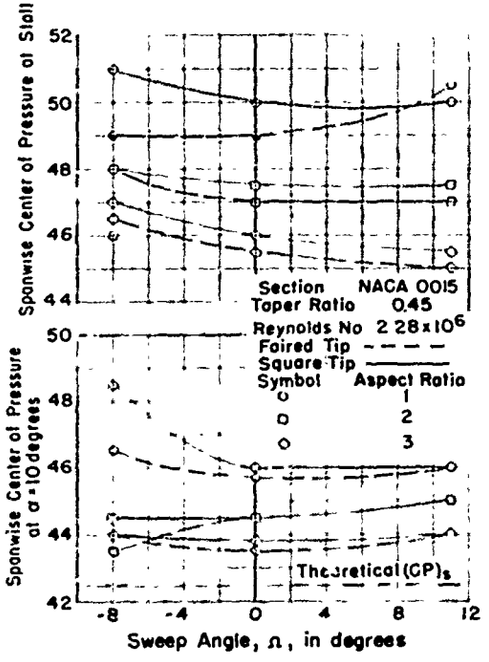

Figure 17 - Effect of Sweep Angle on Location of Spanwise Center of Pressure of Control Surfaces with NACA 0015 Section

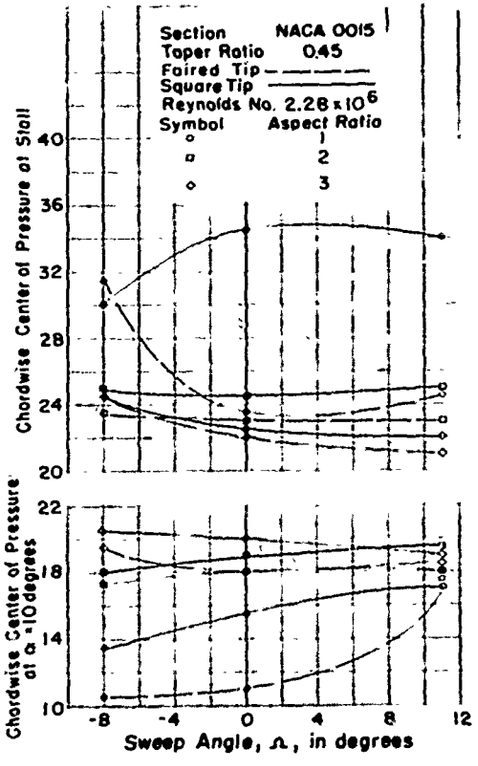

Figure 18 - Effect of Sweep Angle on Location of Chordwise Center of Pressure of Control Surfaces with NACA 0015 Section

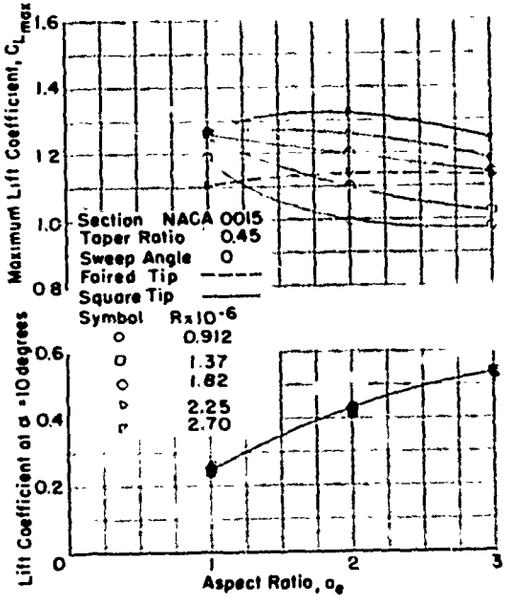

Figure 19 - Effect of Aspect Ratio on Lift Coefficient of Control Surfaces with NACA 0015 Section

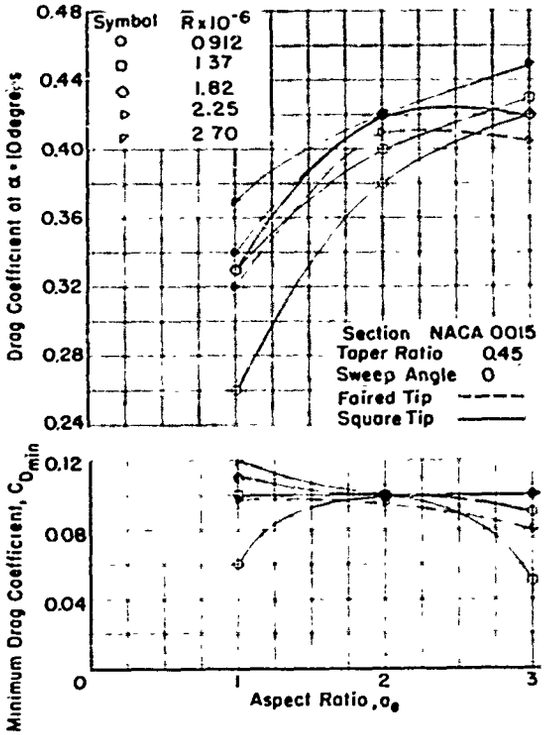

Figure 20 - Effect of Aspect Ratio on Drag Coefficient of Control Surfaces with NACA 0015 Section

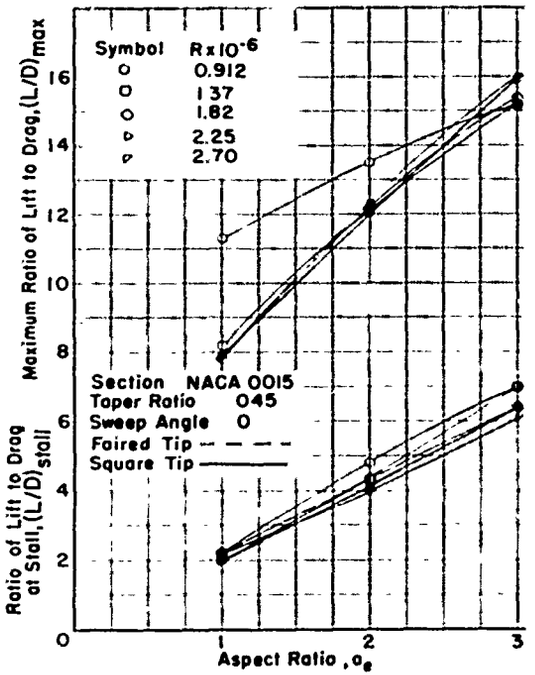

Figure 21 - Effect of Aspect Ratio on Lift/Drag Ratio of Control Surfaces with NACA 0015 Section

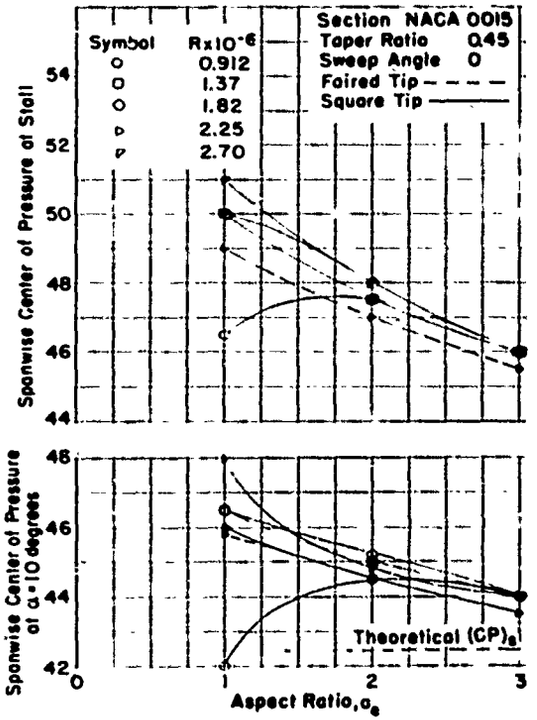

Figure 22 - Effect of Aspect Ratio on Location of Spanwise Center of Pressure of Control Surfaces with NACA 0015 Section

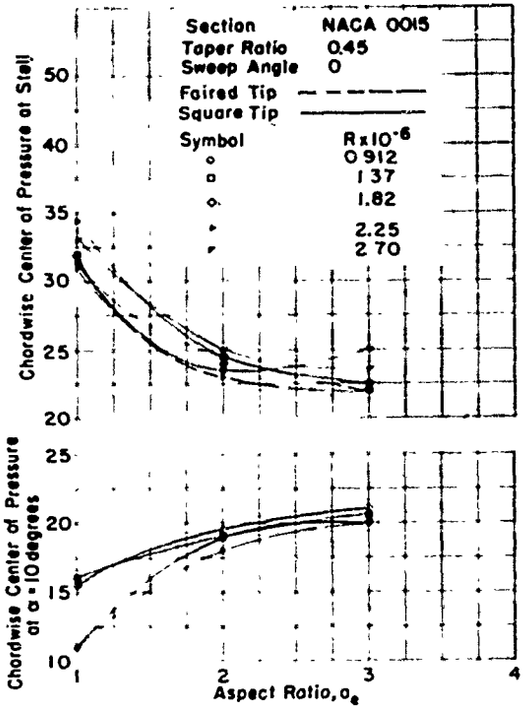

Figure 23 - Effect of Aspect Ratio on Location of Chordwise Center of Pressure of Control Surfaces with NACA 0015 Section

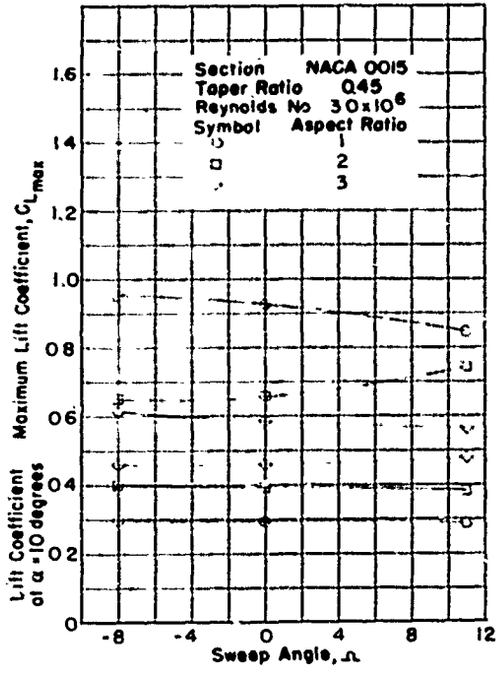

Figure 24 - Effect of Sweep Angle on Lift Coefficient of Control Surfaces with NACA 0015 Section in Astern Condition

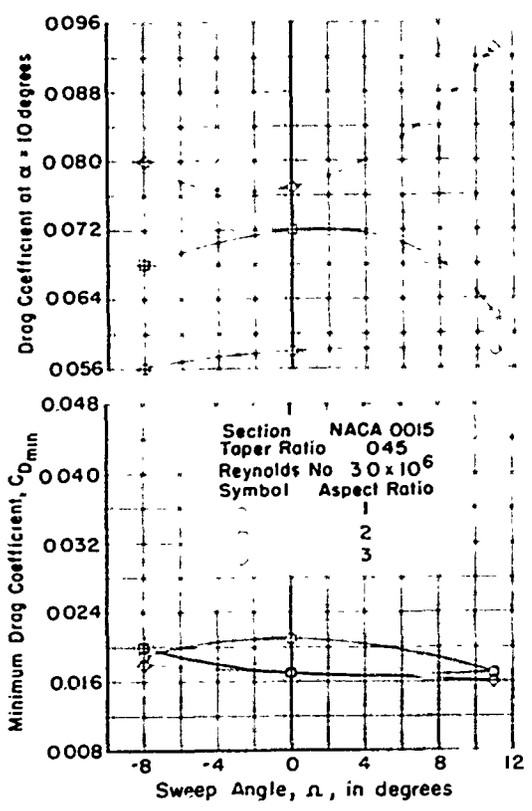

Figure 25 - Effect of Sweep Angle on Drag Coefficient of Control Surfaces with NACA 0015 Section in Astern Condition

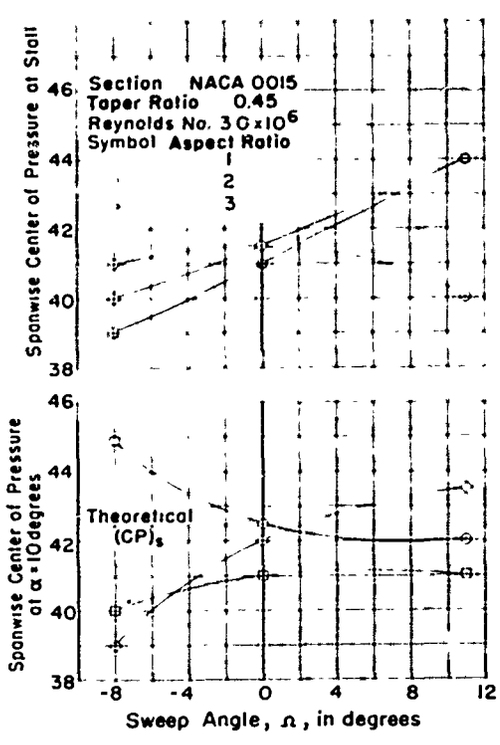

Figure 26 - Effect of Sweep Angle on Location of Spanwise Center of Pressure of Control Surfaces with NACA 0015 Section in Astern Condition

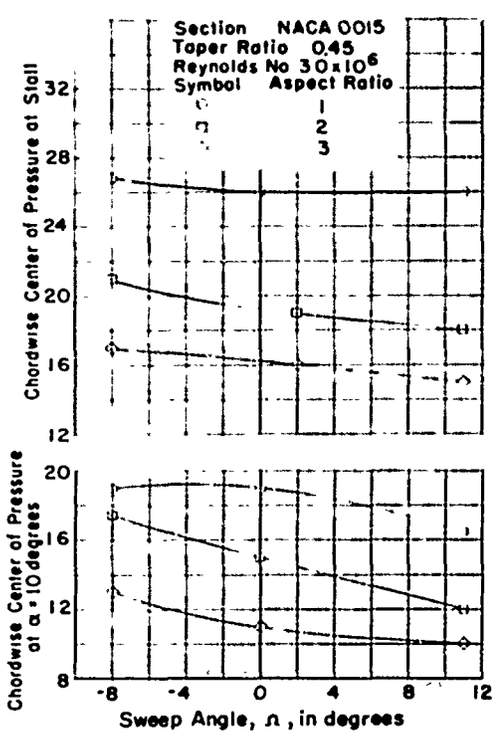

Figure 27 - Effect of Sweep Angle on Location of Chordwise Center of Pressure of Control Surfaces with NACA 0015 Section in Astern Condition

EFFECTS OF REYNOLDS NUMBER

The Reynolds number (ratio of inertia forces to viscous forces) is generally used as a criterion for similarity of flow around the model and the full-scale body. The Reynolds number effect (i.e., effect of viscosity) on the maximum lift coefficient is shown in Figure 7 for the control surface with an NACA 0015 section. The variation in maximum lift coefficient with Reynolds number is seen to be of considerable magnitude for surfaces with aspect ratios of 2 and 3, as well as for infinite aspect ratio surfaces.[10] This plot shows the effect of fairing the tip, as well as roughness effects.

The variation of stall angle with Reynolds number is shown in Figure 8, and over the range tested, the maximum variation was 5 degrees. This was obtained with a surface having an effective aspect ratio of 2 with a square tip. The stall angle also increased slightly with increasing Reynolds number for an aspect ratio of 3, but for an aspect ratio of 1 the stall angle remained almost constant.

Figure 9 is a plot of maximum lift coefficient and lift coefficient at a 10-degree angle of attack versus Reynolds number for all five sections of the series. All surfaces had the same taper ratio, sweep angle, and aspect ratio. The greatest variation in $C_{L_{max}}$ was noted for the TMB-No. 07507515 and TMB-Fairing No. 7. This was to be expected, since both sections have circular leading edges. However, $C_{L_{(\alpha = 10 \text{ degrees})}}$ is almost constant over the Reynolds number range for all surfaces tested.

Figure 10 shows that the drag of surfaces with TMB-No. 07507515 and TMB-Fairing No. 7 section shapes varies in much the same way as the lift. However, the minimum drag coefficient for these two surfaces is almost one and one-half times greater than the minimum drag coefficient of the others tested.

The plot of lift-drag ratio (L/D) versus Reynolds number (Figure 11) shows that surfaces with TMB No. 07507515 and TMB Fairing No. 7 section shapes have a lower $(L/D)_{max}$ than the other sections tested. These two surfaces also exhibit a greater Reynolds number effect on the location of the center of pressure, as shown in Figures 12 and 13.

EFFECTS OF GEOMETRIC PARAMETERS

AHEAD CONDITION

Sweep Angle

Studies were made of the effect of sweep on the characteristics of control surfaces with an NACA 0015 section and effective aspect ratios of 1, 2, and 3. Measurements were made for angles of sweep of the quarter-chord line of 11 degrees aft, zero degrees, and 8 degrees forward. Figure 14 shows that this limited variation of sweep has little effect on the lift coefficient at $\alpha = 10$ degrees. The effect of sweep on the drag coefficient was as much as

20 percent, with the greatest variation occurring for an effective aspect ratio of 3, as shown in Figure 15.

Figures 16, 17, and 18 show the variation of L/D ratio and location of the spanwise and chordwise centers of pressure with sweep angle. It should be noted that the location of the spanwise center of pressure is always slightly out board of the theoretical value $4/3\pi \ b/2$ for a surface with elliptical loading. This confirms expectations for a taper ratio of 0.45, as shown in Figure 3, for swept-back surfaces, but is contrary to the results expected for swept-forward surfaces. However, in the latter case this variation was only 2 to 6 percent from the theoretical value for $\alpha = 10$ degrees.

Aspect Ratio

The "aspect ratio" referred to throughout this report is the effective aspect ratio (or b^2/S) when the surface is mounted on a ground board. Figure 19 shows that at $\alpha = 10$ degrees the lift coefficient of a surface with an NACA 0015 section increases with increasing aspect ratio over the range covered. However, the maximum lift coefficient decreases with increasing aspect ratio over the lower part of the Reynolds number range. The drag coefficient, L/D ratio, and location of the spanwise center of pressure of the surfaces with an NACA 0015 section and zero sweep are shown on Figures 20, 21, and 22.

Figure 23 shows that as the aspect ratio is increased, when $\alpha = 10$ degrees, the chordwise center of pressure moves aft toward the quarter chord of the control surface. However, near the stall angle the chordwise center of pressure moves forward toward the nose as the aspect ratio is increased.

Tip Shape

The control surfaces with the NACA 0015 section were tested with square and faired tips. From Figure 7, for an aspect ratio of 2, a higher value of $C_{L_{max}}$ was obtained with square tips than was obtained with faired tips. At the highest Reynolds number the faired tip reduced the stall angle approximately 2 degrees.

Figures 10, 12, and 13 show the effect of the tip shape on the drag coefficient, the spanwise center of pressure locations, and the chordwise center of pressure location, respectively.

ASTERN CONDITION

Surfaces with an NACA 0015 section with square tips were tested at a Reynolds number of 3 million in the astern condition. Cross plots of the coefficients as a function of the sweep angle are presented in Figures 24 through 27 for surfaces with three different aspect ratios. For most control-surface design problems, the behavior of the surfaces in reverse flow are of secondary importance. However, for situations where this information is required, the

cross-plots show the effect of sweep and aspect ratio on the coefficients. Also, the results of the wind-tunnel tests are presented in Appendixes C and D for the surface in the astern condition.

CORRELATION WITH THEORY

Several theoretical and semi-empirical equations are available in the aerodynamic and hydrodynamic literature for estimating the characteristics of low-aspect-ratio surfaces. All of these existing equations exhibit poor agreement with experimental results or agree with the experimental results for only one specific control surface. The experimental results for low-aspect-ratio surfaces exhibit a nonlinear effect which may be of considerable importance in the calculation of the coefficients. A semi-empirical approach is therefore employed to arrive at equations suitable for engineering computations.

LIFT COEFFICIENT

A modification of the Helmbold[11] equation with a nonlinear term of the form suggested by Betz and others will be presented for the lift coefficient. When the form of the lift coefficient is chosen as

$$C_L = f_1 \alpha + f_2 \alpha^2$$

where

$$f_1 = f_3 (a_0, a_e, \Omega)$$

$$f_2 = f_4 (a_e, C_{D_c})$$

satisfactory agreement has been achieved in isolated cases by properly selecting the functions f_1 and f_2. Taking derivatives of C_L with respect to α yields

$$\frac{\partial C_L}{\partial \alpha} = f_1 + 2 f_2 \alpha$$

and

$$\frac{\partial^2 C_L}{\partial \alpha^2} = 2 f_2$$

Hence, the function f_1 is the lift-curve slope at $\alpha = 0$ and f_2 is 1/2 the curvature of the lift curve. From a survey of the aerodynamic literature it is seen that the Helmbold equation, as mofified by Polhamus[12] to account for sweep, is a satisfactory relationship for f_1. From consideration of the semi-empirical equation proposed in Reference 13, which included an α^2 term, there appears to be a dependence of the nonlinear portion of the lift coefficient on aspect ratio. If the form of f_2 is selected as

$$f_2 = \frac{C_{D_c}}{a_e}\left(\frac{\alpha}{57.3}\right)^2$$

then, in the limit as $a_e \to \infty$, $f_2 \to 0$, which is in agreement with experimental evidence. Then, using the Polhamus equation for f_1 and the proposed form for f_2, the lift coefficient can be written as

$$C_L = \left[\frac{a_0 a_e}{\cos\Omega\sqrt{\frac{a_e^2}{\cos^4\Omega} + 4 + \frac{57.3\,a_0}{\pi}}}\right]\alpha + \frac{C_{D_c}}{a_e}\left(\frac{\alpha}{57.3}\right)^2 \qquad [1]$$

and the lift-curve slope at $\alpha = 0$ is

$$\left(\frac{\partial C_L}{\partial \alpha}\right)_{\alpha=0} = \left[\frac{a_0 a_e}{\cos\Omega\sqrt{\frac{a_e^2}{\cos^4\Omega} + 4 + \frac{57.3\,a_0}{\pi}}}\right] \qquad [1a]$$

where a_0 is the section lift-curve slope corrected from experimental observations, $a_0 = 0.9\ (2\pi/57.3)$ per degree,

a_e is the effective aspect ratio,

Ω is the sweep of quarter-chord line,

C_{D_c} is the cross flow-drag coefficient, and

α is the angle of attack in degrees.

The crossflow drag coefficient, which is a function of the tip shape and taper ratio, was evaluated at a single point from the wind-tunnel results for both the square and faired tips. These values ($C_{D_c} = 0.80$ for squared tips and $C_{D_c} = 0.40$ for faired tips) were used in the semi-empirical equation for the lift coefficient. Figure 28 presents an experimentally determined relationship for the crossflow drag coefficient as a function of the taper ratio for both square and faired tips. These two curves were deduced from the experimental data obtained from this investigation and from Reference 14.

Figures 29 and 30 are comparisons of the theoretical and measured lift coefficient as a function of angle of attack for surfaces with an NACA 0015 section with square and faired tips, respectively.

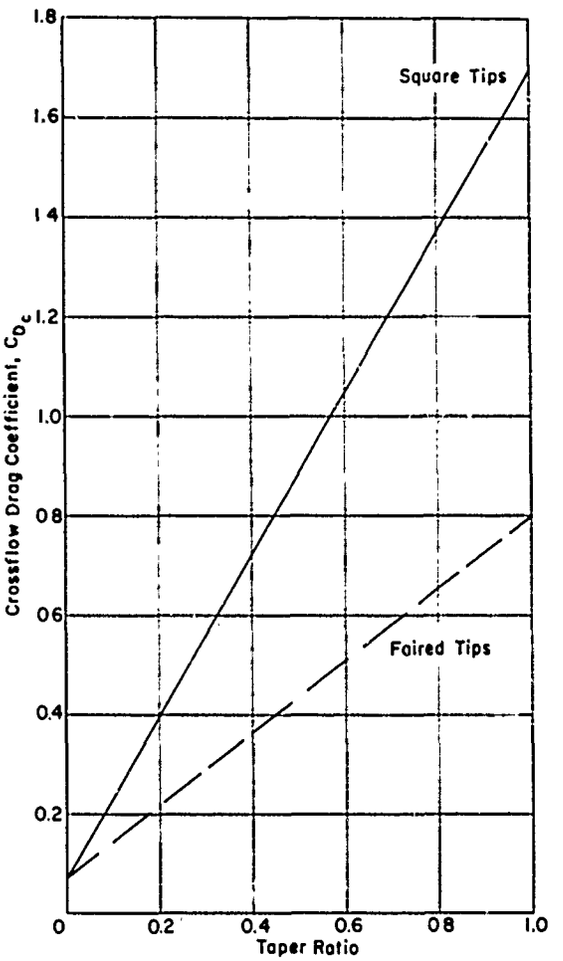

Figure 28 - Effect of Tip Shape and Taper Ratio on Crossflow Drag Coefficient

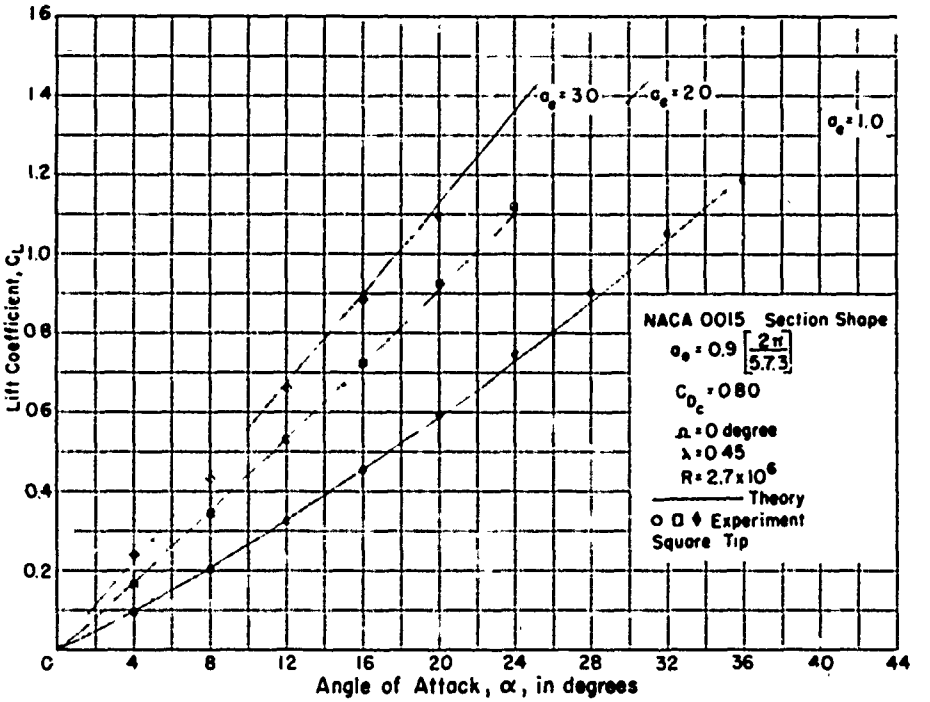

Figure 29 - Comparison of Experimental and Calculated Lift Coefficients for Square-Tip Control Surfaces of Various Aspect Ratios

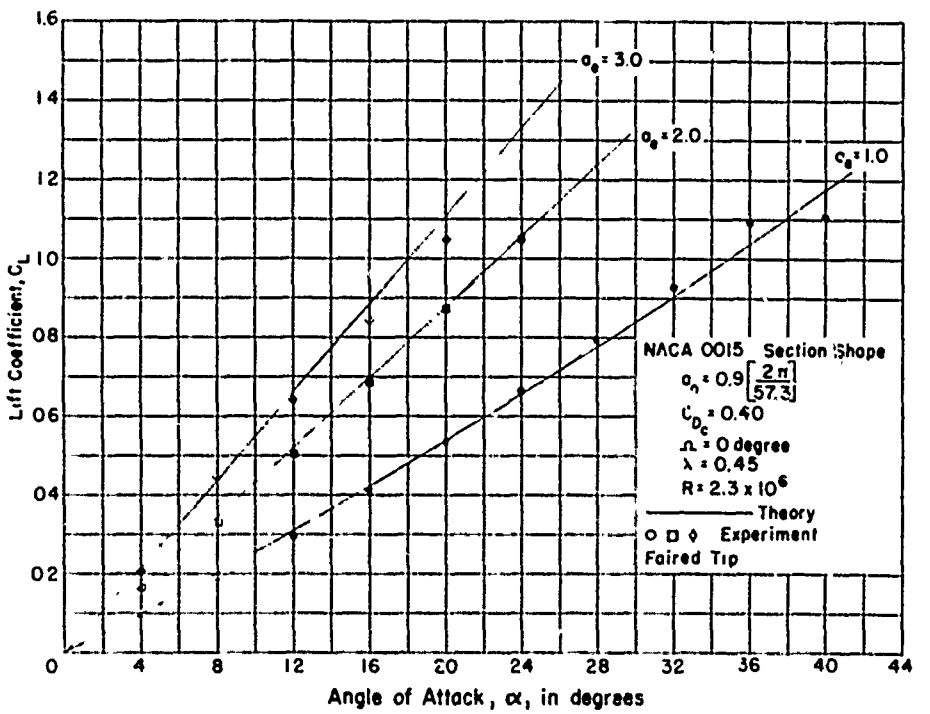

Figure 30 - Comparison of Experimental and Calculated Lift Coefficients for Faired-Tip Control Surfaces of Various Aspect Ratios

DRAG COEFFICIENT

The drag coefficient can be computed with reasonable accuracy from

$$C_D = C_{d_0} + \frac{C_L^2}{\pi a_e e} \qquad [2]$$

where C_{d_0} is the minimum section drag coefficient,

C_L is the lift coefficient,

a_e is the effective aspect ratio, and

e is the Oswald efficiency factor ($e = 0.90$) from Reference 15.

On Figures 31 and 32 this semi-empirical equation is compared with the measured results of the wind-tunnel tests. The value for C_{d_0} of 0.0065 was taken from Reference 16 for the NACA 0015 section.

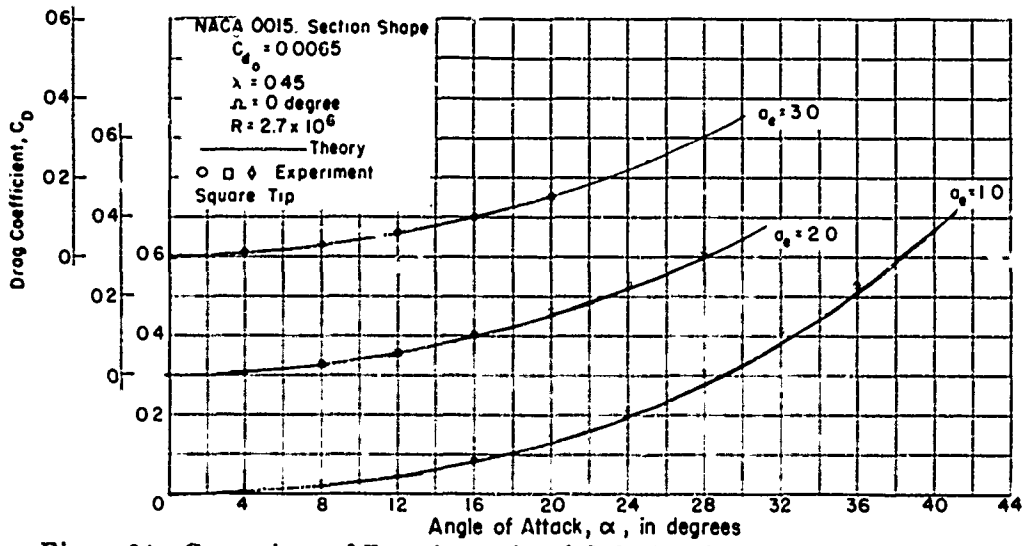

Figure 31 - Comparison of Experimental and Calculated Drag Coefficients for Square-Tip Control Surfaces of Various Aspect Ratios

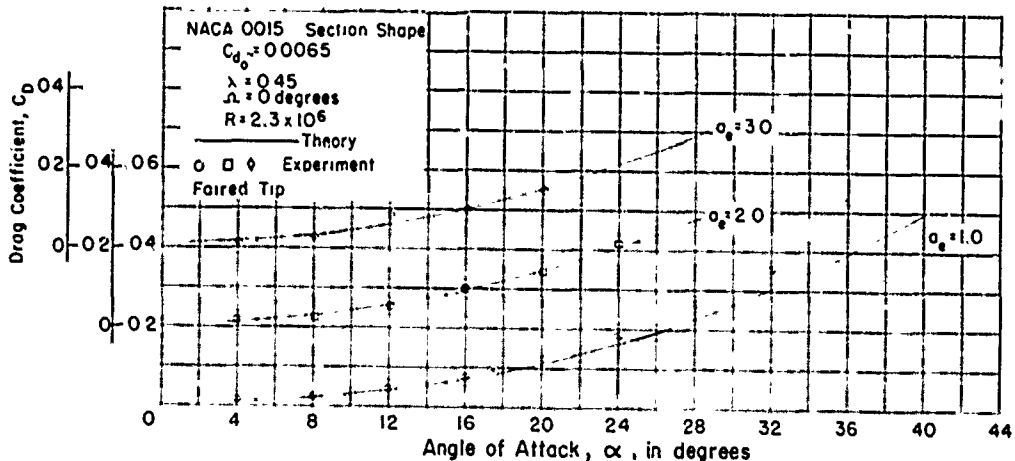

Figure 32 - Comparison of Experimental and Calculated Drag Coefficients for Faired-Tip Control Surfaces of Various Aspect Ratios

PITCHING MOMENT COEFFICIENT

In addition to the lift and drag forces, the pitching moment must be known before the torque on the control surface shaft can be computed. A semi-empirical equation for the pitching moment coefficient can be written as:

$$C_{m_{shaft}} = \left[\left(\frac{x}{c}\right)_{shaft} - \left(\frac{\partial C_m}{\partial C_L}\right)_{C_{L=0}}\right]\left[\left(\frac{\partial C_L}{\partial \alpha}\right)_{C_L=0}\right]\alpha \quad -\frac{1}{2}\frac{C_{D_c}}{a_e}\left(\frac{\alpha}{57.3}\right)^2 \qquad [3]$$

where the nonlinear correction term is of the same form as for the lift coefficient. When the shaft is located at $x/c = 0.25$, as was the case in this investigation, Equation [3] becomes

$$C_{m_{c/4}} = \left[0.25 - \left(\frac{\partial C_m}{\partial C_L}\right)_{C_L=0}\right]\left(\frac{\partial C_L}{\partial \alpha}\right)_{C_L=0}\alpha \quad -\frac{1}{2}\frac{C_{D_c}}{a_e}\left(\frac{\alpha}{57.3}\right)^2 \qquad [4]$$

where $\left(\frac{\partial C_m}{\partial C_L}\right)_{C_L=0}$ is given by Hembold's equation,[17]

$$\left(\frac{\partial C_m}{\partial C_L}\right)_{C_L=0} = \frac{1}{2} - \frac{\frac{2\pi}{57.3 a_0}\sqrt{a_e^2+4}+2}{4\,(a_e+2)} \qquad [5]$$

and $(\partial C_L/\partial \alpha)_{C_L=0}$ is computed from Equation [1a]. A plot of the lift-curve slope is presented in Reference 3 as a function of several geometric parameters. The computed values of $(\partial C_m/\partial C_L)_{C_L=0}$ are compared with experimental values[18] in Figure 33. The theoretical and experimental[14] lift-curve slopes are shown in Figure 34 as a function of the aspect ratio. The results of Equation [4], using the above values for $(\partial C_L/\partial \alpha)_{C_L=0}$ and $(\partial C_m/\partial C_L)_{C_L=0}$ are compared with the experimental data in Figures 35 and 36.

For comparative purposes the pitching moment curve from Jossel's equation[19]

$$C_{m_{\bar{c}/4}} = \frac{0.0434 - 0.241 \sin\alpha}{0.195 + 0.305 \sin\alpha}\sin\alpha \qquad [6]$$

is also plotted on Figures 35 and 36.

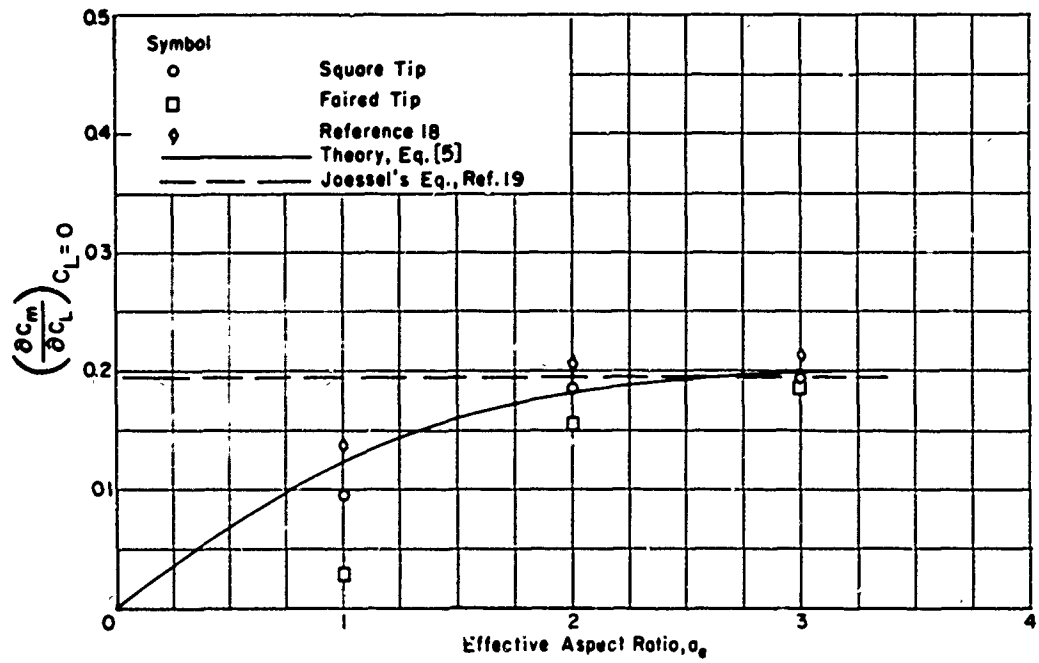

Figure 33 - Effect of Aspect Ratio on Location of Chordwise Center of Pressure

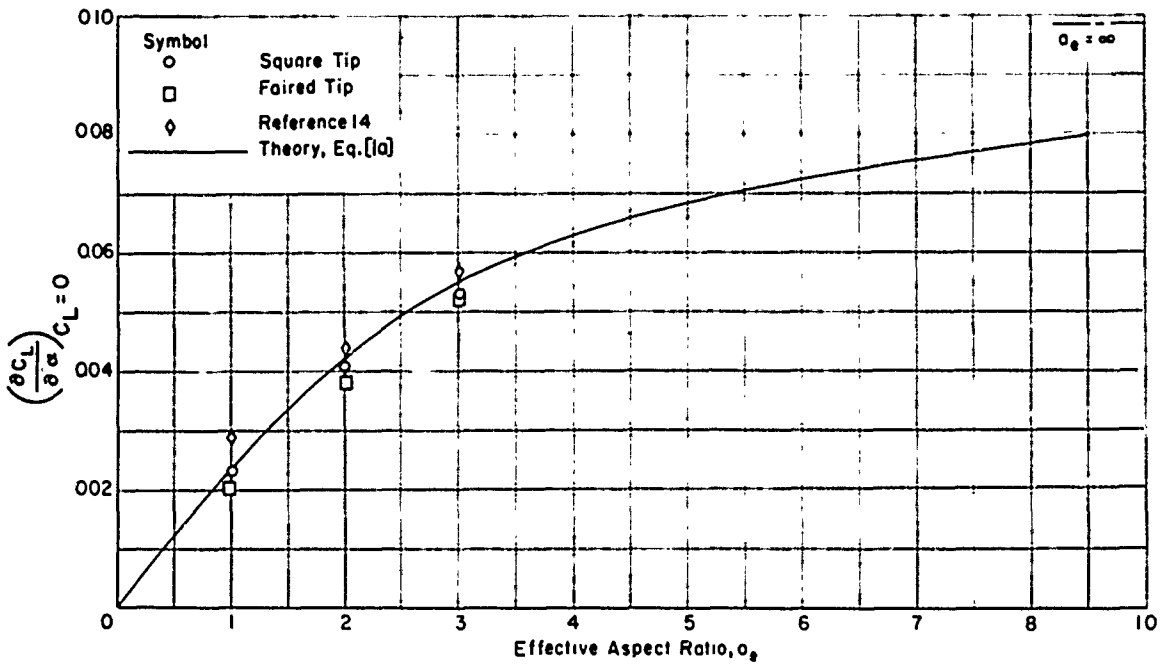

Figure 34 - Effect of Aspect Ratio on Lift-Curve Slope

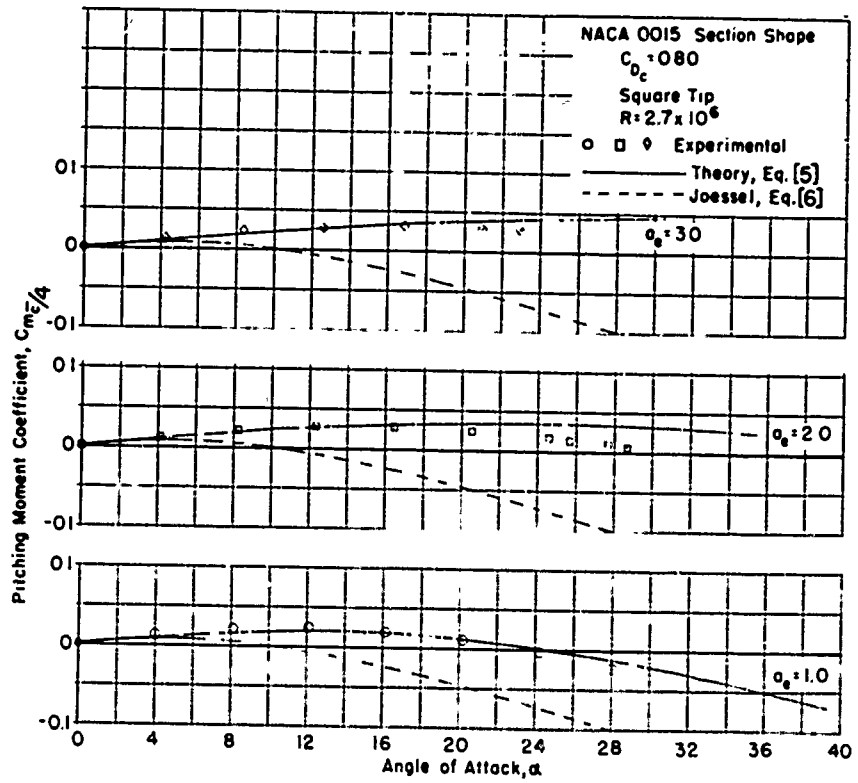

Figure 35 - Comparison of Experimental and Calculated Pitching Moment Coefficient for Square-Tip Control Surfaces of Various Aspect Ratios

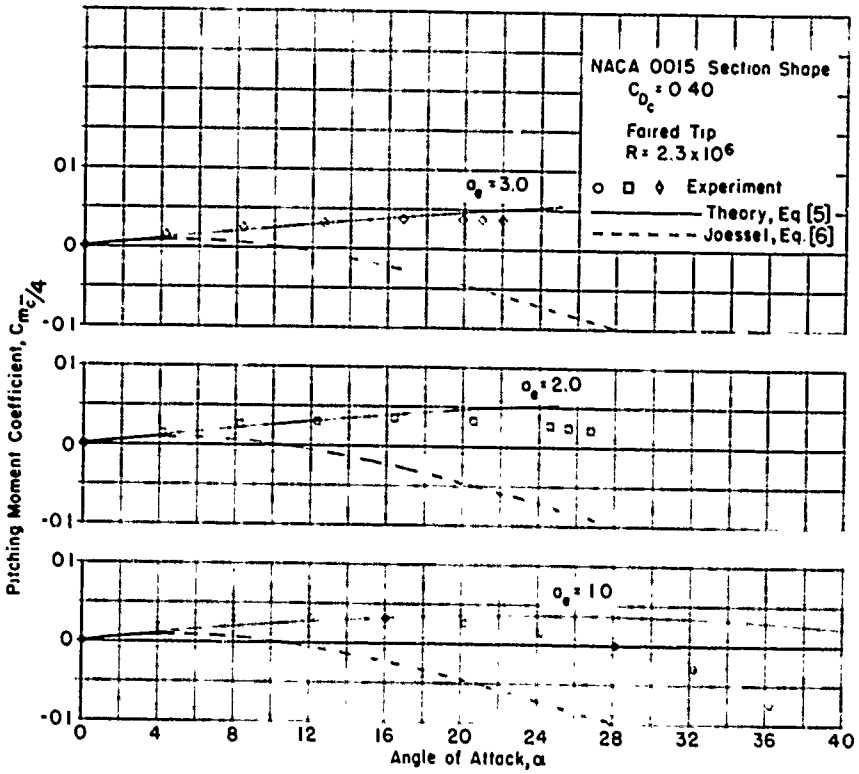

Figure 36 - Comparison of Experimental and Calculated Pitching Moment Coefficient for Faired-Tip Control Surfaces of Various Aspect Ratios

CENTER OF PRESSURE LOCATION

The location of the chordwise center of pressure, for control surfaces that are different from the ones tested, can be computed from

$$(CP)_{\bar{c}} = 0.25 - \frac{C_{m_{\bar{c}/4}}}{C_L \cos\alpha + C_D \sin\alpha} \qquad [7]$$

Also, from the geometry of the control surface shown in Figure 1, an approximate equation for the spanwise center of pressure for lifting surfaces having an elliptical load distribution can be written as

$$(CP)_s = \frac{C_L \left(\frac{4}{3\pi}, \frac{b}{2}\right) \cos\alpha + C_D \left(\frac{b}{2}\right) \sin\alpha}{b\,(C_L \cos\alpha + C_D \sin\alpha)} \qquad [8]$$

where C_L, C_D, and $C_{M_{\bar{c}/4}}$ can be computed from Equations [1], [2], and [4], respectively.

COMPUTATION OF CONTROL SURFACE SHAFT TORQUE

Since the control surface shaft is not usually located at the center of pressure of the hydrodynamic forces, a method of computing the resulting shaft torques is presented. First, from consideration of section shape, effective aspect ratio, sweep angle, and Reynolds number, the proper curve is selected from the data presented in the Appendices. If the taper ratio or other geometric parameters differ from those for which model data are available, the characteristics can be calculated using the equations of the previous section. After the curve has been selected, the moment coefficient about a shaft lying in the symmetry plane and normal to the chordal plane of the control surface can be computed from:

$$C_{M_{\text{shaft}}} = \left(\frac{l_3 - l_1}{l_2 - l_1}\right) C_{M_{\bar{c}/4}}$$

where the symbols are defined in Figure 37.

Hence, the torque on the control surface shaft is given by:

$$M_{\text{shaft}} = C_{M_{\text{shaft}}} \frac{\rho}{2} S V^2 \bar{c} \qquad [9]$$

However, this is the torque produced by the hydrodynamic forces only; therefore, the frictional torque produced by the bearings and linkages also must be considered when computing the size of the shaft and equipment.

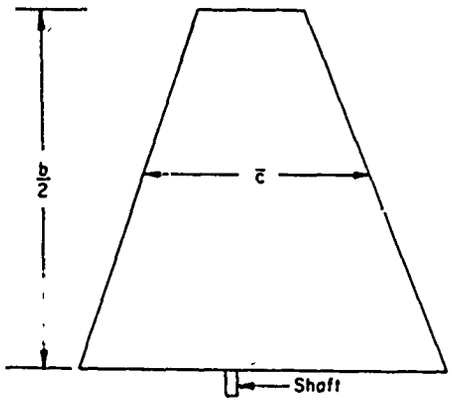

Figure 37 – Sketch Defining Method of Computing Control Surface Shaft Torque

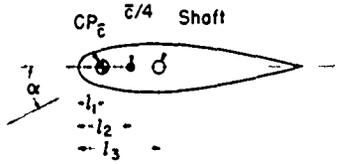

SUMMARY OF THEORETICAL AND SEMI-EMPIRICAL EQUATIONS

The proposed theoretical and semi-empirical equations for computing the control surface characteristics required by the designer are summarized here for convenience.

Lift Coefficient:

$$C_L = \left[\frac{a_0 \, a_e}{\cos \Omega \sqrt{\frac{a_e^2}{\cos^4 \Omega} + 4 + \frac{57.3 \, a_0}{\pi}}} \right] \alpha + \frac{C_{D_c}}{a_e} \left(\frac{\alpha}{57.3} \right)^2 \qquad [1]$$

Drag Coefficient:

$$C_D = C_{d_0} + \frac{C_L^2}{\pi a_e e} \qquad [2]$$

Pitching Moment Coefficient:

$$C_{m_{\bar{c}/4}} = \left[0.25 - \left(\frac{\partial C_m}{\partial C_L} \right)_{C_L = 0} \right] \left(\frac{\partial C_L}{\partial \alpha} \right)_{C_L = 0} \alpha \; - \frac{1}{2} \frac{C_{D_c}}{a_e} \left(\frac{\alpha}{57.3} \right)^2 \qquad [4]$$

Chordwise Center of Pressure:

$$(CP)_{\bar{c}} = 0.25 - \frac{C_{m_{\bar{c}/4}}}{C_L \cos\alpha + C_D \sin\alpha} \qquad [7]$$

and Spanwise Center of Pressure:

$$(CP)_s = \frac{C_L\left(\frac{4}{3\pi}\cdot\frac{b}{2}\right)\cos\alpha + C_D\left(\frac{b}{2}\right)\sin\alpha}{\frac{b}{2}(C_L\cos\alpha + C_D\sin\alpha)} \qquad [8]$$

The computed values of C_L, C_D, and $C_{M_{\bar{c}/4}}$ have been compared with the experimental values in Figures 29 through 32, 35, and 36, respectively. The computed value of the lift coefficient for a control surface with different geometric characteristics is compared (Figure 38) with the experimental results obtained from Reference 14. Here also the agreement between the theoretical and experimental values is quite satisfactory.

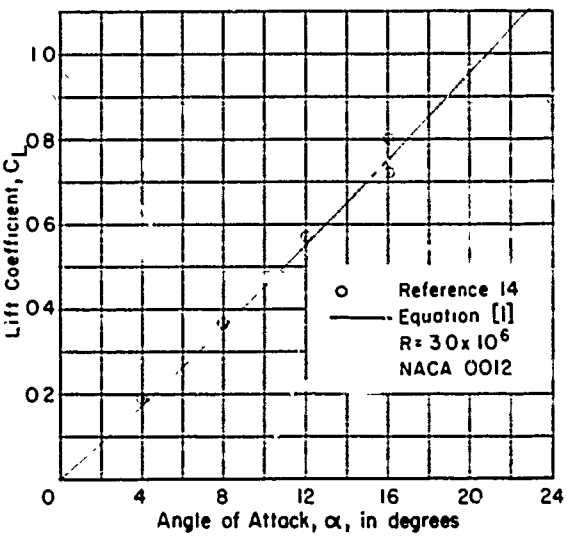

Figure 38 - Comparison of Experimental and Calculated Lift Coefficient for Square-Tip Control Surface of Aspect Ratio 2 and Taper Ratio of 1.0

CONCLUSIONS AND RECOMMENDATIONS

From the experimental results of this investigation, the effects of aspect ratio, sweep angle, tip shape, and section shape are evaluated and presented in the cross-plots. Based on these results, control surfaces with square tips, an NACA 0015 section, and a moderately swept quarter-chord line (if needed) are recommended for most naval applications. These semi-empirical equations are compared with the experimentally determined lift, drag, and pitching moment coefficients for the models with an NACA 0015 section. As can be seen from the comparison, the agreement is sufficiently good to recommend use of these equations for design purposes.

It should be pointed out that these results are the free-stream model characteristics; hence the effect of the particular hull configuration on these characteristics must be considered for each specific design application.

ACKNOWLEDGMENTS

The authors wish to express their appreciation to Mr. S.M. Gay, Jr., of the Hydromechanics Laboratory for his assistance in preparing the models, and Mr. T.J. Schmitt and Mr. H.R. Chaplin of the Aerodynamics Laboratory for conducting the wind-tunnel tests.

Also, the authors wish to thank Mr. A. Goodman of the Hydromechanics Laboratory for his contributions to the section concerning correlation of the experimental data with theory.

REFERENCES

1. Johnson, J.L., "A Bibliography of Reports on Low-Aspect-Ratio Lifting Surfaces and Elongated Bodies in Subsonic Flow," David Taylor Model Basin Report C-523 (Nov 1952) CONFIDENTIAL.

2. Fehlner, L.F., "The Design of Control Surfaces for Hydrodynamic Applications," David Taylor Model Basin Report C-358 (Jan 1951).

3. DeYoung, J. and Harper, C.W., "Theoretical Symmetrical Span Loading at Subsonic Speeds for Wings Having Arbitrary Plan Form," National Advisory Committee for Aeronautics Report 921 (1948).

4. Freeman, H.B., "Calculated and Observed Speeds of Cavitation about Two- and Three-Dimensional Bodies in Water," David Taylor Model Basin Report 495 (Nov 1942).

5. Design Data Sheet, Navy Department, Bureau of Ships, Section DDS 1108-1 "Shaft Struts, Twin Arm Type," (May 1947).

6. Fehlner, L.F. and Pode, L., "The Development of a Fairing for Tow Cables," David Taylor Model Basin Report C-433 (Jan 1952) CONFIDENTIAL.

7. Swanson, R.S. and Toll, T.A., "Jet-Boundary Corrections for Reflection-Plane Models in Rectangular Wind Tunnels," National Advisory Committee for Aeronautics Report 770 (1943).

8. Schmitt, T.J. "Wind-Tunnel Test Results of Submarine Control Surfaces," David Taylor Model Basin Aero Test A295 (Aug 1951-Jan 1953).

9. Chaplin, H.R., "Wind-Tunnel Tests of Low-Aspect-Ratio Control Surfaces with Trailing Edge to Wind," David Taylor Model Basin Report 944 (Feb 1954).

10. Loftin, K. Jr. and Smith, H.A., "Aerodynamic Characteristics of 15 NACA Airfoil Sections at Seven Reynolds Numbers from 0.7×10^6 to 9.0×10^6," National Advisory Committee for Aeronautics TN 1945 (Oct 1949).

11. Hembold, H.B., "Der Unverwundene Ellipsenflügel als trägendeFläche," Jahrb. 1942 der Deutschen Luftfahrt-forschung, Sect. 1, pp. 111-113.

12. Polhamus, E.C., "A Simple Method of Estimating the Subsonic Lift and Damping in Roll of Sweptback Wings," National Advisory Committee for Aeronautics TN 1862 (1949).

13. Flax, A.H. and Laurence, H.R., "The Aerodynamics of Low-Aspect-Ratio Wings and Wing-Body Combinations,"Cornell Aeronautical Laboratory Report 37 (1951).

14. Jones, W., Jr., "Investigation of the Effects of Variations in the Reynolds Number Between 0.4×10^6 and 3.0×10^6 on the Low-Speed Aerodynamics Characteristics of Three Low-Aspect-Ratio Symmetrical Wings with Rectangular Plan Forms," National Advisory Committee for Aeronautics Research Memorandum L52G18 (1952).

15. Perkins, C.D. and Hage, R.E., "Airplane Performance Stability and Control," John Wiley and Sons, Inc. (1949).

16. Jacobs, N. and Abbott, I.H., "Airfoil Section Data Obtained in the NACA Variable-Density Tunnel as Affected by Support Interference and other Corrections," National Advisory Committee for Aeronautics Report 669 (1939).

17. Voepel, H., "Tests on Wings of Small Aspect Ratio," Royal Aircraft Establishment Library Translation No. 276 (1948). (Translation of A.V.A. Goettingen Report 19/9/46, "Messungen an Tragflugeln kleiner Streckung!")

18. Scholz, N., "Kraft-und Druckverteilungsmessungen an Tragflachen kleiner Streckung," Forschung auf dem Gebiete des Ingenieurwesens, Part B, Vol. 16, No. 3 (1949-1950), pp. 85-91.

19. Rossell, H.E. and Chapman, L.B., "Principles of Naval Architecture," Volume II. The Society of Naval Architects and Marine Engineers, New York (1939), p. 203.

APPENDIX A

FREE-STREAM CHARACTERISTICS OF SQUARE-TIP CONTROL SURFACES WITH AN NACA 0015 SECTION SHAPE IN THE AHEAD CONDITION

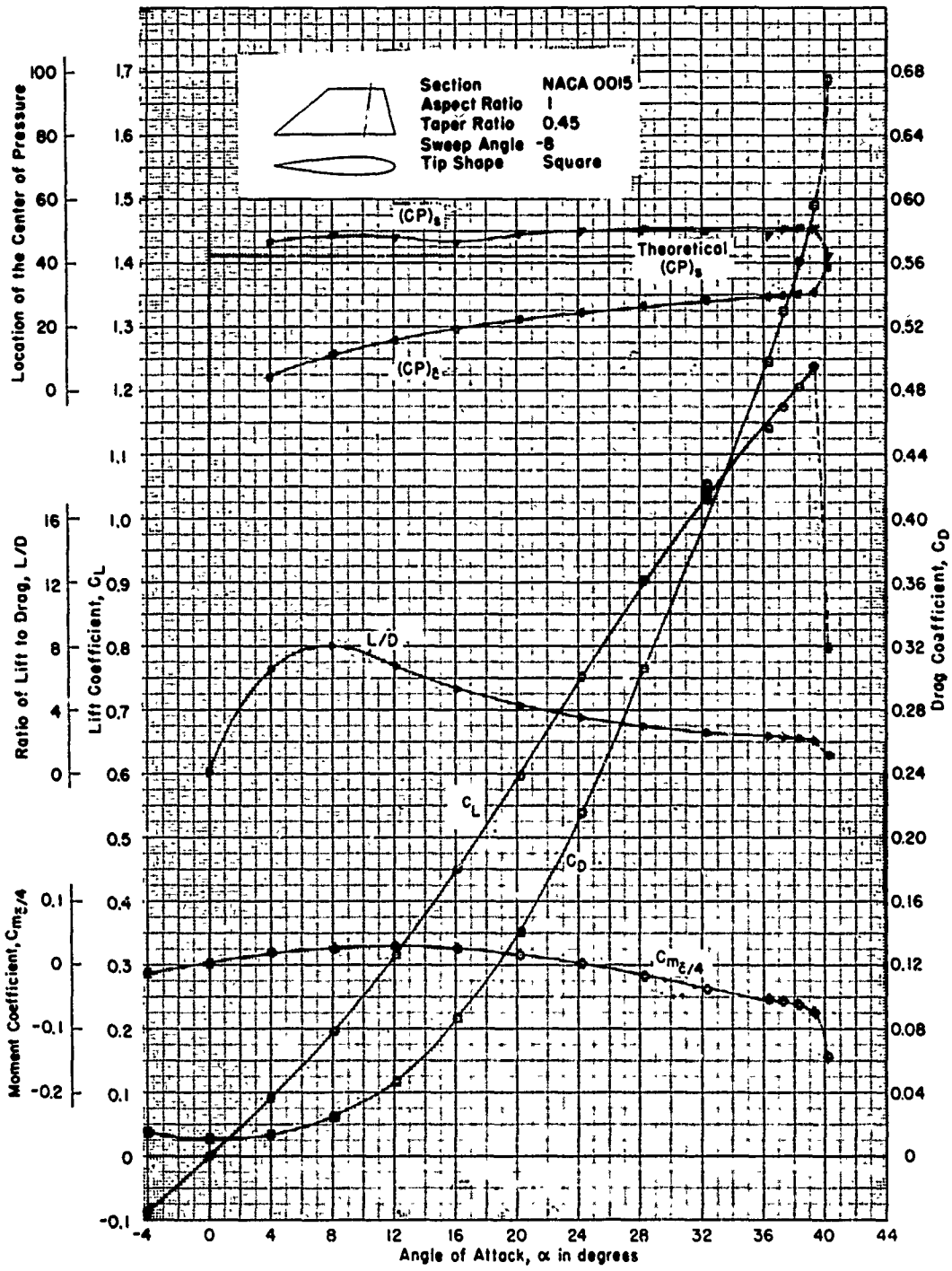

Figure 39 - Reynolds Number of 2.25×10^6

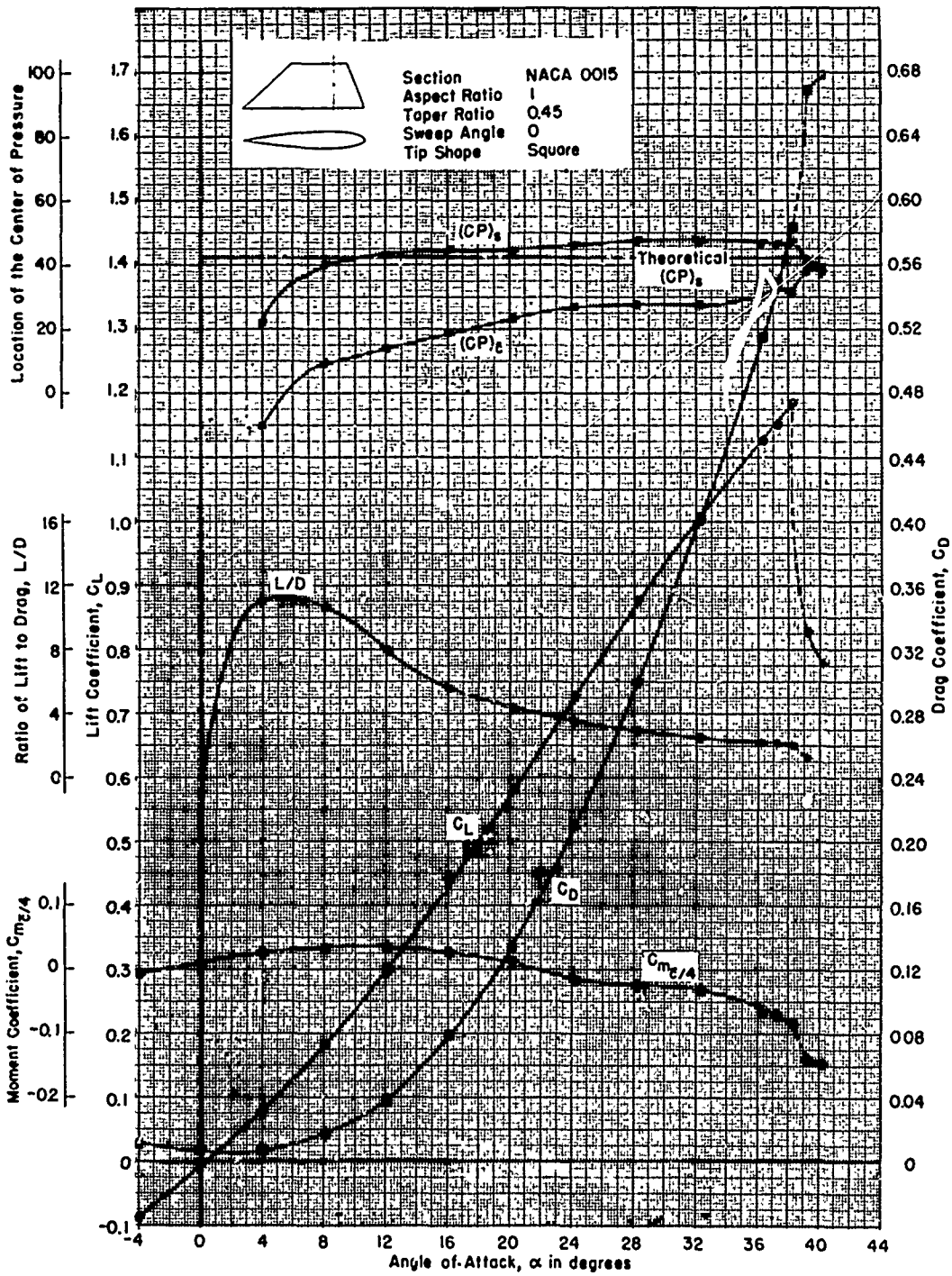

Figure 40 - Reynolds Number of 0.912×10^6

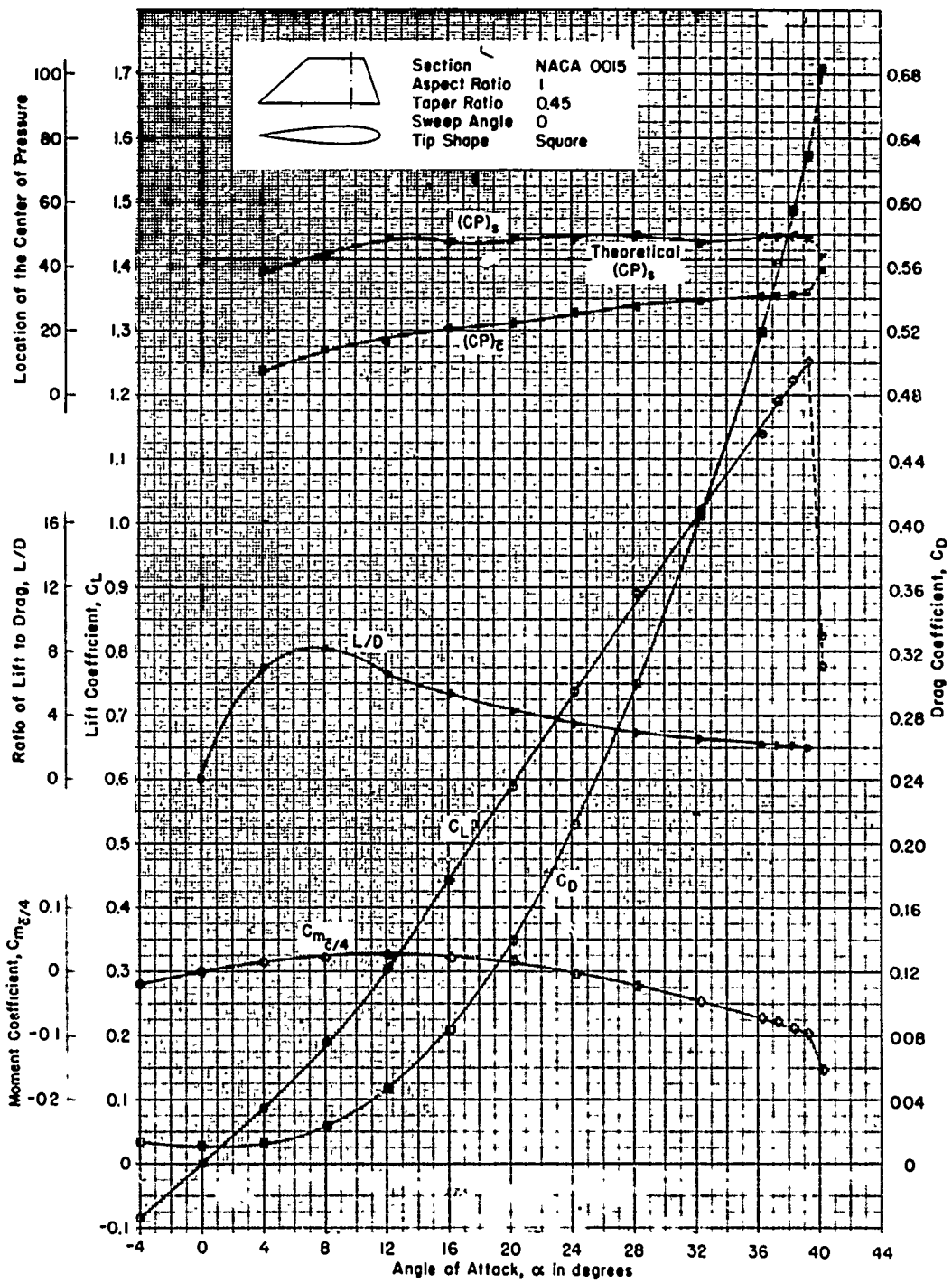

Figure 41 - Reynolds Number of 1.37×10^6

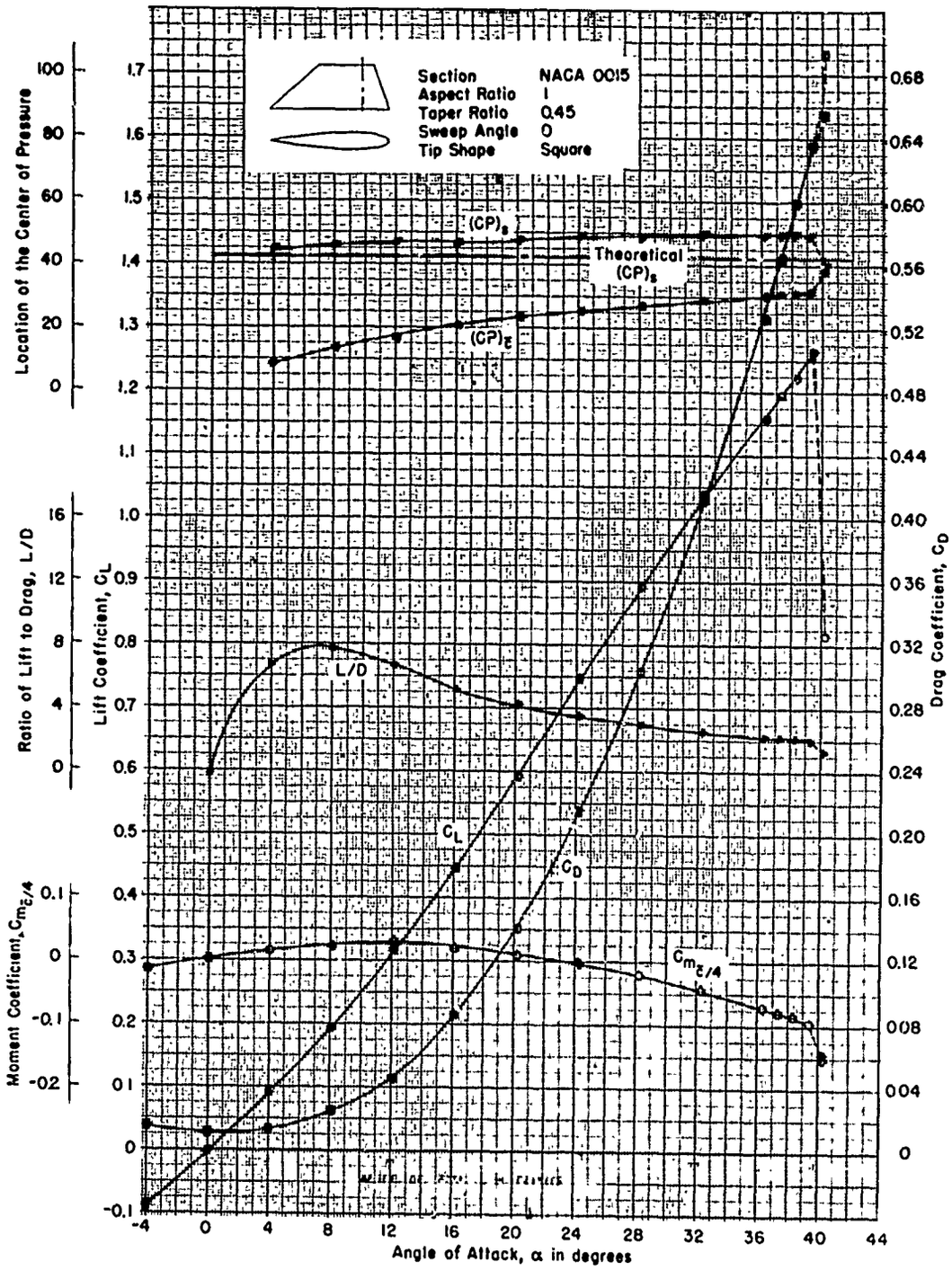

Figure 42 - Reynolds Number of 1.82×10^6

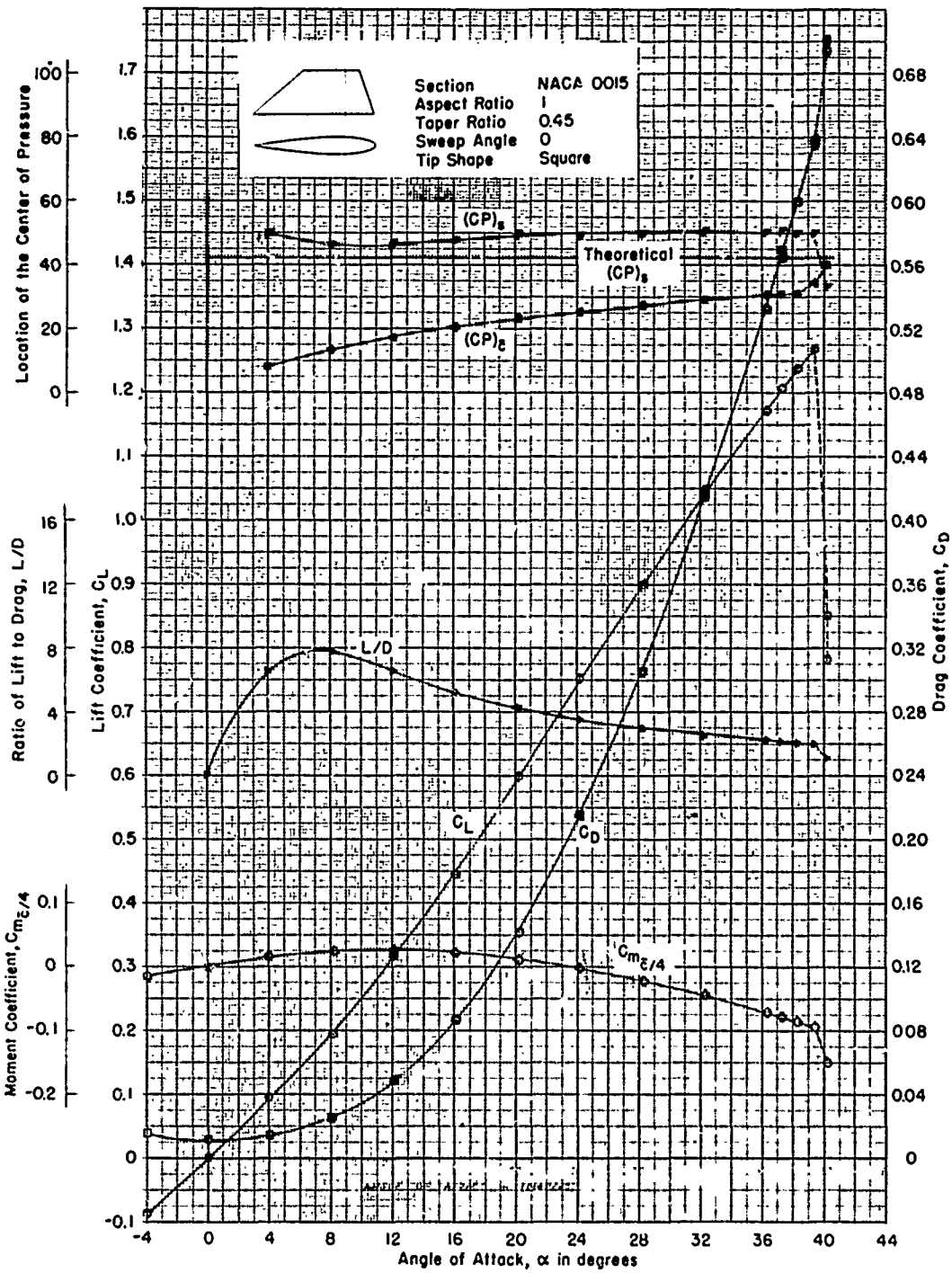

Figure 43 - Reynolds Number of 2.25×10^6

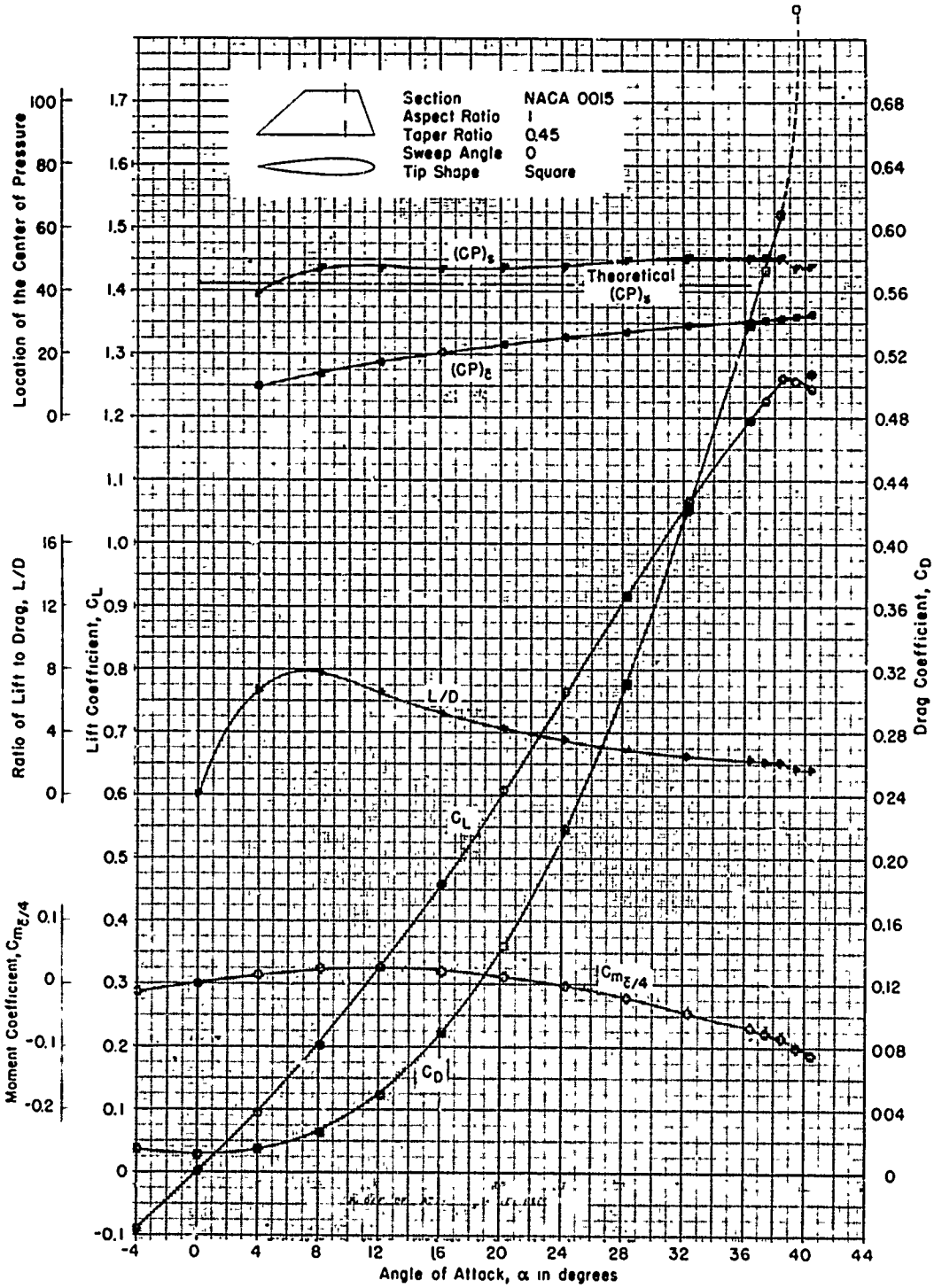

Figure 44 - Reynolds Number of 2.70×10^6

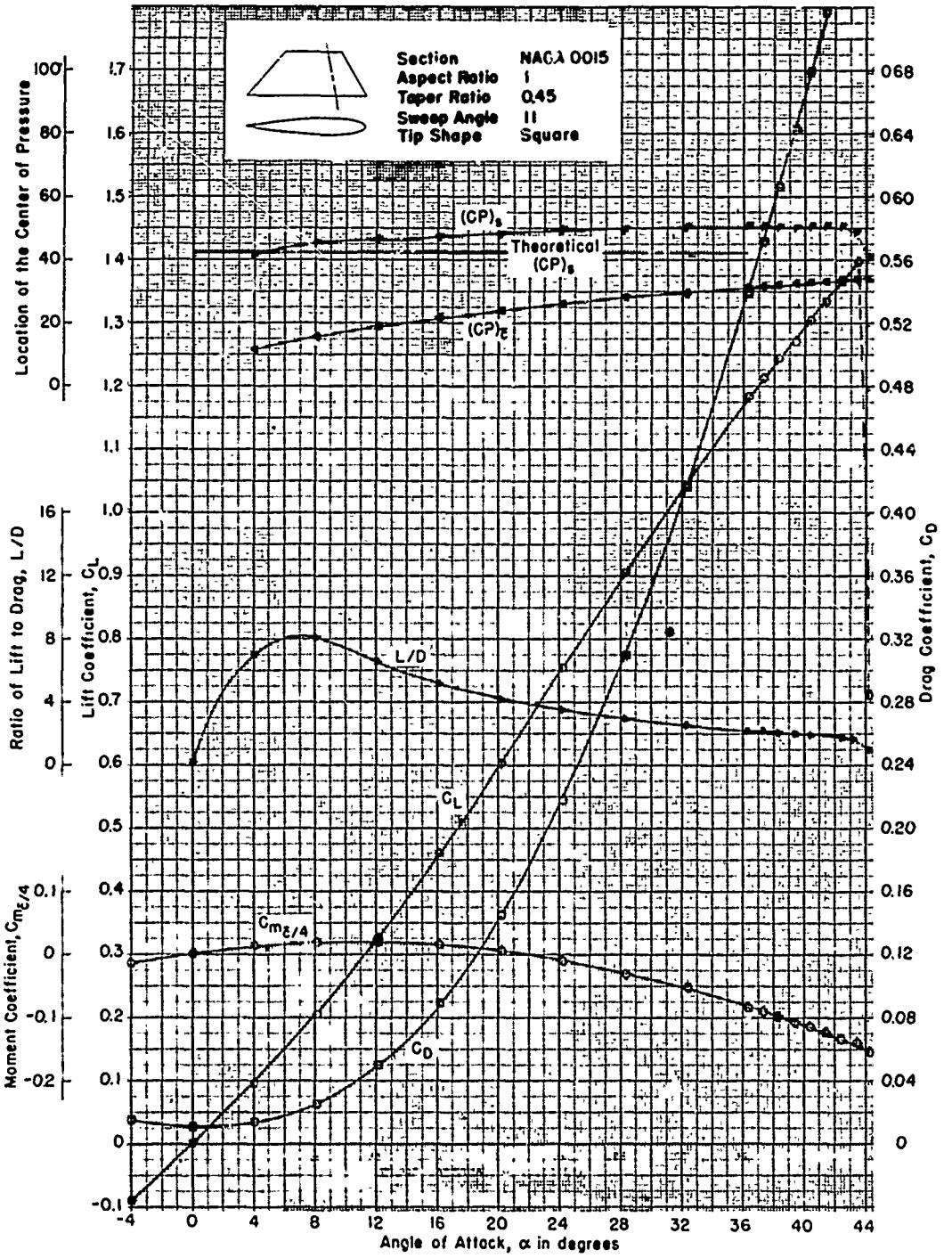

Figure 45 - Reynolds Number of 2.28×10^6

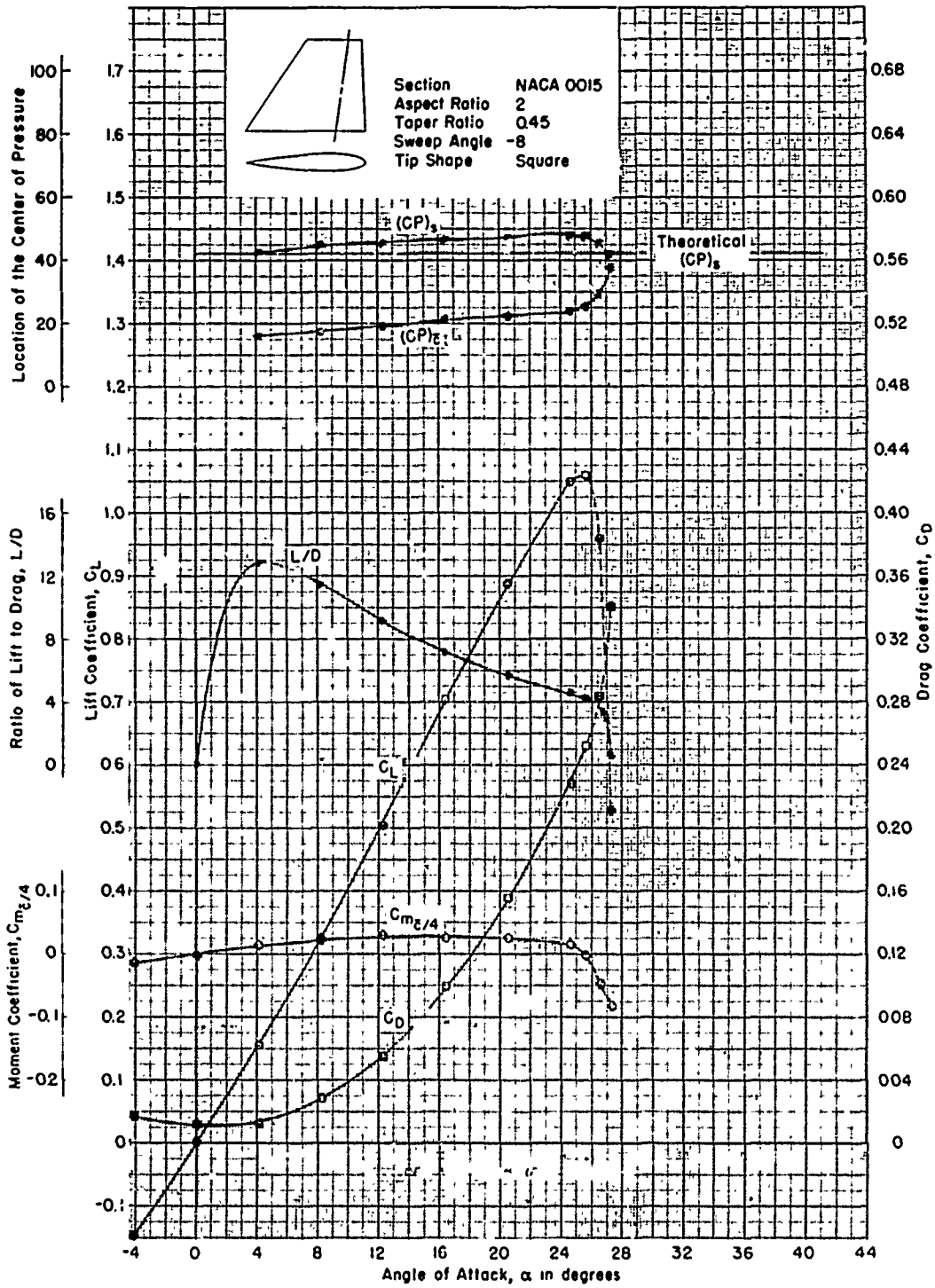

Figure 46 - Reynolds Number of 0.931×10^6

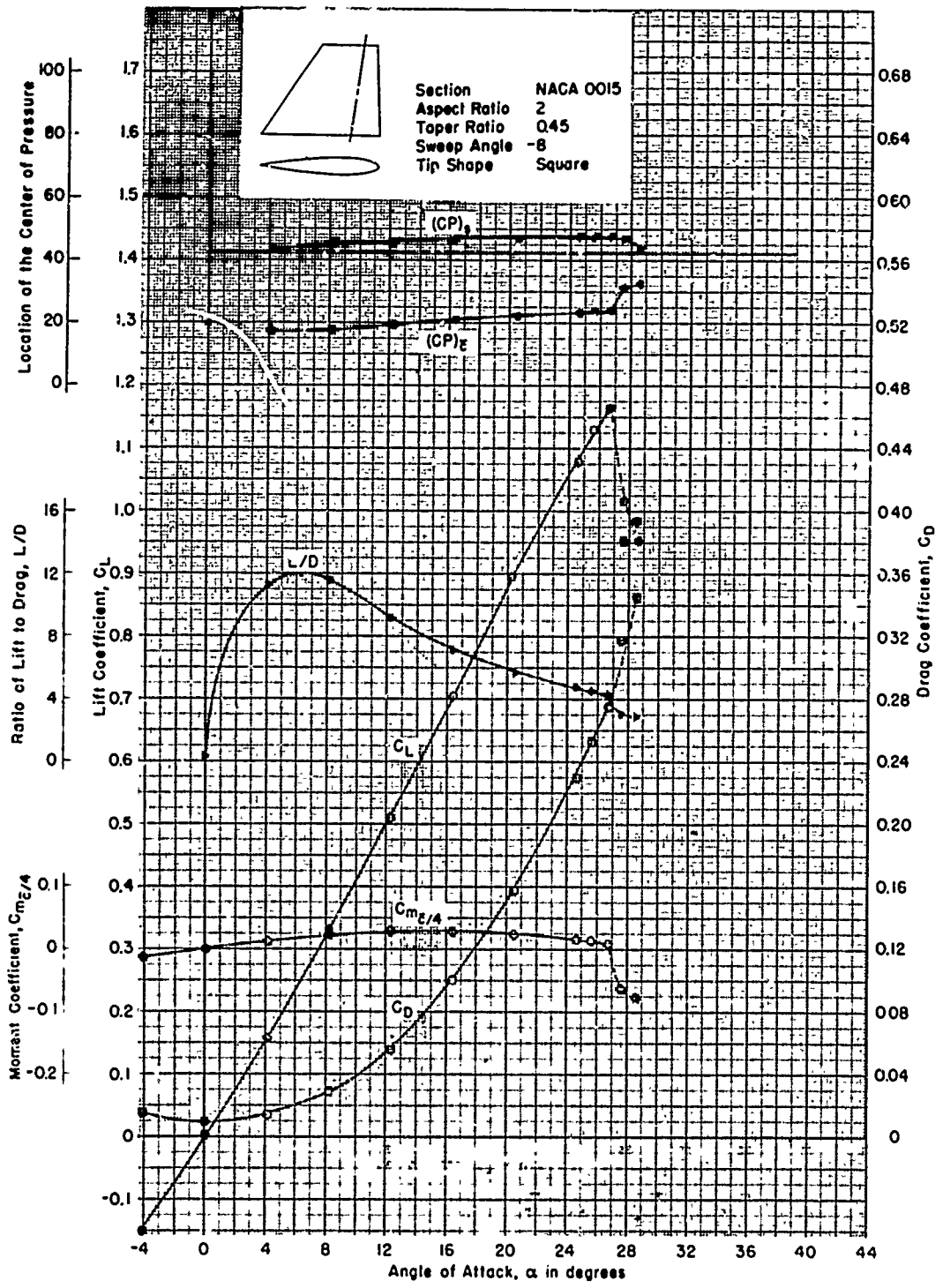

Figure 47 - Reynolds Number of 1.40×10^6

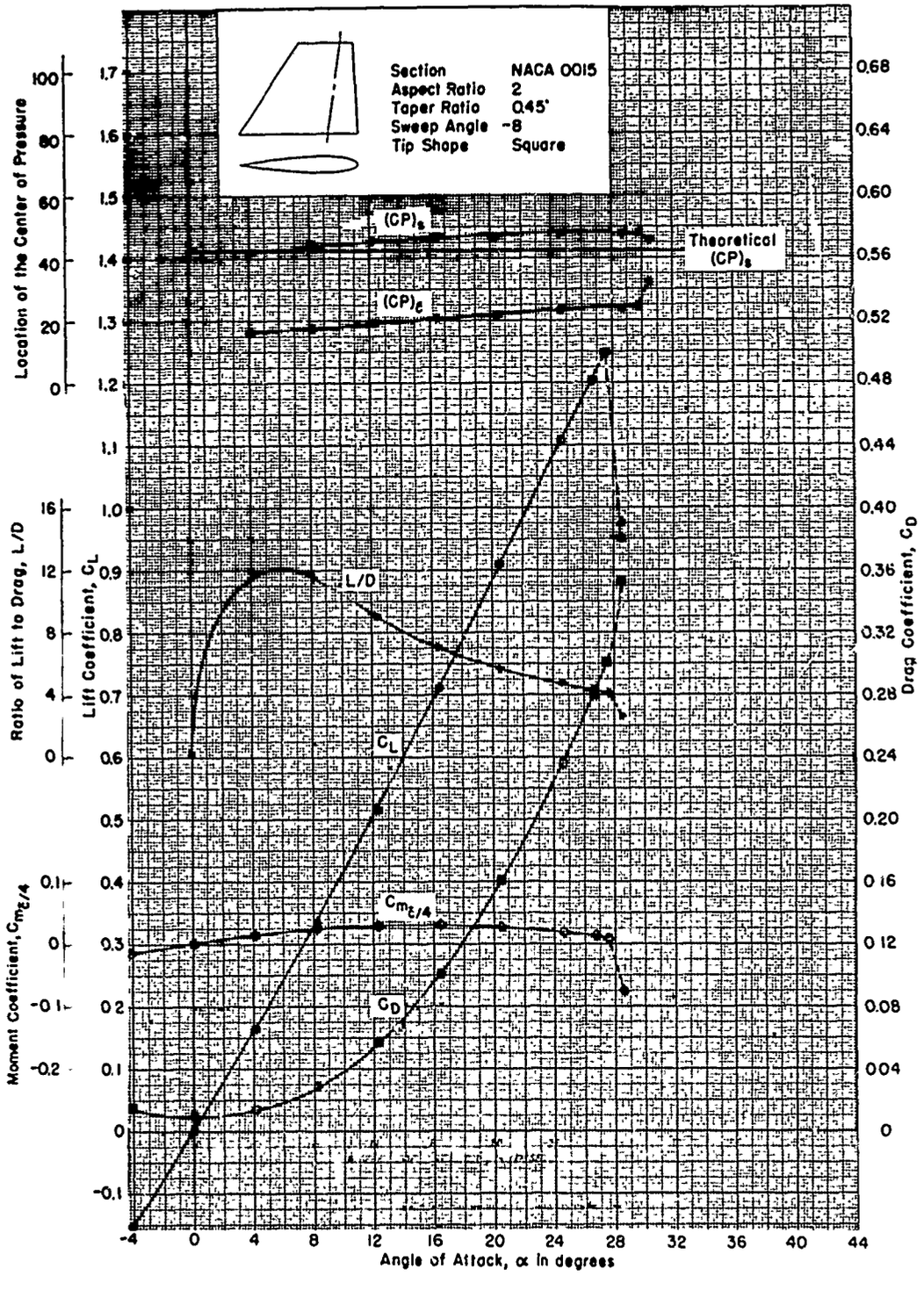

Figure 48 - Reynolds Number of 1.84×10^6

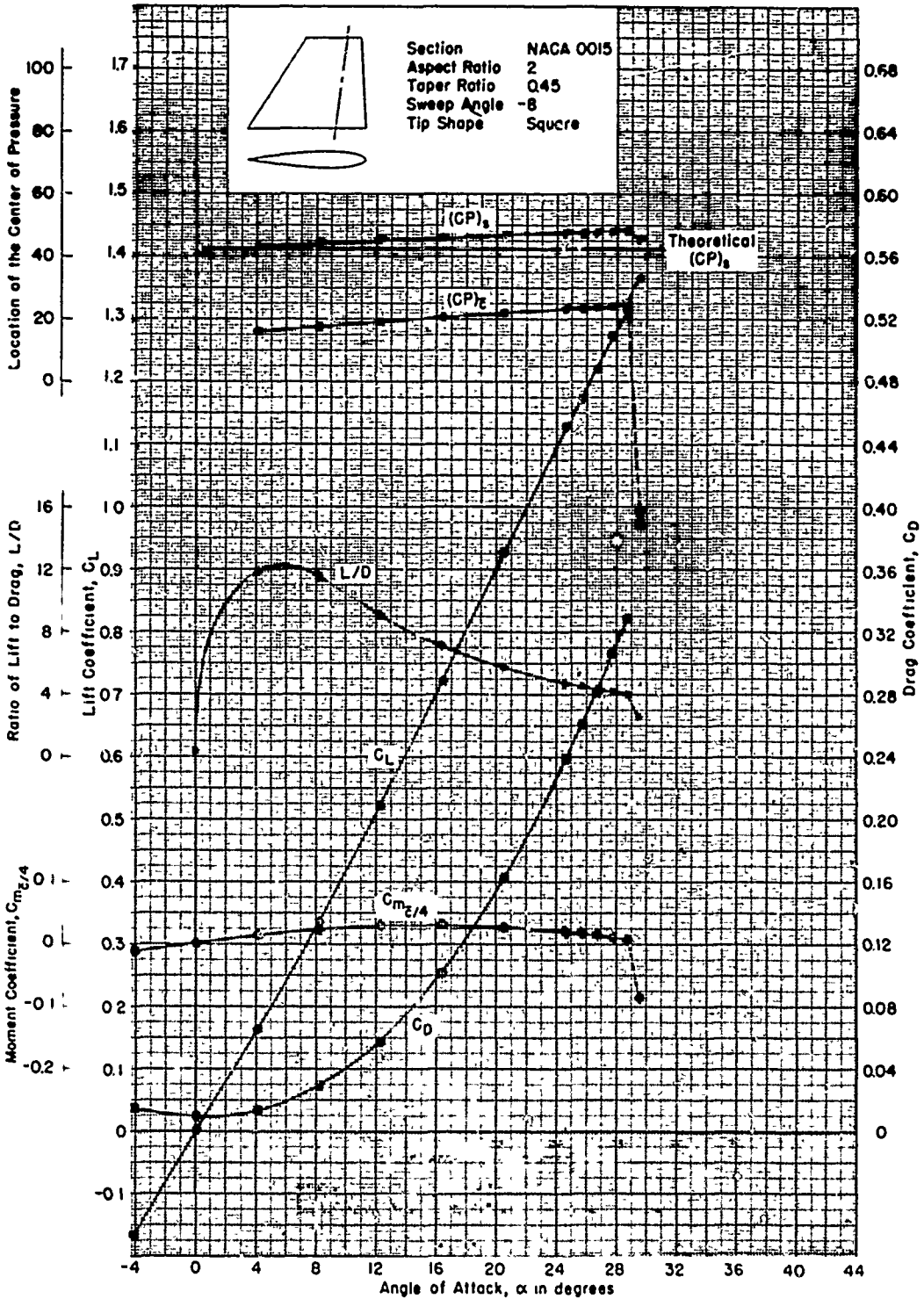

Figure 49 - Reynolds Number of 2.29×10^6

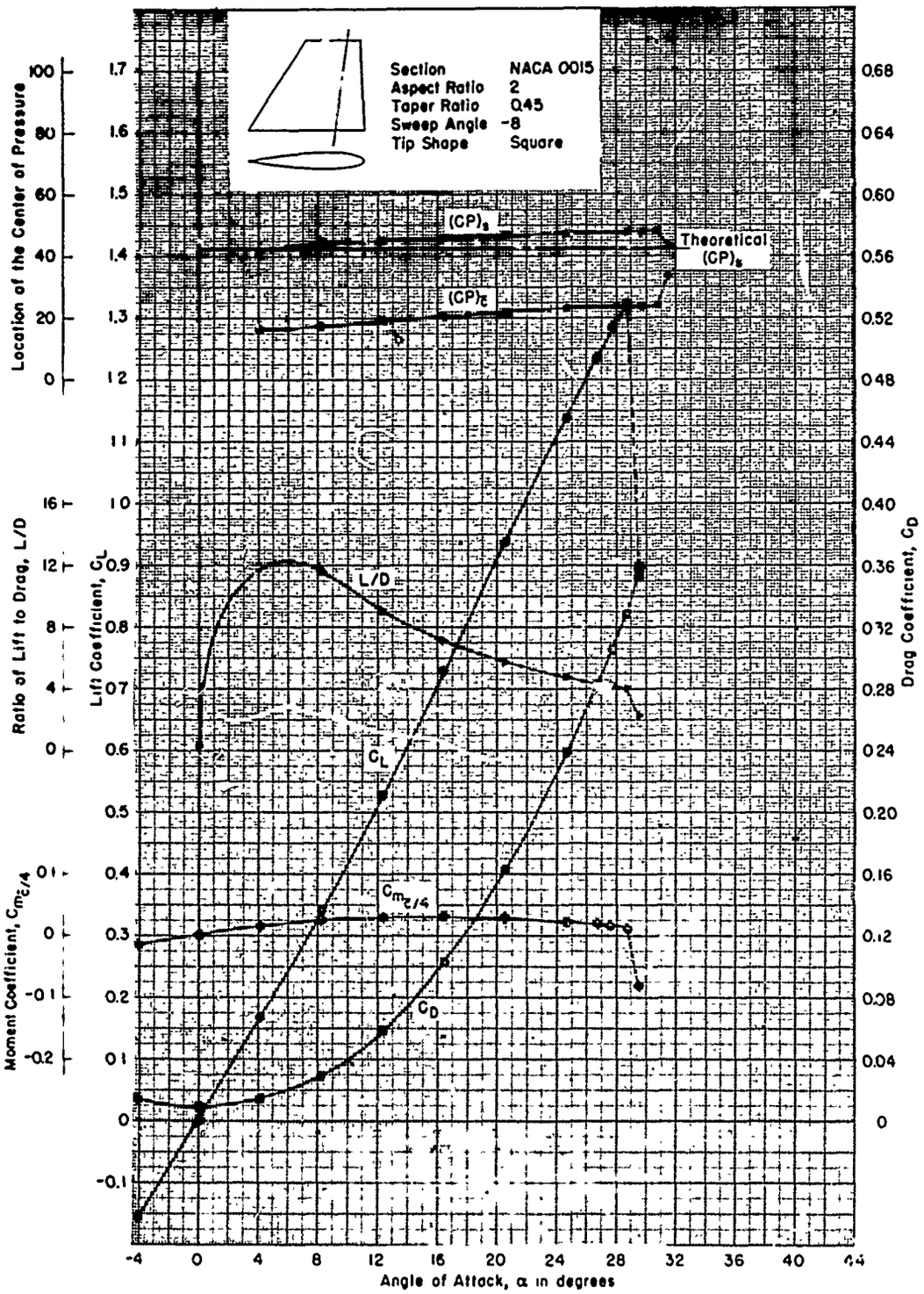

Figure 50 - Reynolds Number of 2.72×10^6

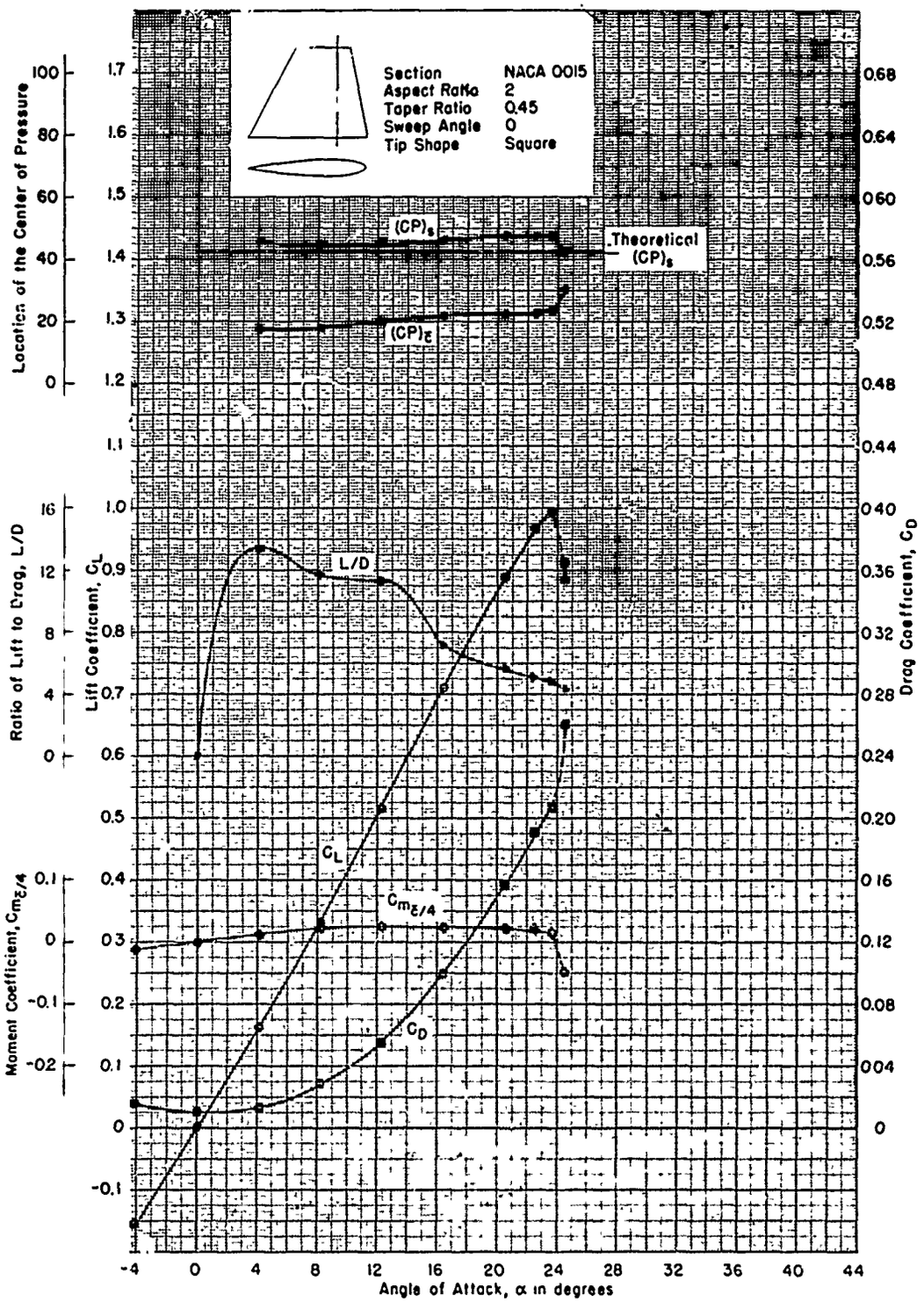

Figure 51 - Reynolds Number of 0.931×10^6

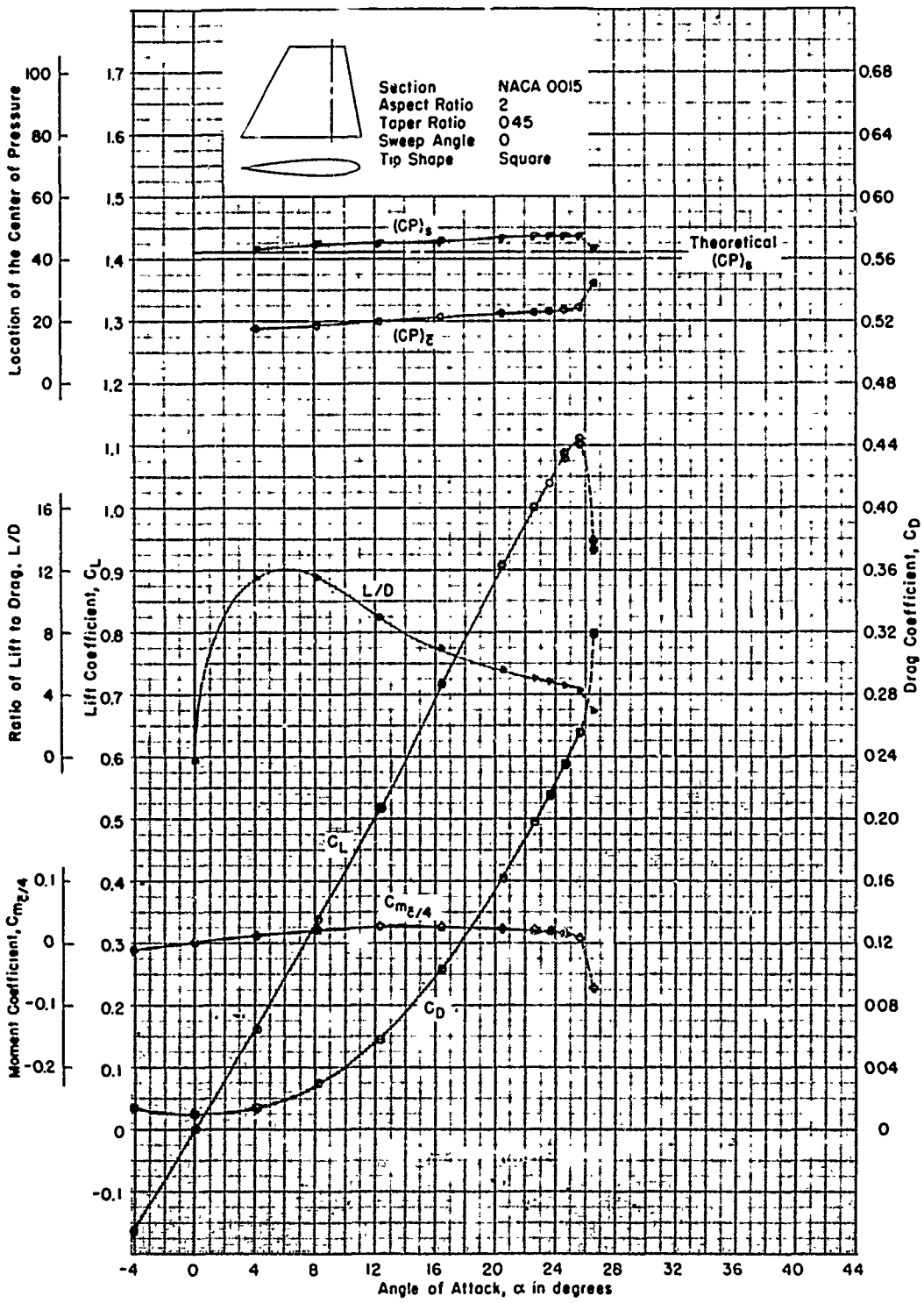

Figure 52 - Reynolds Number of 1.40×10^6

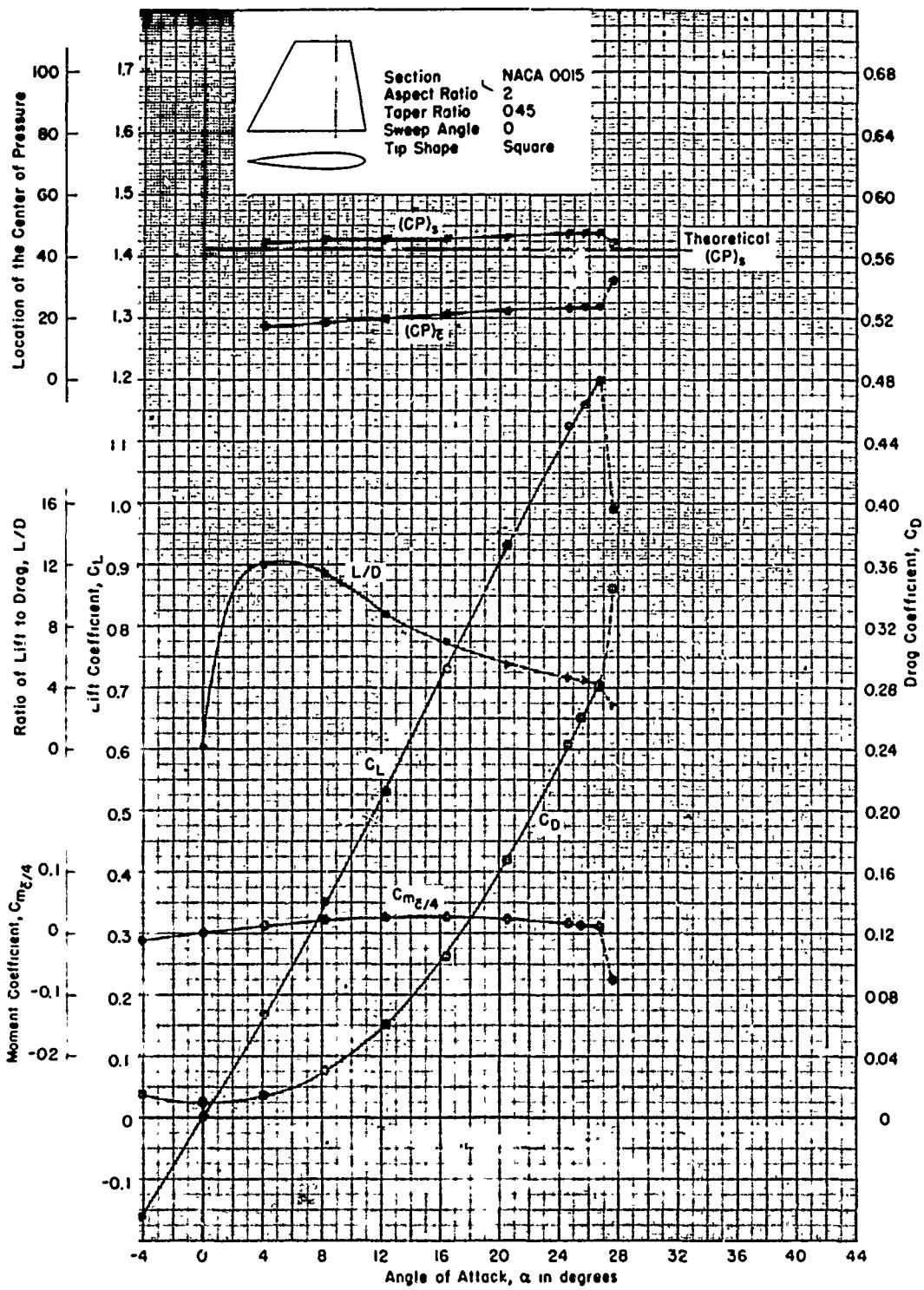

Figure 53 - Reynolds Number of 1.84×10^6

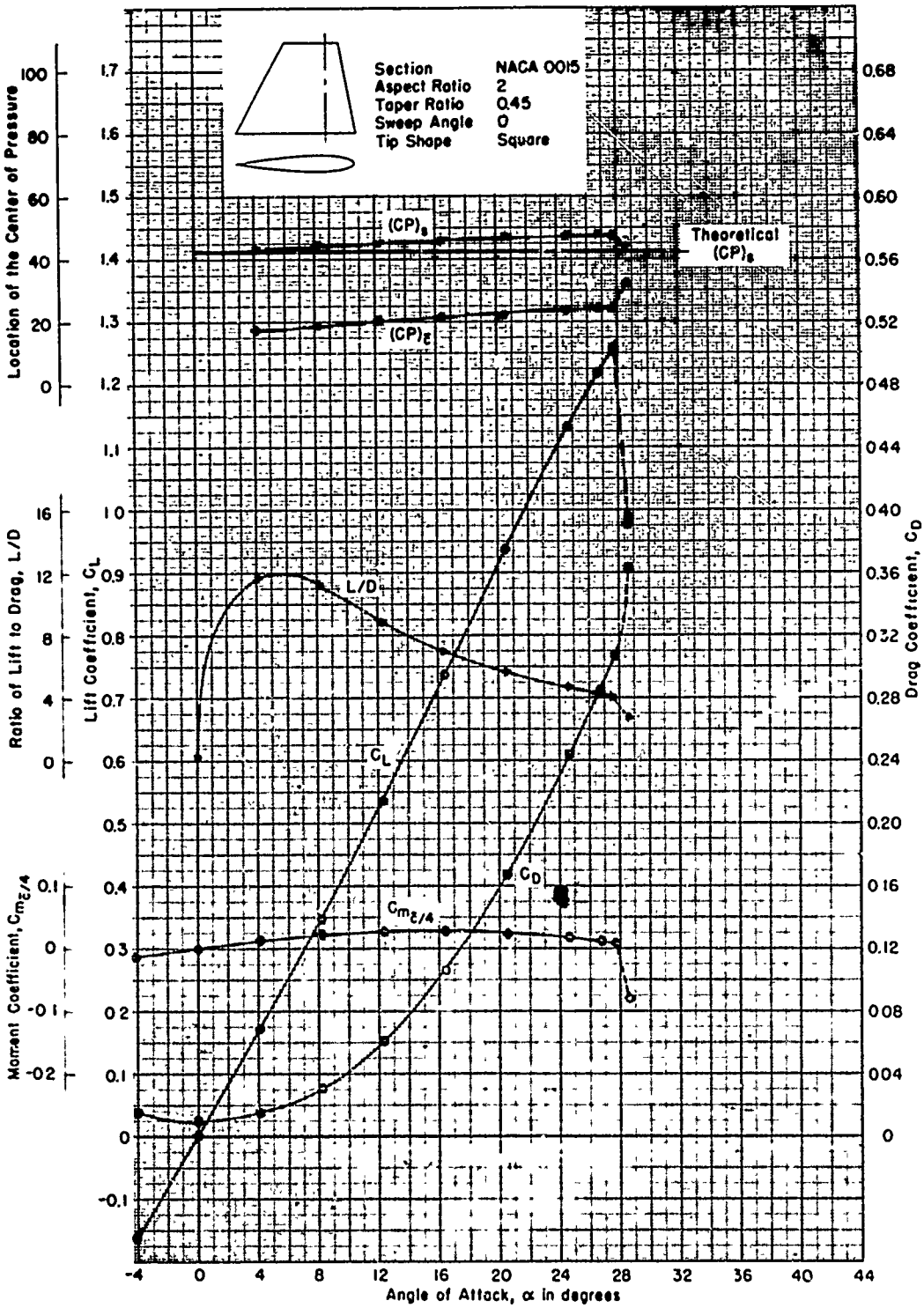

Figure 54 - Reynolds Number of 2.29×10^6

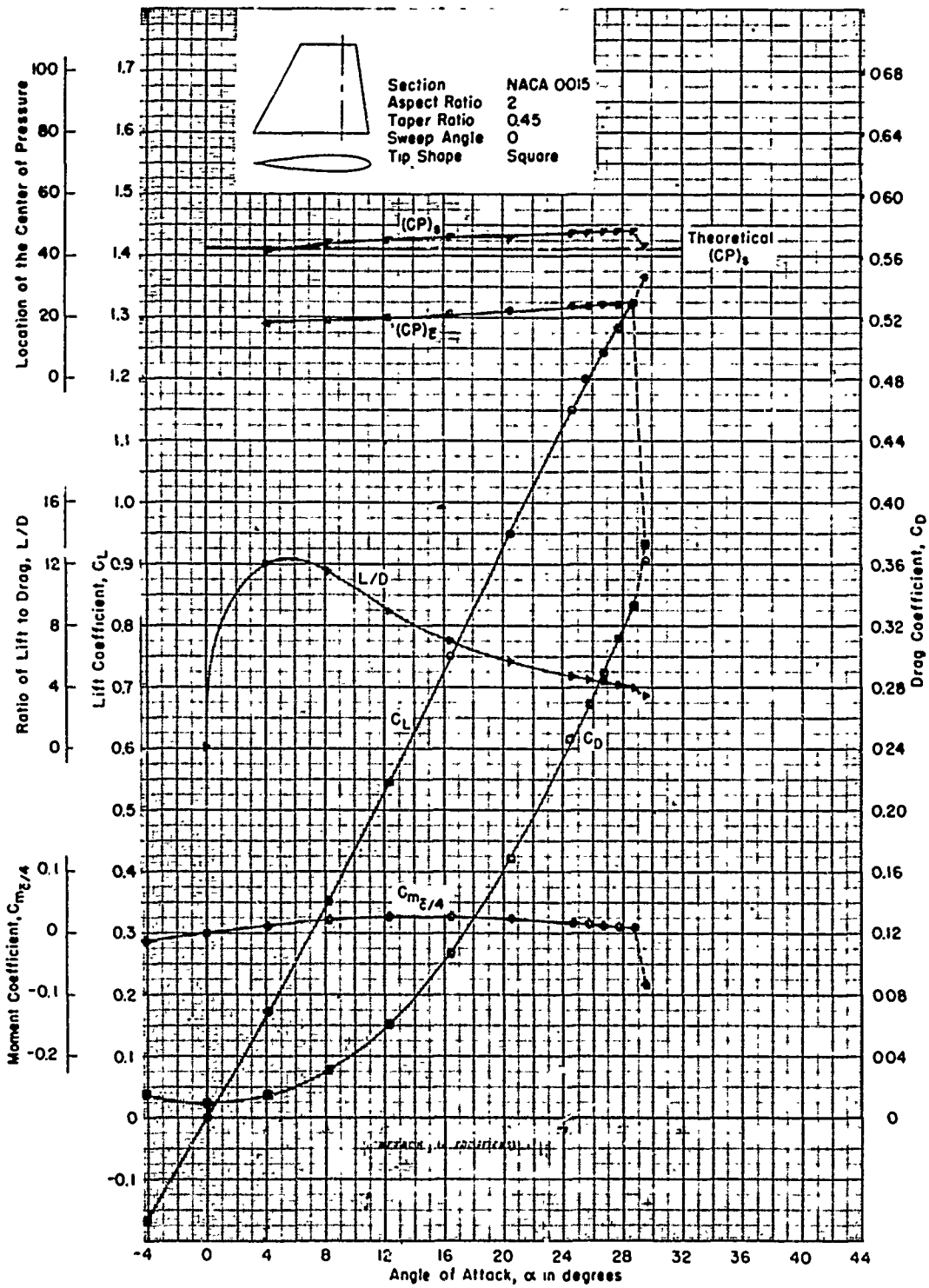

Figure 55 - Reynolds Number of 2.72×10^6

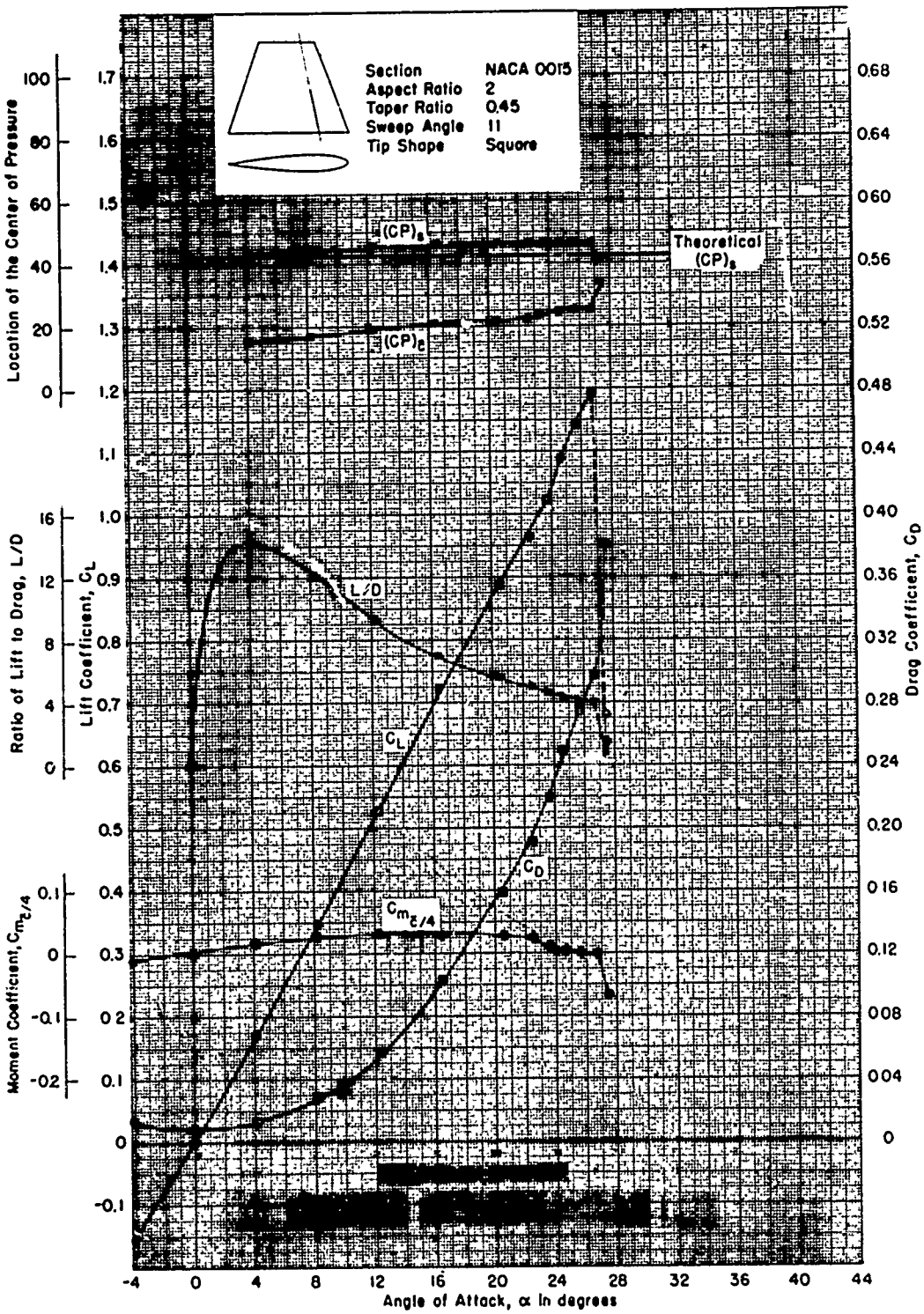

Figure 56 - Reynolds Number of 0.931×10^6

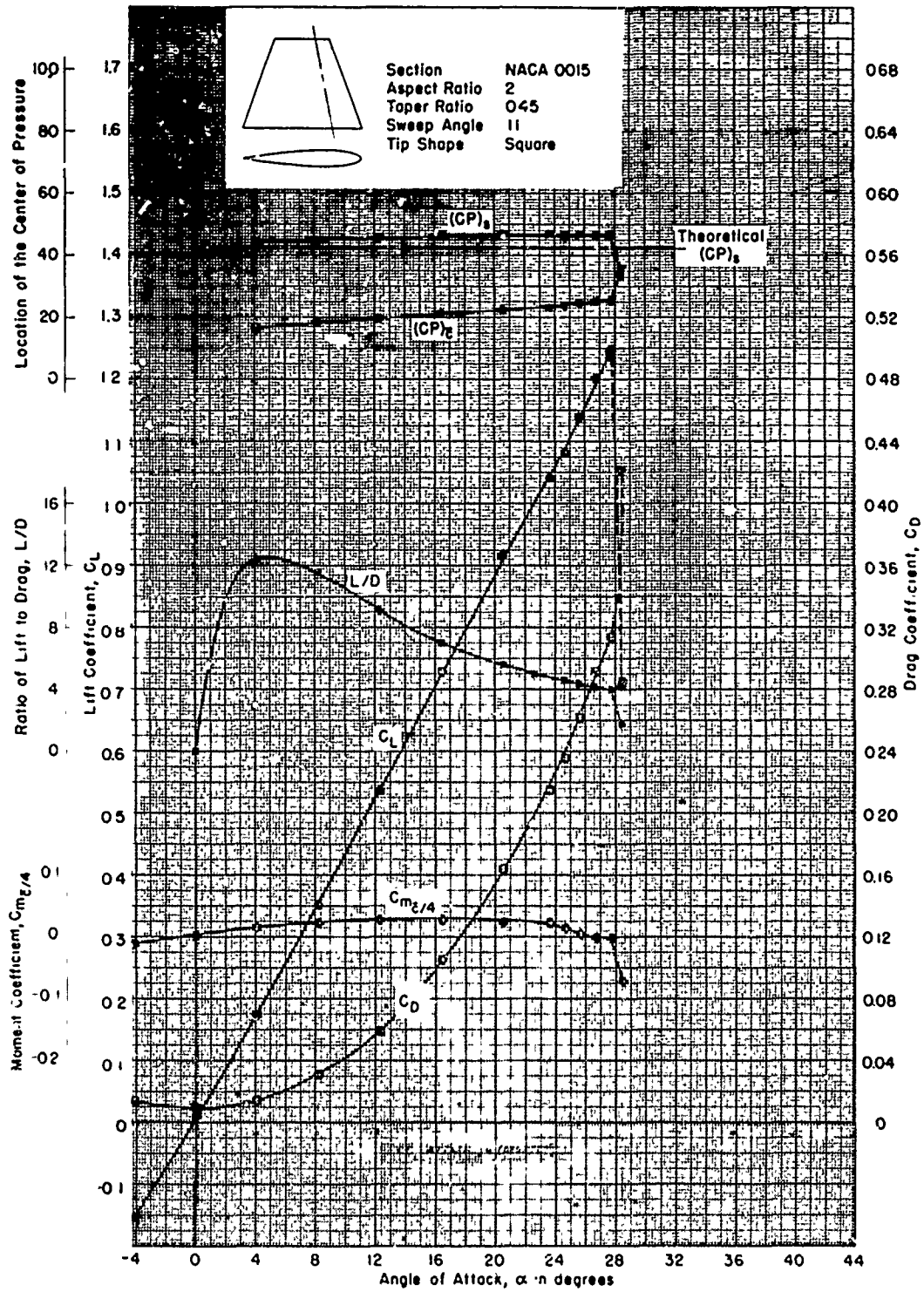

Figure 57 - Reynolds Number of 1.40×10^6

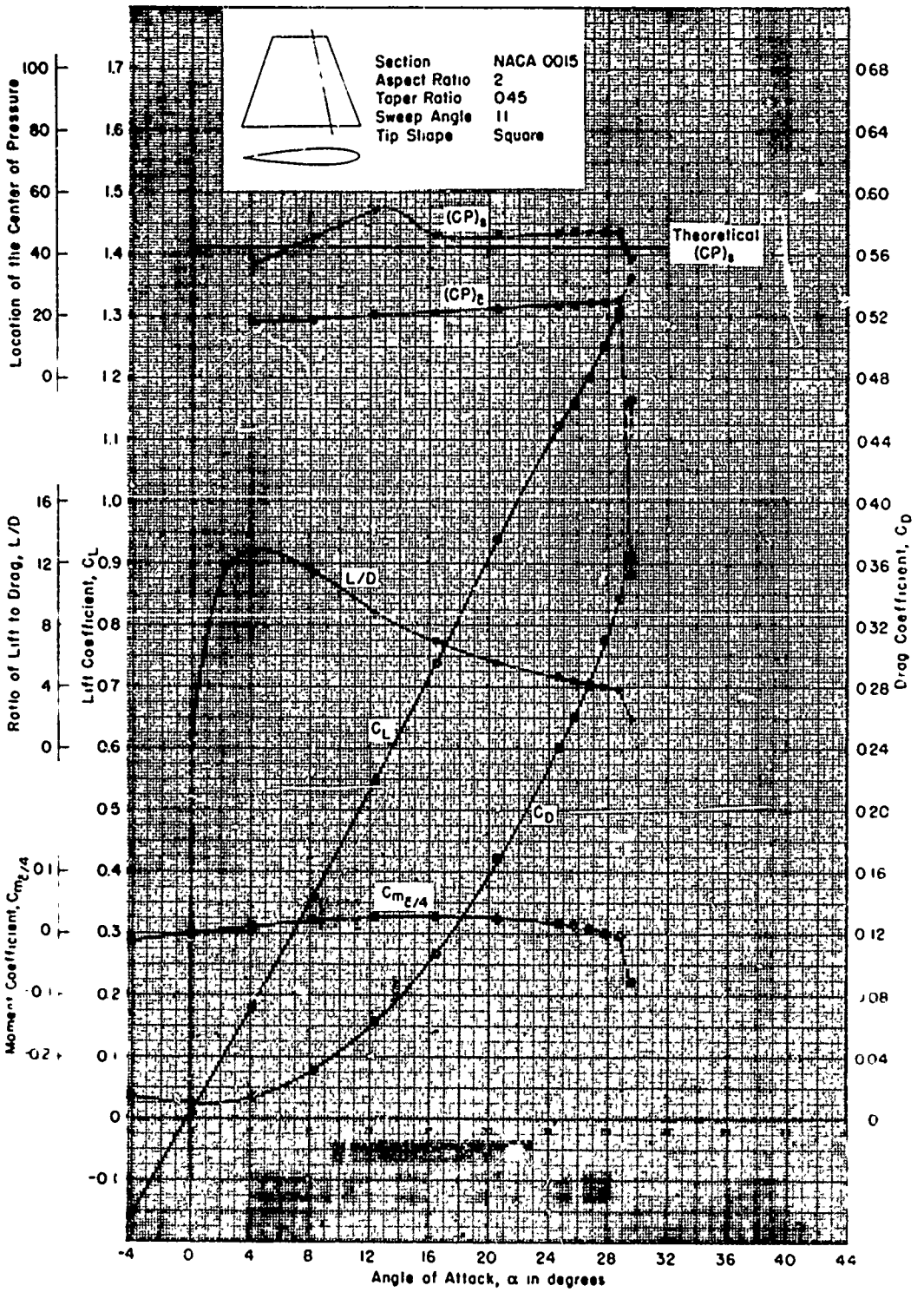

Figure 58 - Reynolds Number of 1.84×10^6

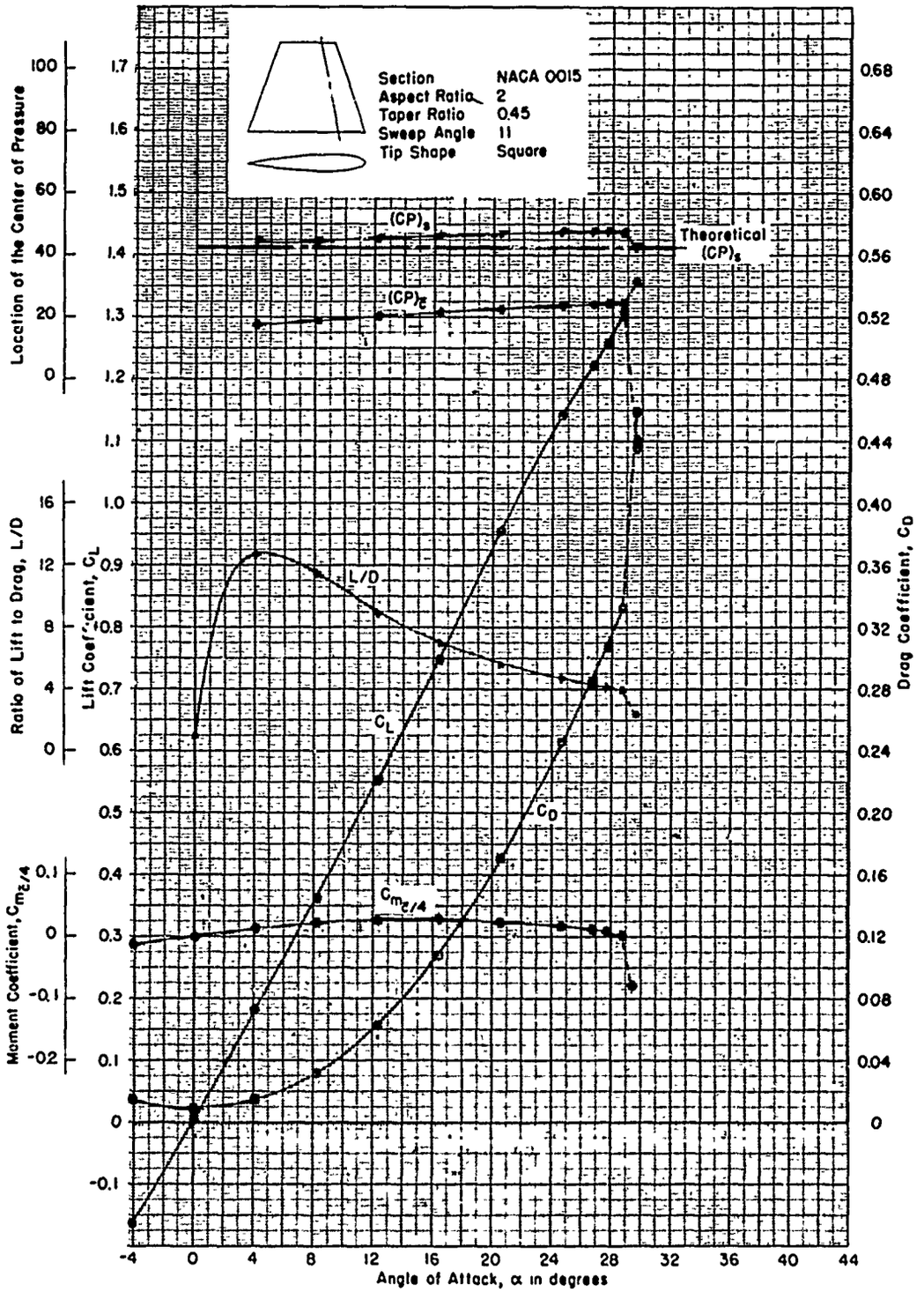

Figure 59 - Reynolds Number of 2.29×10^6

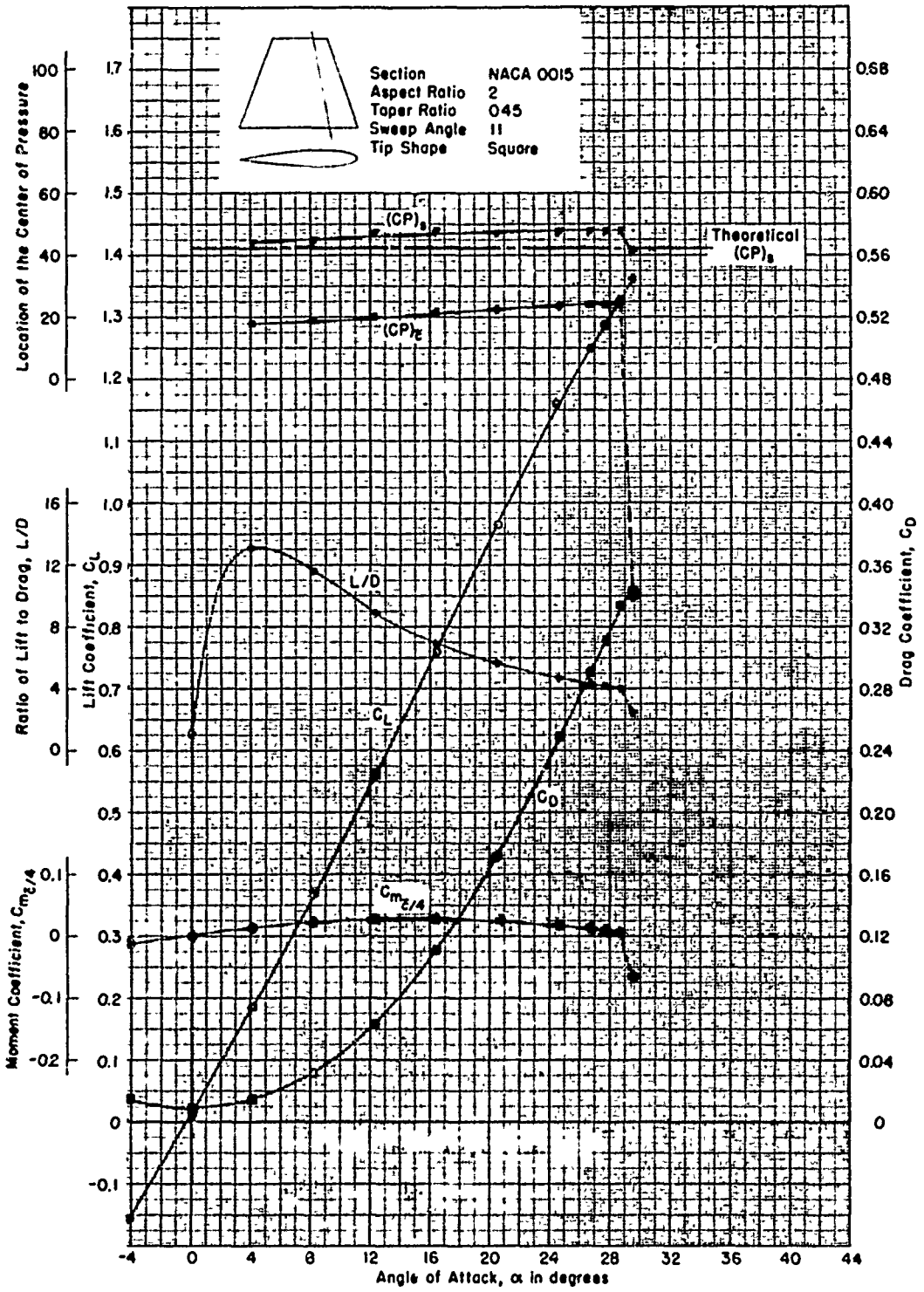

Figure 60 - Reynolds Number of 2.72×10^6

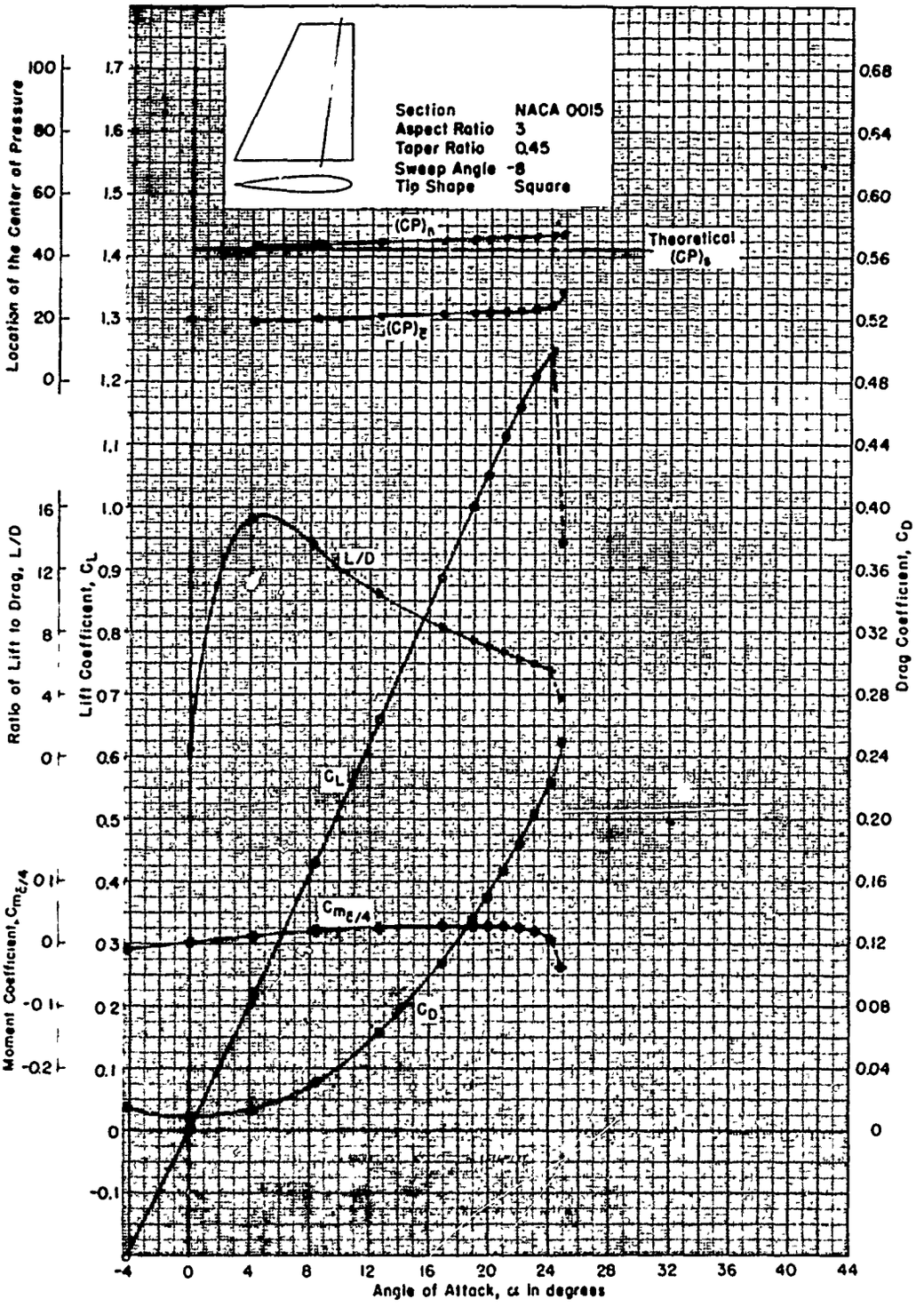

Figure 61 - Reynolds Number of 2.26×10^6

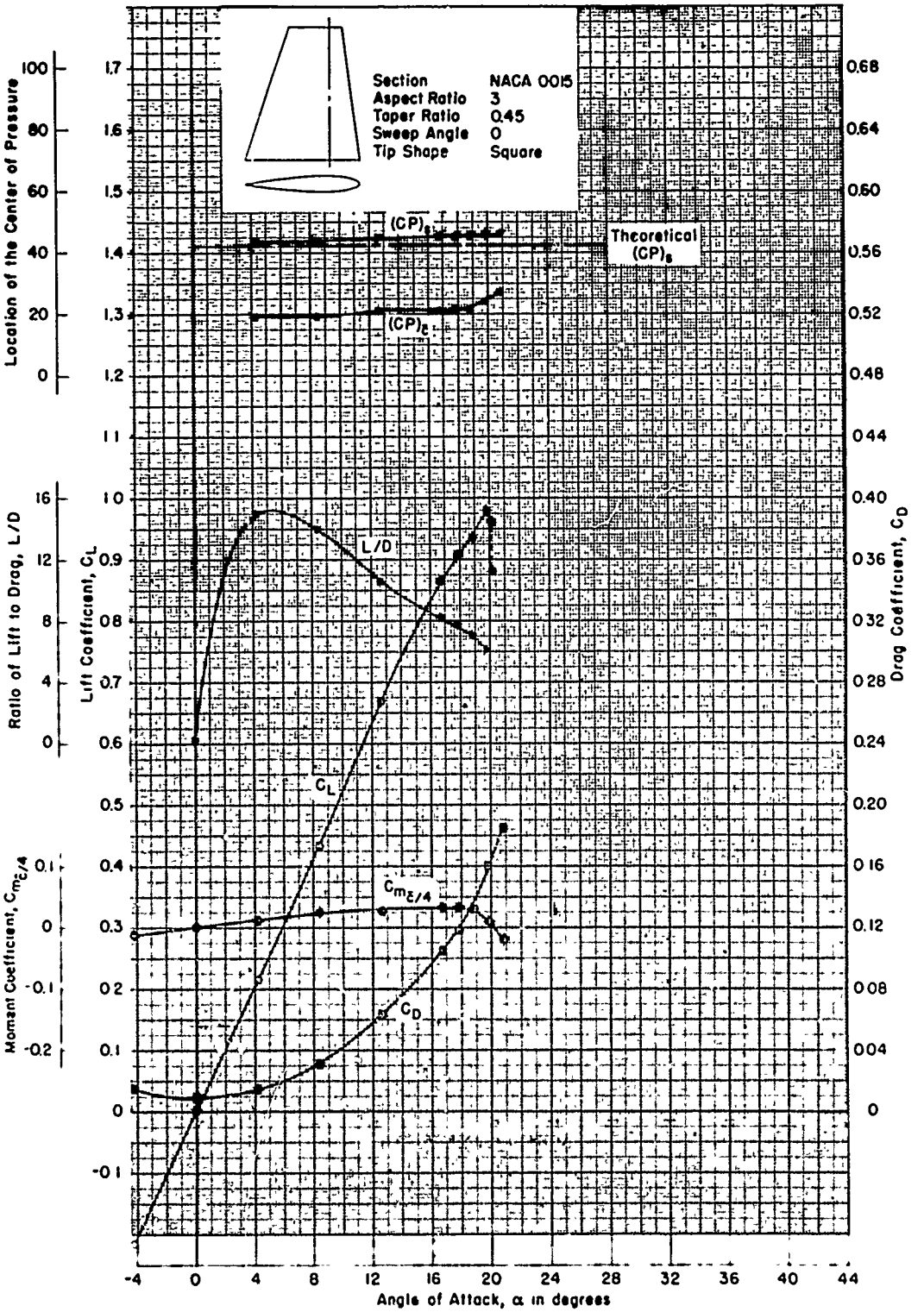

Figure 62 - Reynolds Number of 0.912×10^6

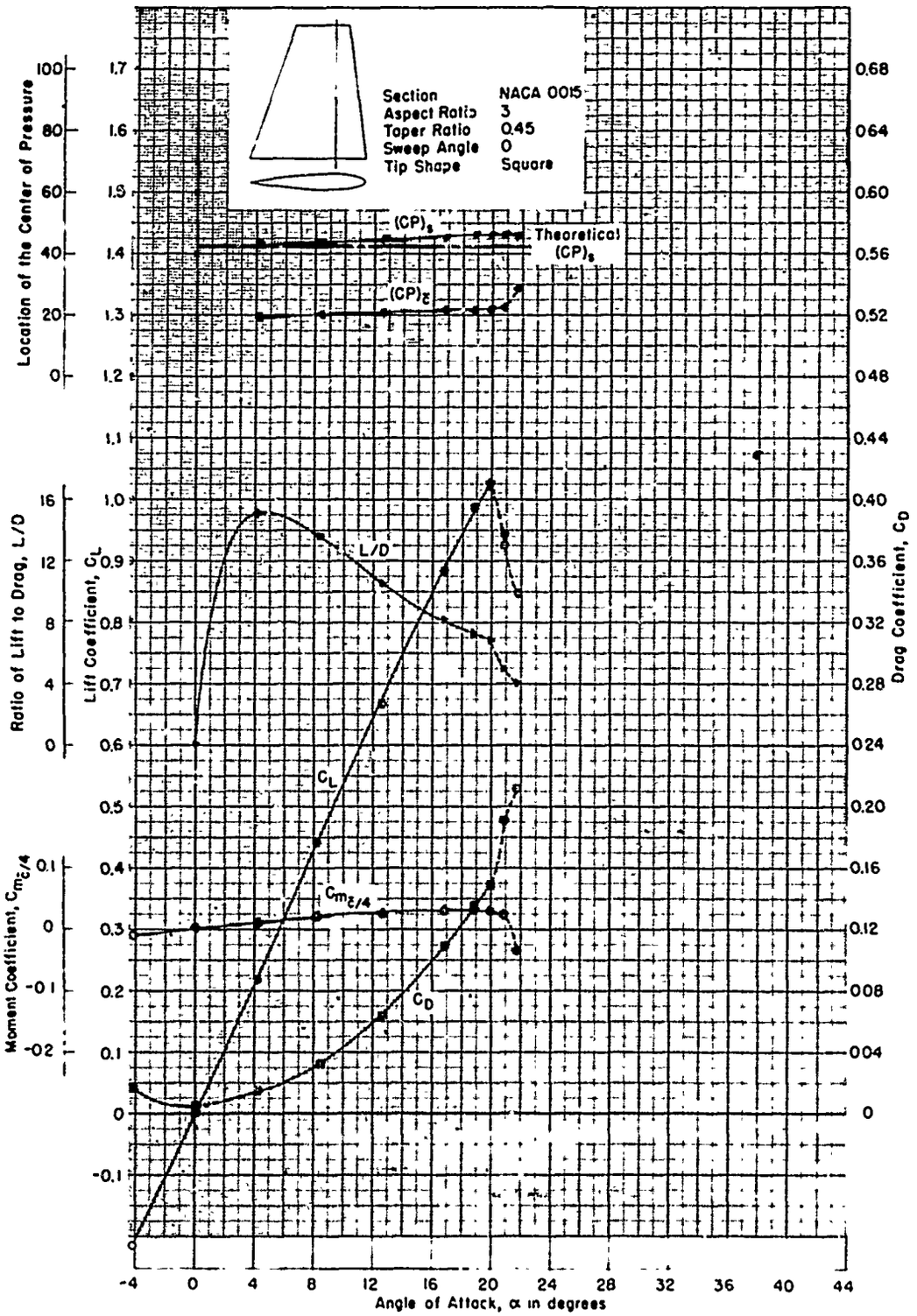

Figure 63 - Reynolds Number of 1.37×10^6

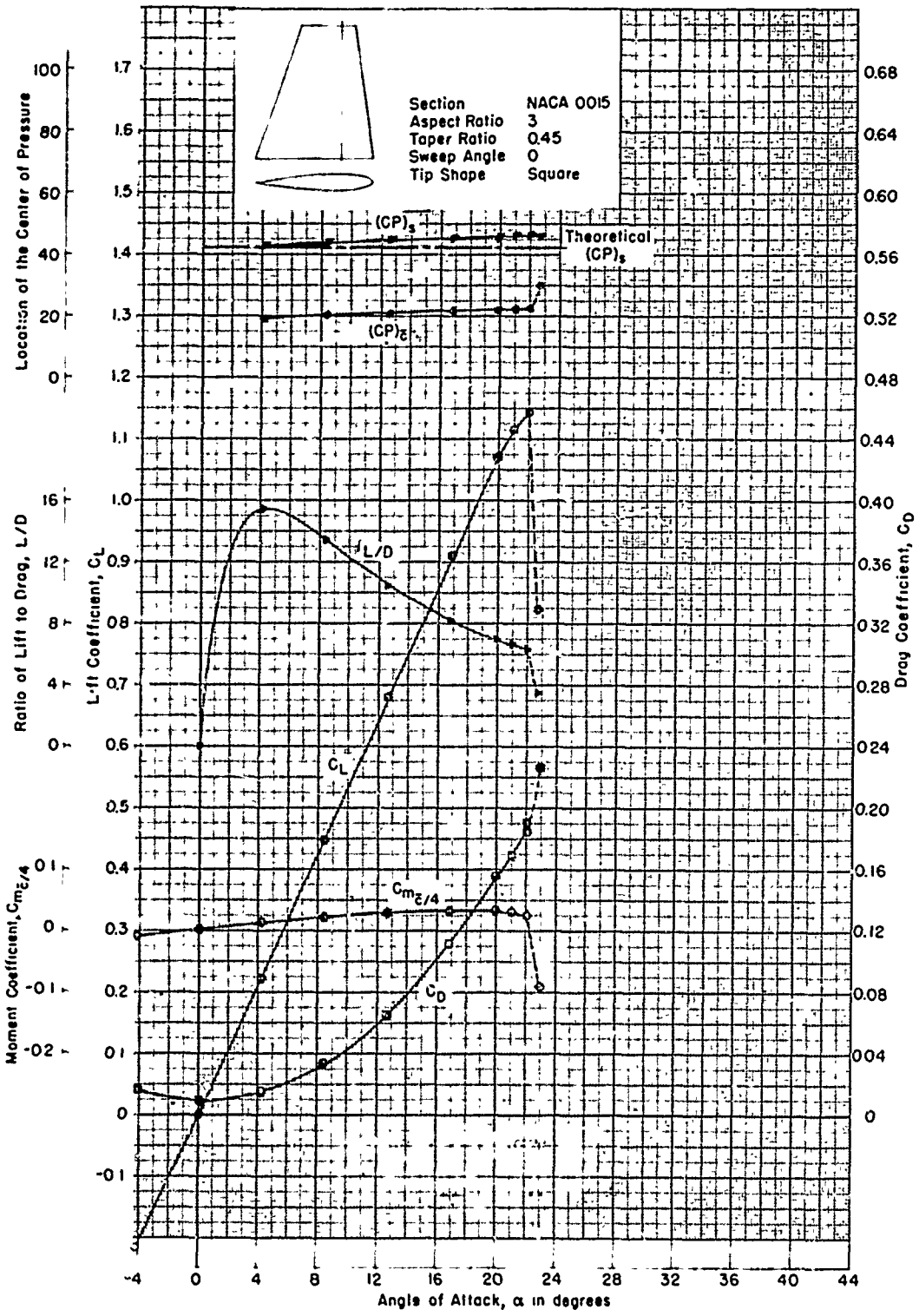

Figure 64 - Reynolds Number of 1.82×10^6

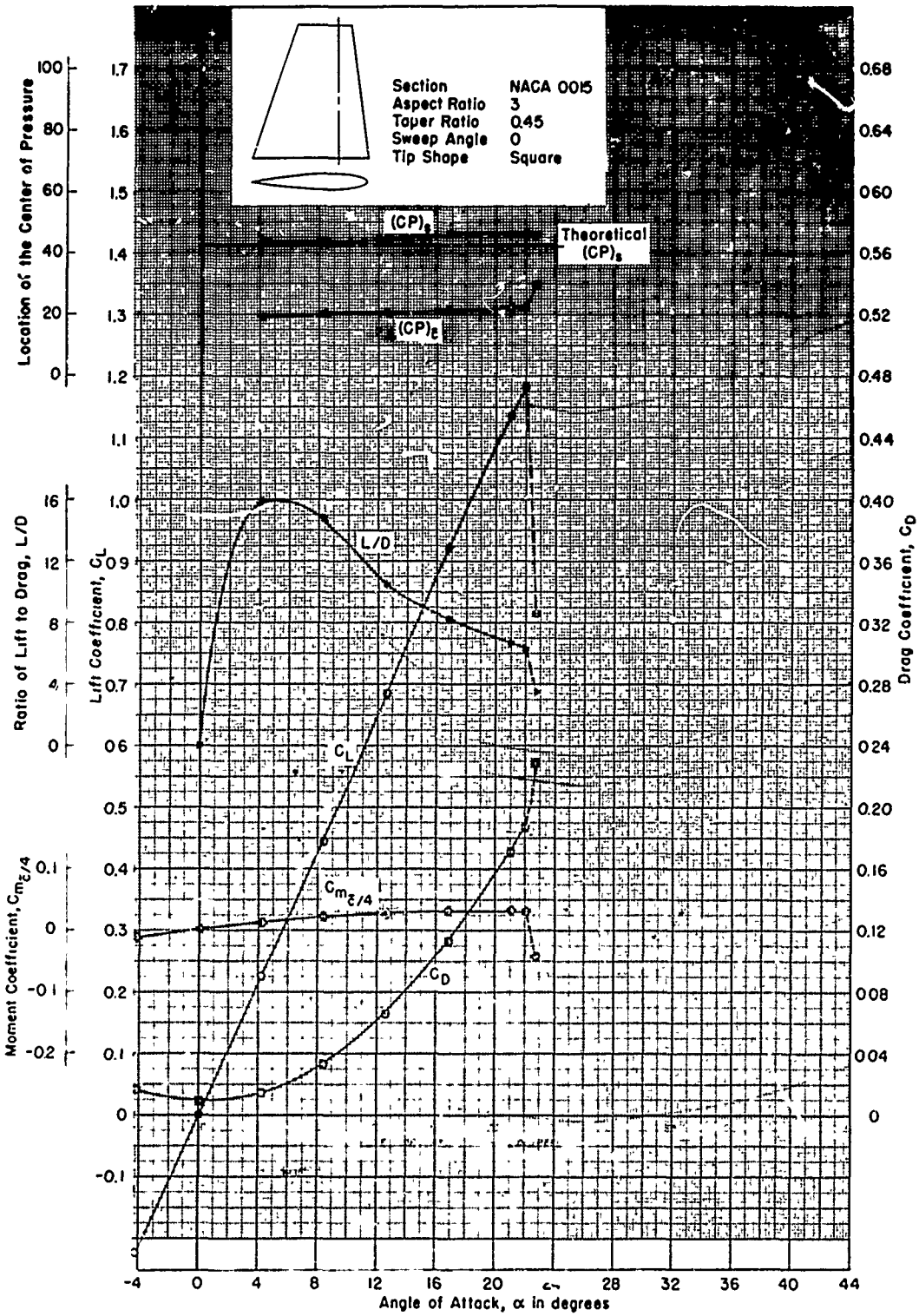

Figure 65 - Reynolds Number of 2.25×10^6

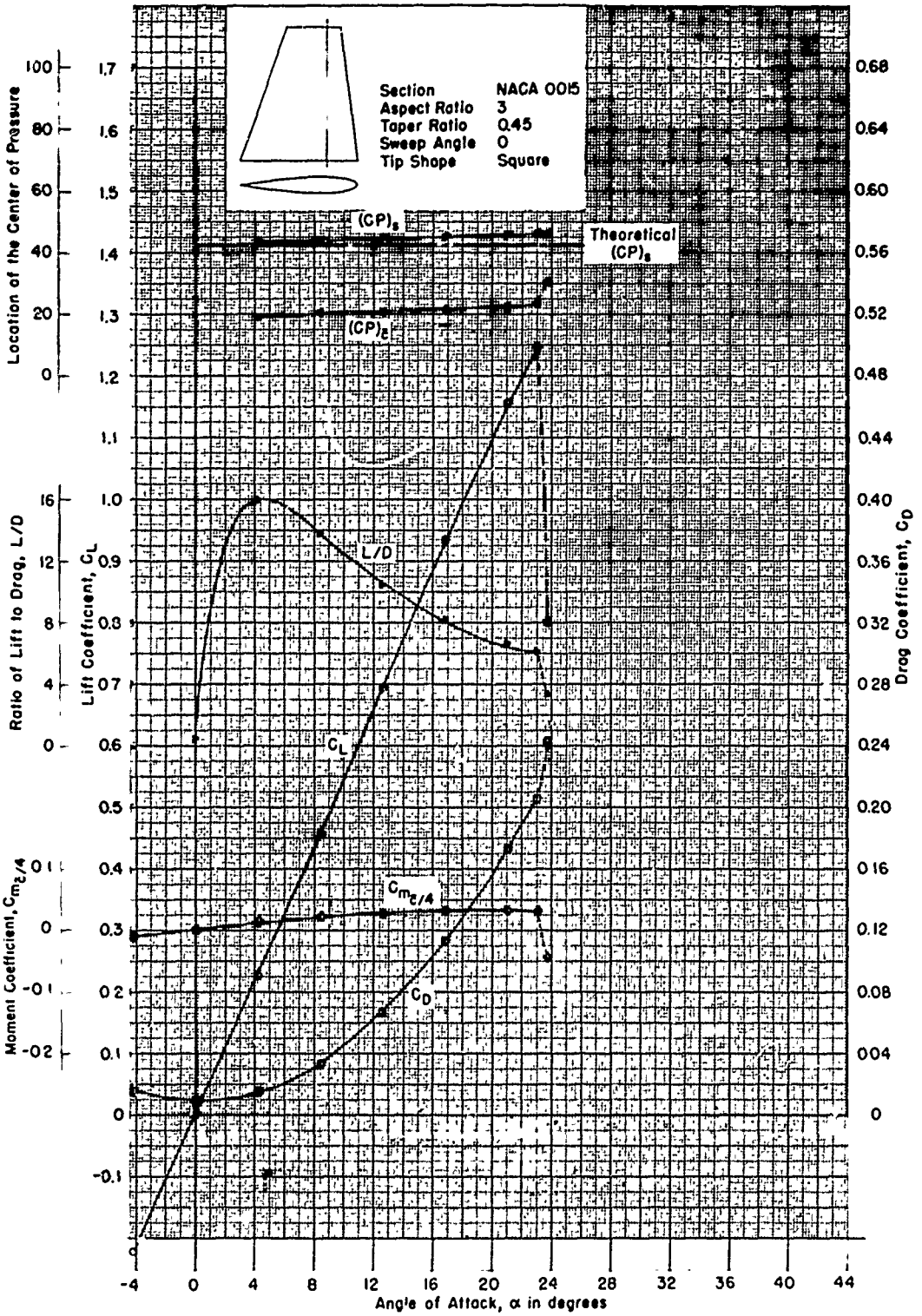

Figure 66 - Reynolds Number of 2.70×10^6

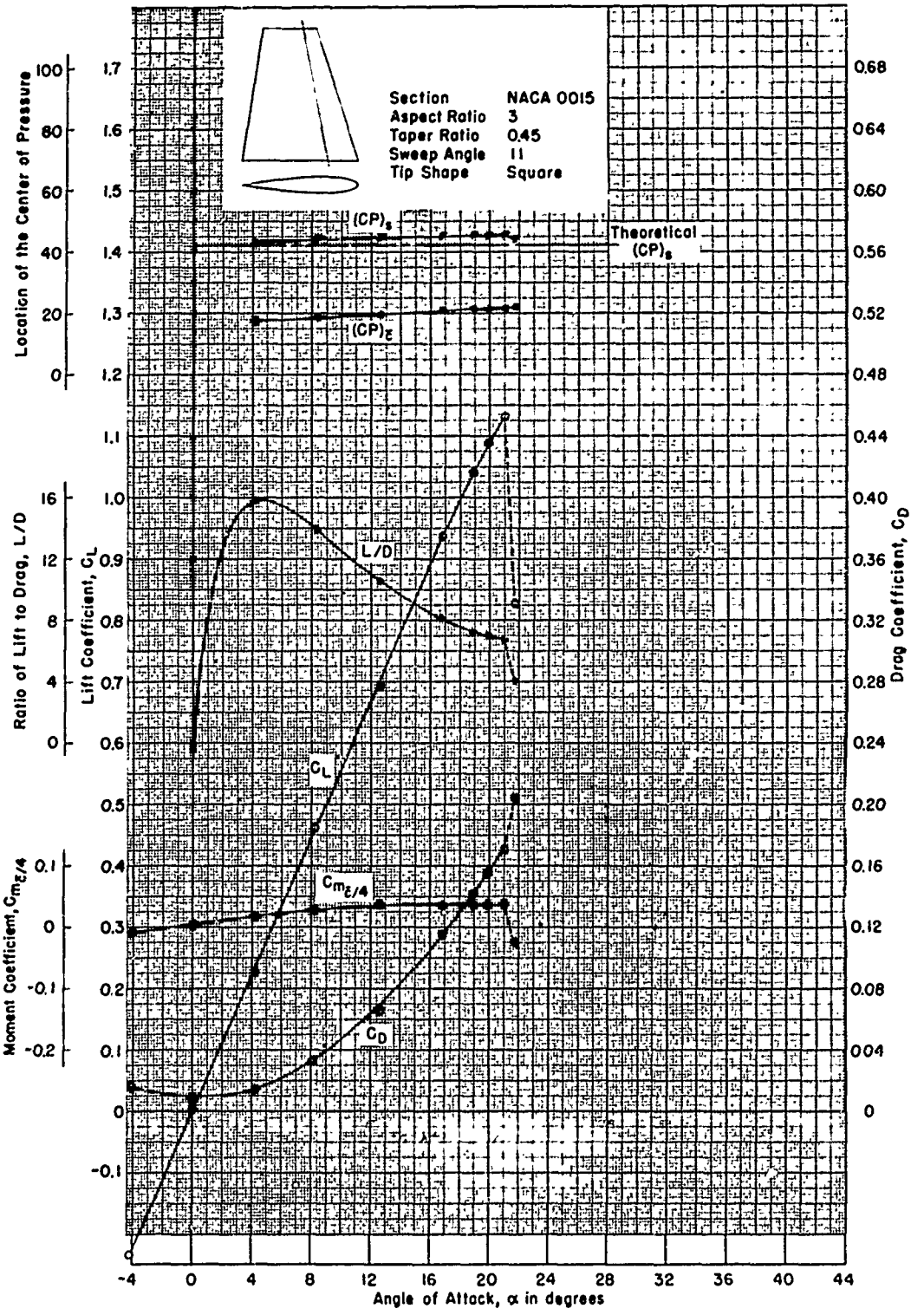

Figure 67 - Reynolds Number of 2.26×10^6

APPENDIX B

FREE-STREAM CHARACTERISTICS OF FAIRED-TIP CONTROL SURFACES WITH AN NACA 0015 SECTION SHAPE IN THE AHEAD CONDITION

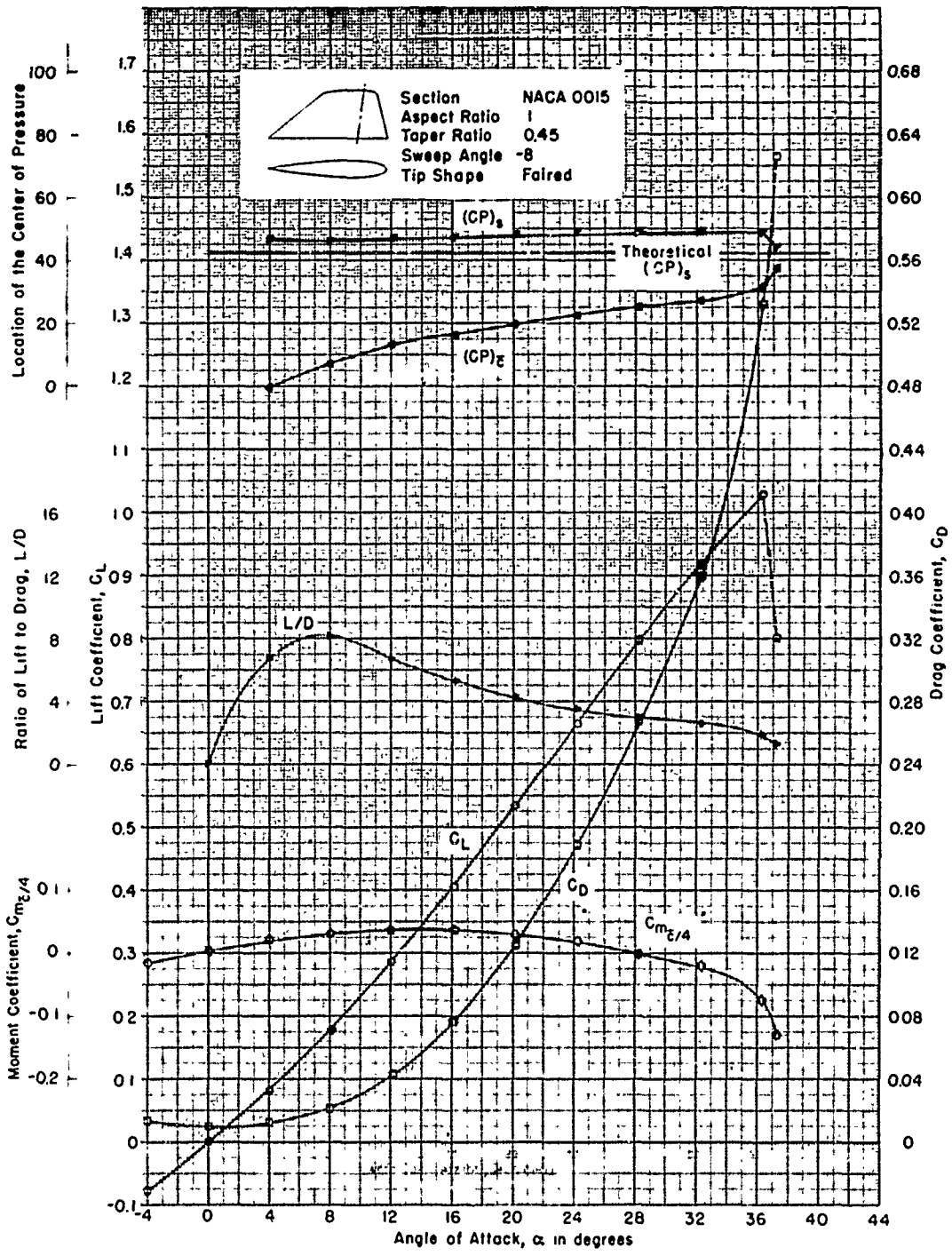

Figure 68 - Reynolds Number of 2.28×10^6

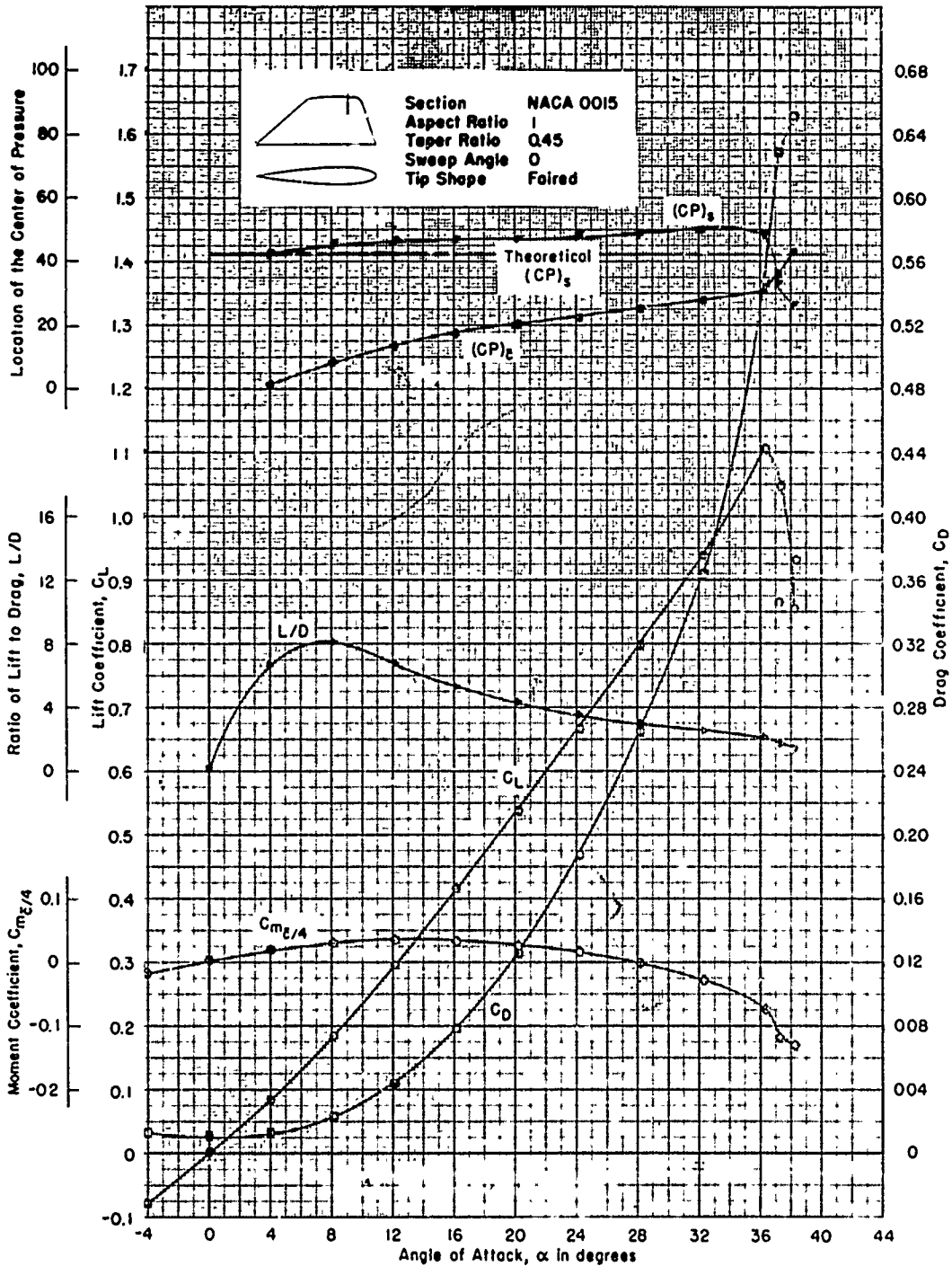

Figure 69 - Reynolds Number of 2.29×10^6

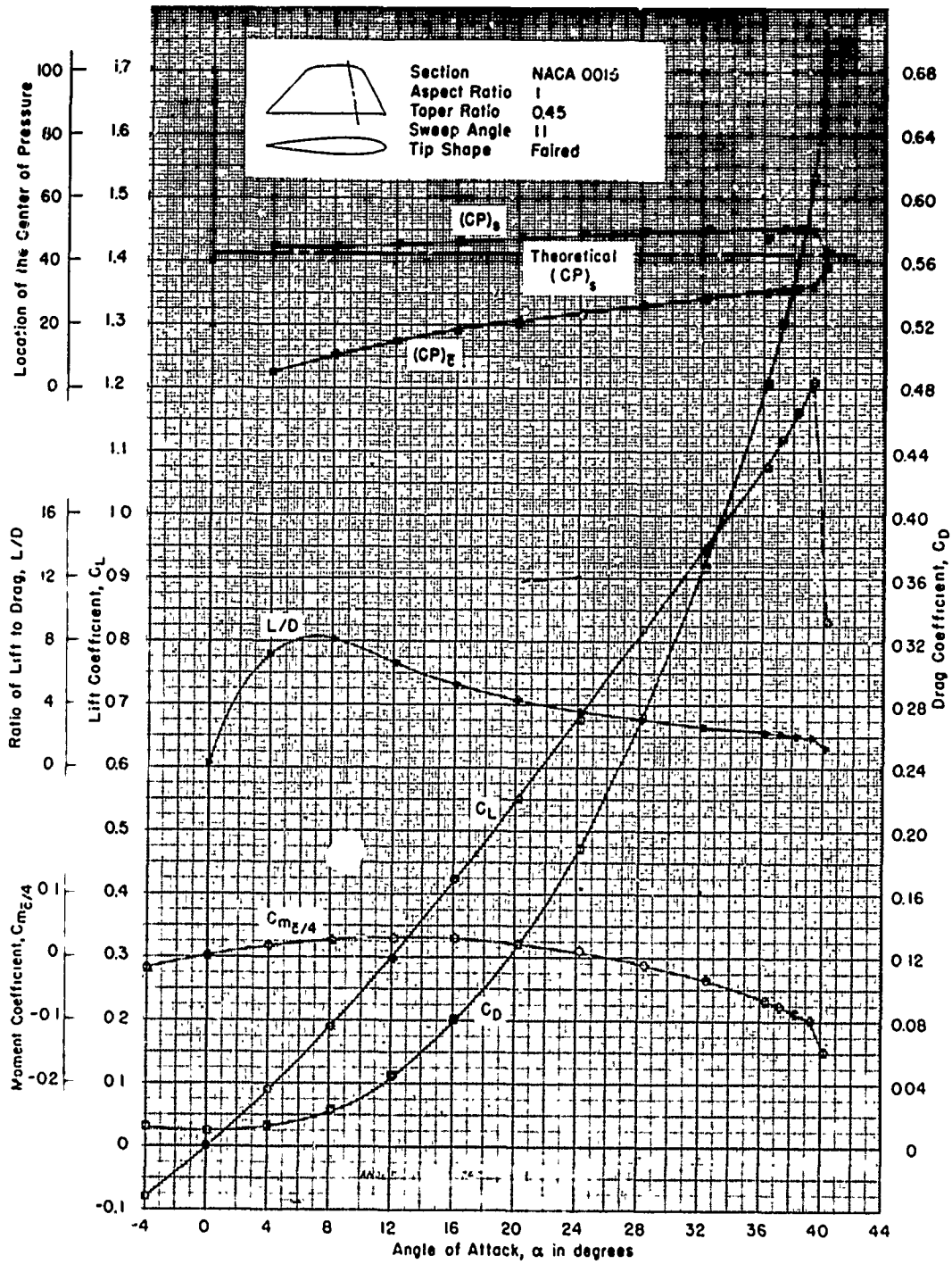

Figure 70 - Reynolds Number of 2.28×10^6

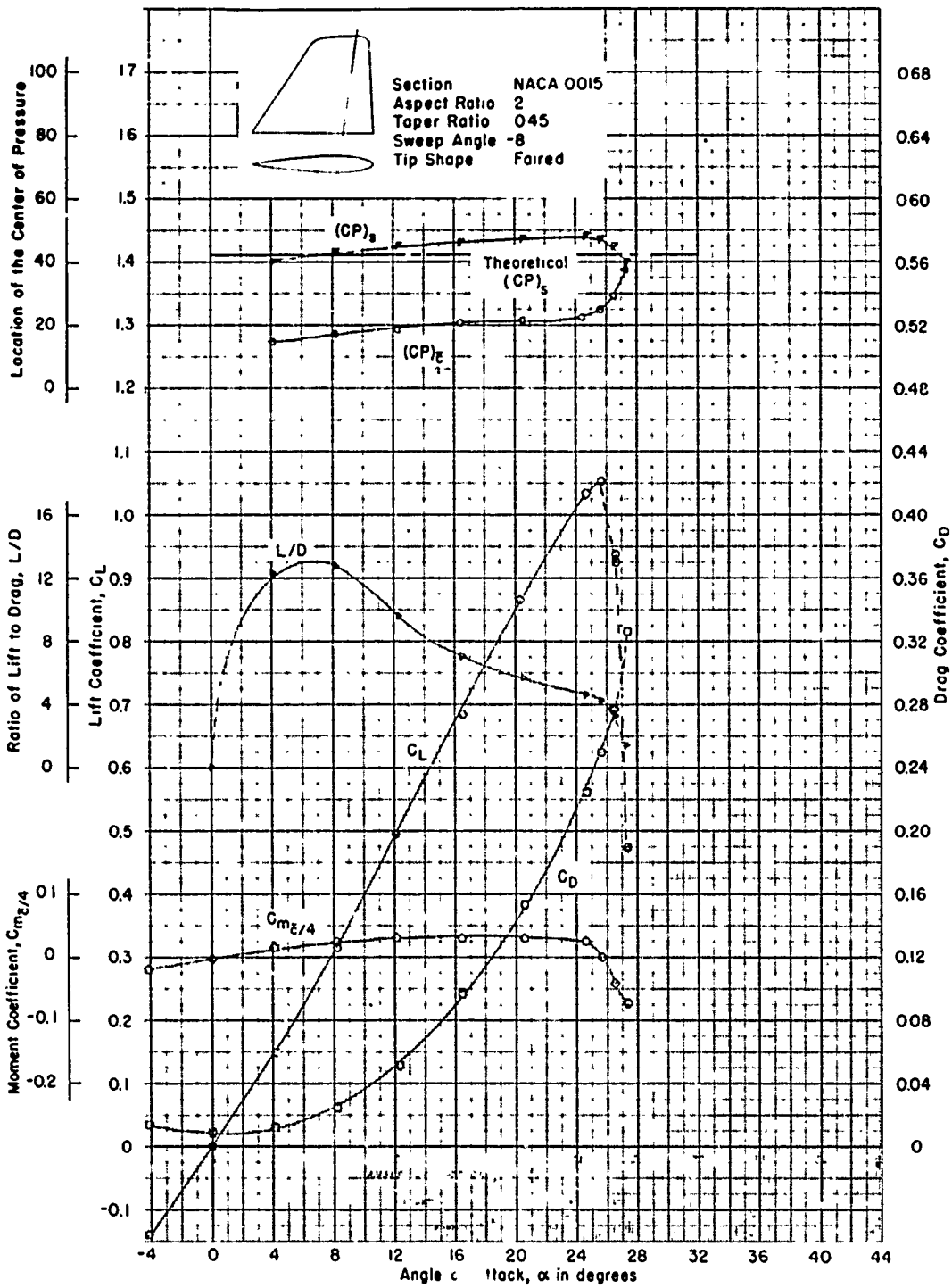

Figure 71 - Reynolds Number of 0.931×10^6

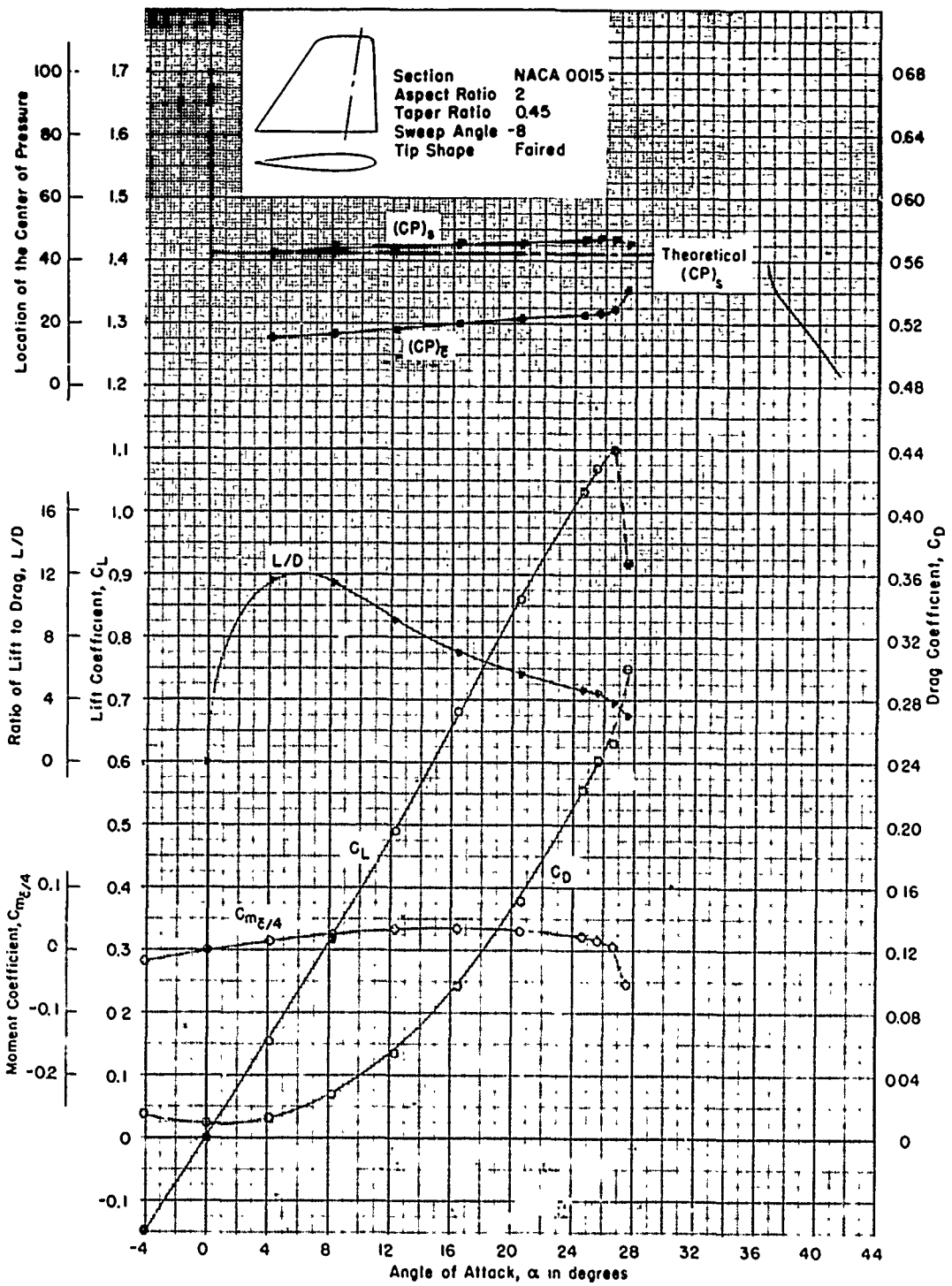

Figure 72 - Reynolds Number of 1.40×10^6

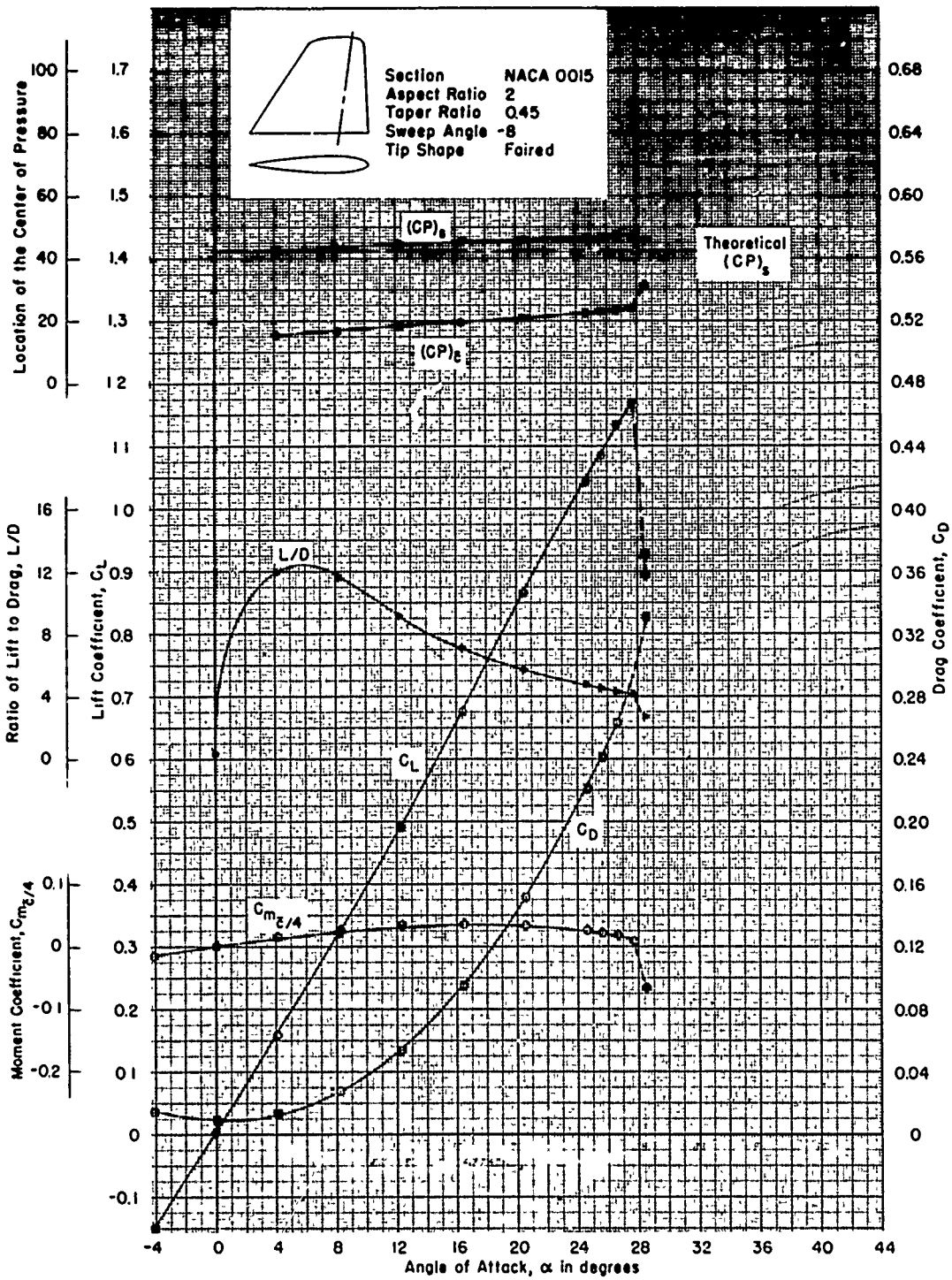

Figure 73 - Reynolds Number of 1.84×10^6

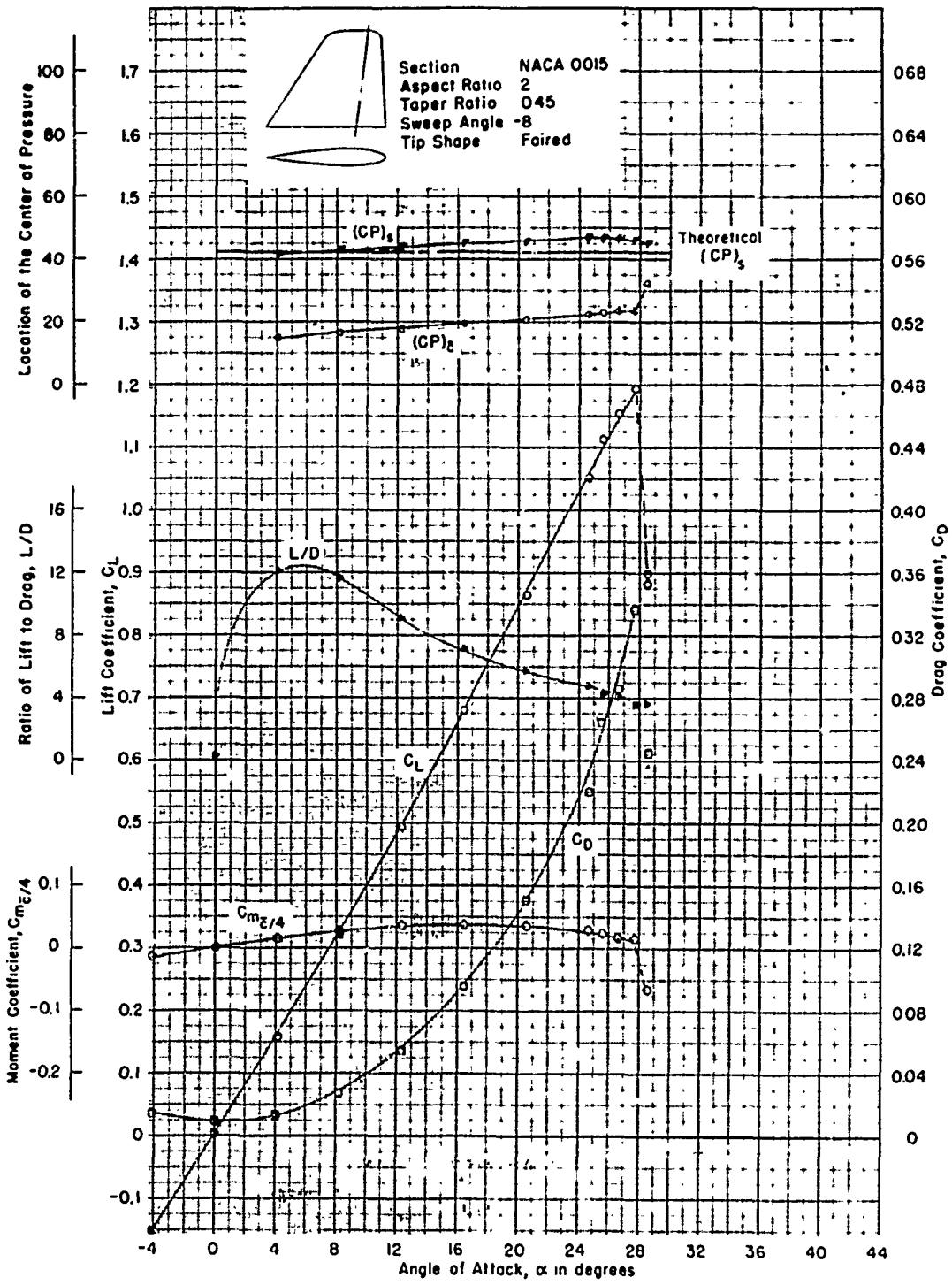

Figure 74 - Reynolds Number of 2.29×10^6

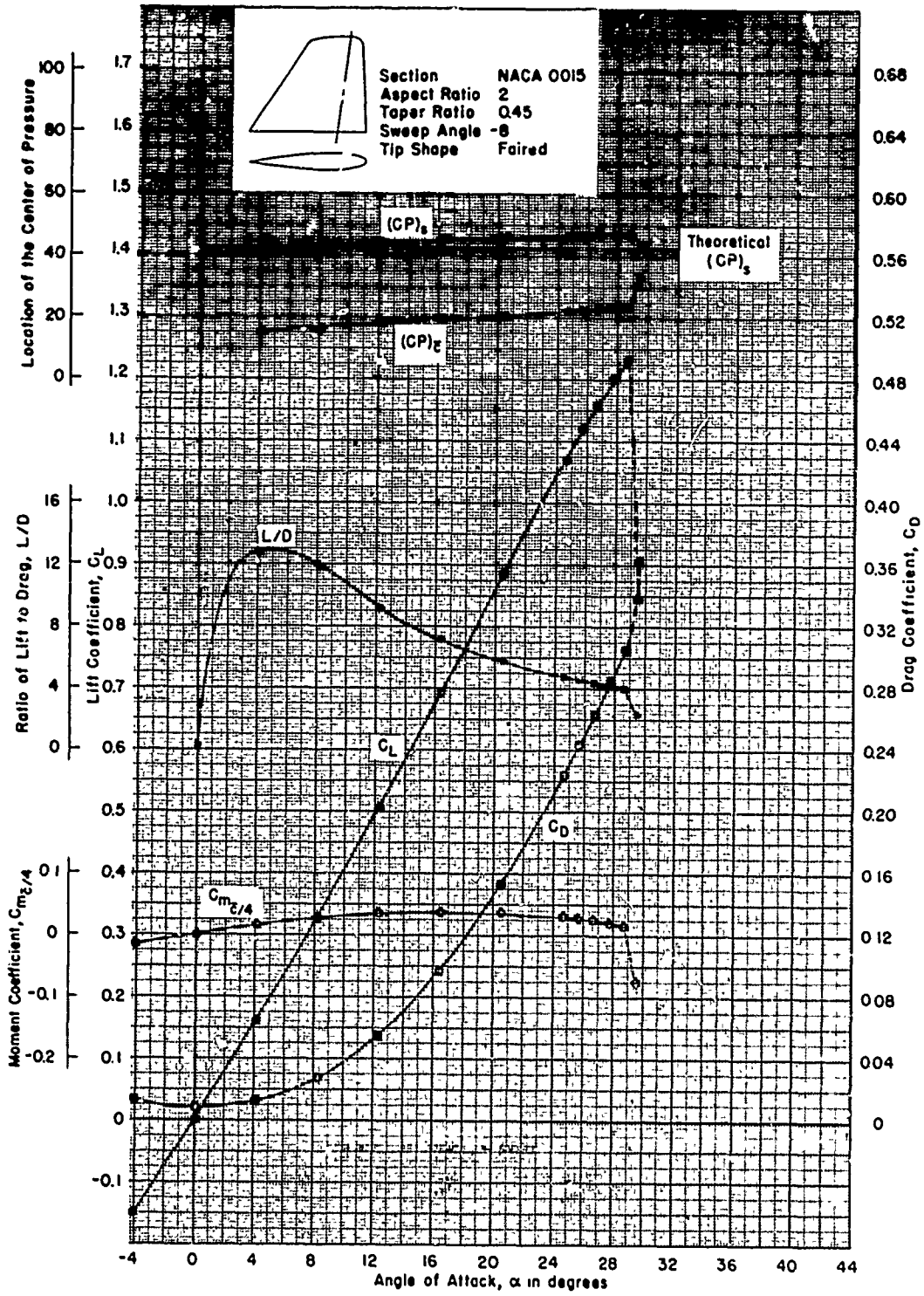

Figure 75 - Reynolds Number of 2.72×10^6

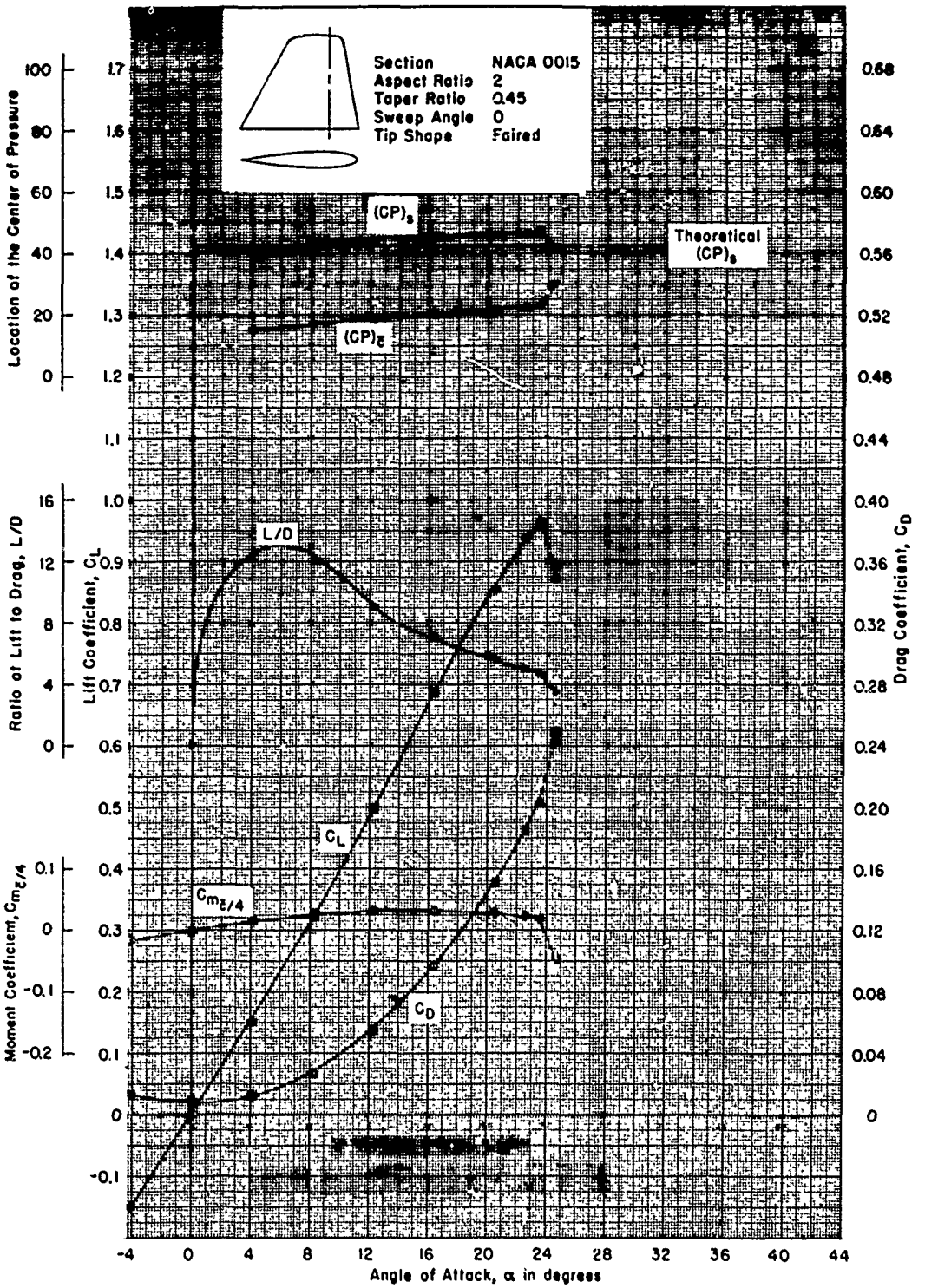

Figure 76 - Reynolds Number of 0.931×10^6

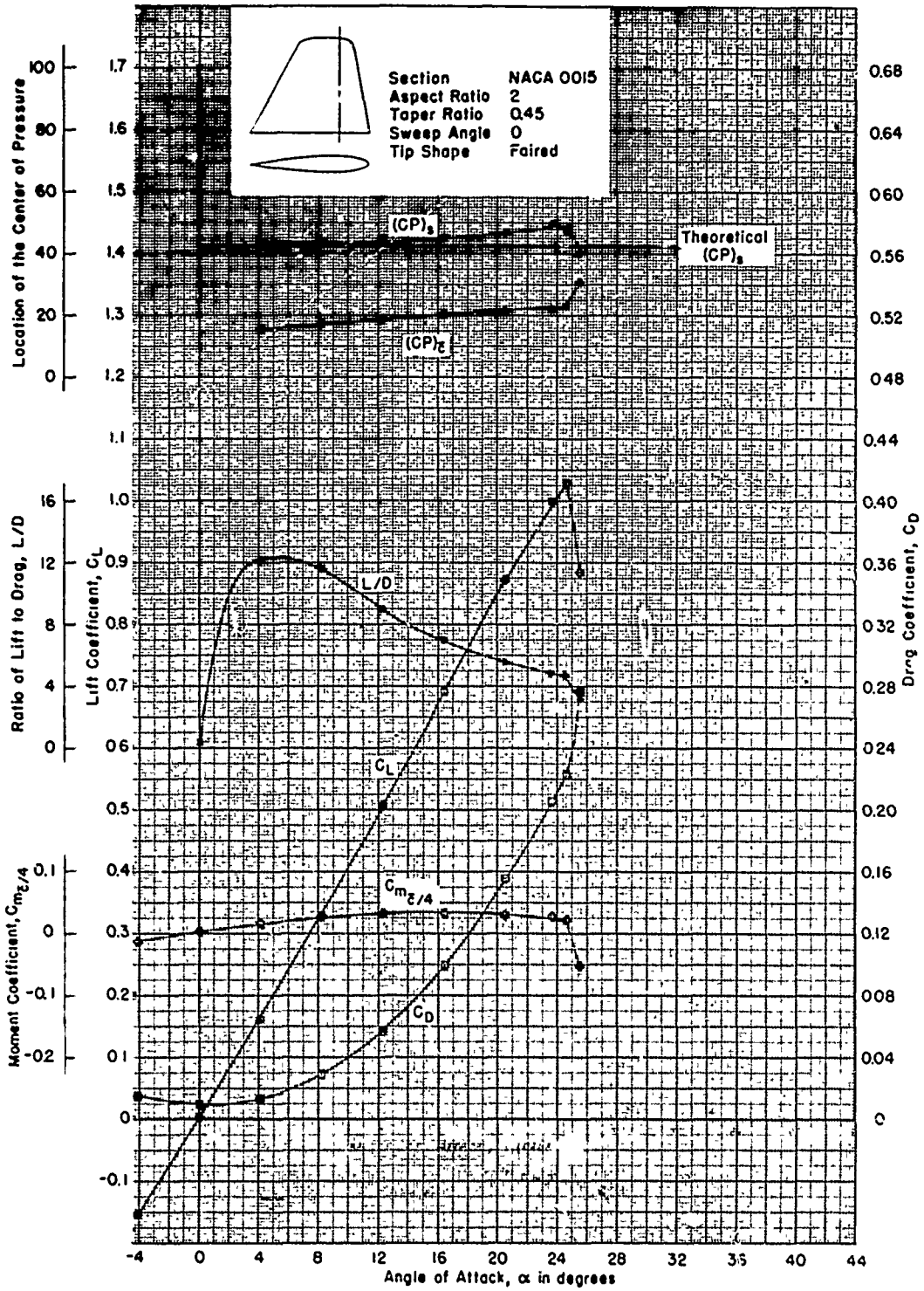

Figure 77 - Reynolds Number of 1.40×10^6

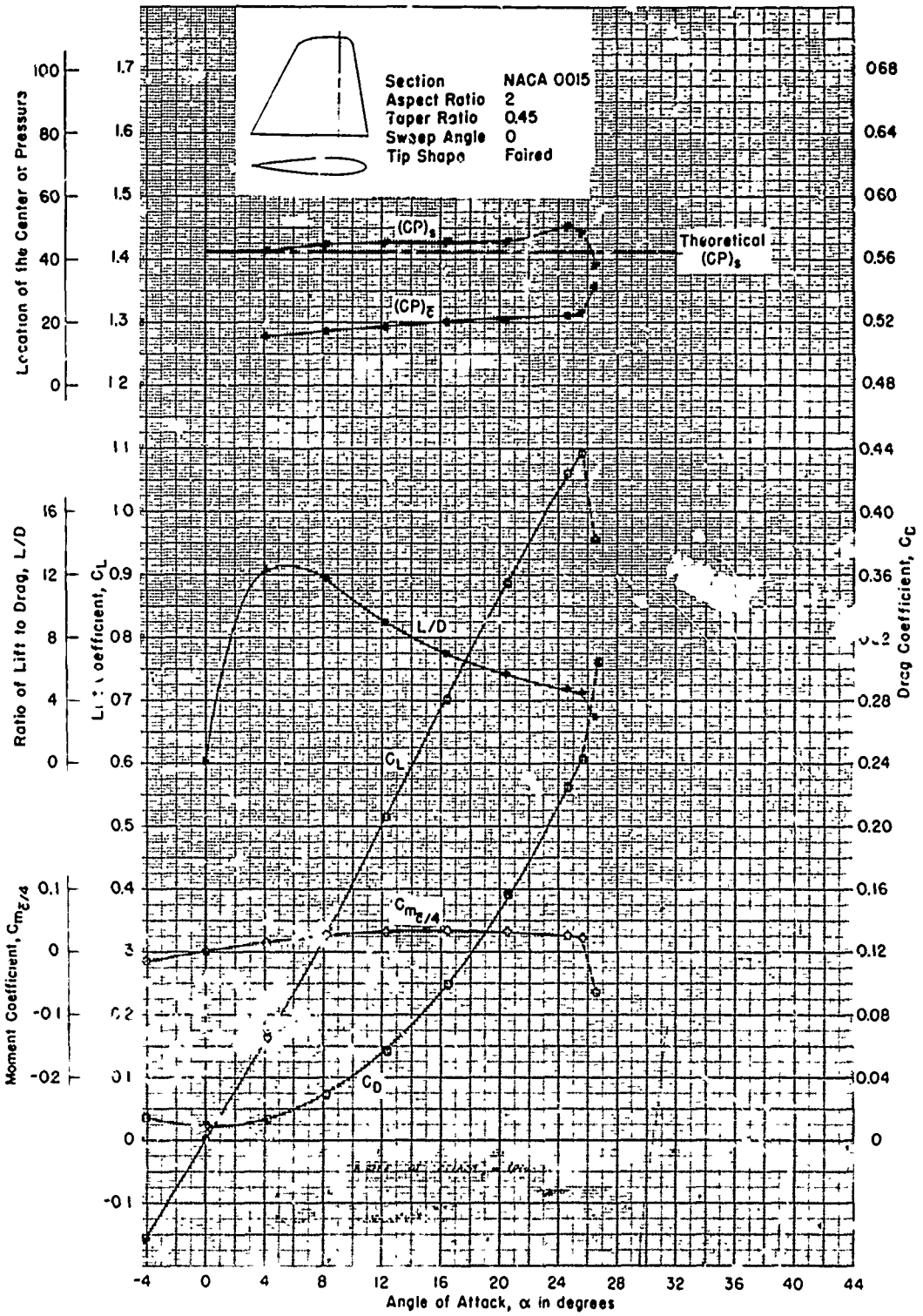

Figure 78 - Reynolds Number of 1.80×10^6

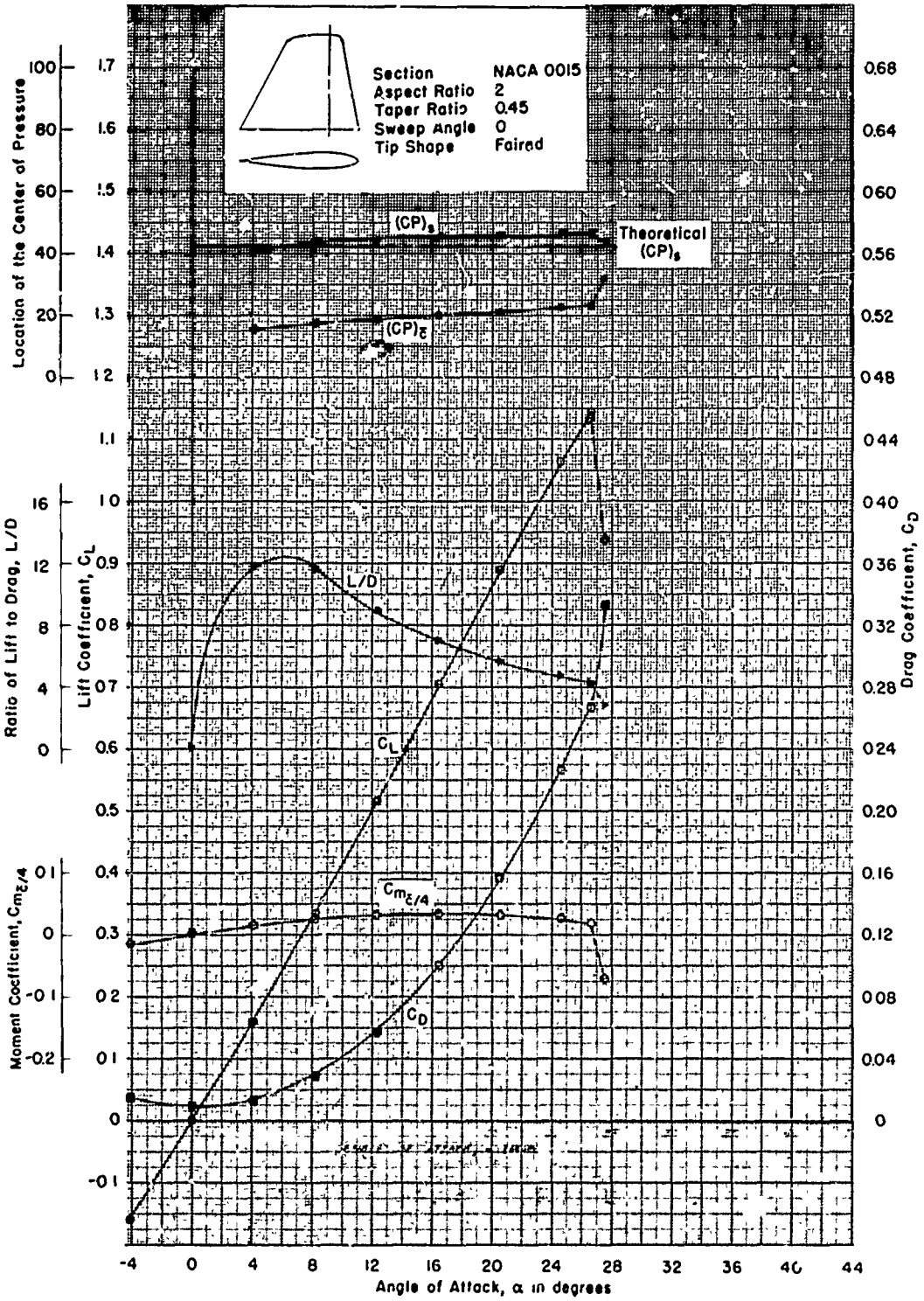

Figure 79 - Reynolds Number of 2.29×10^6

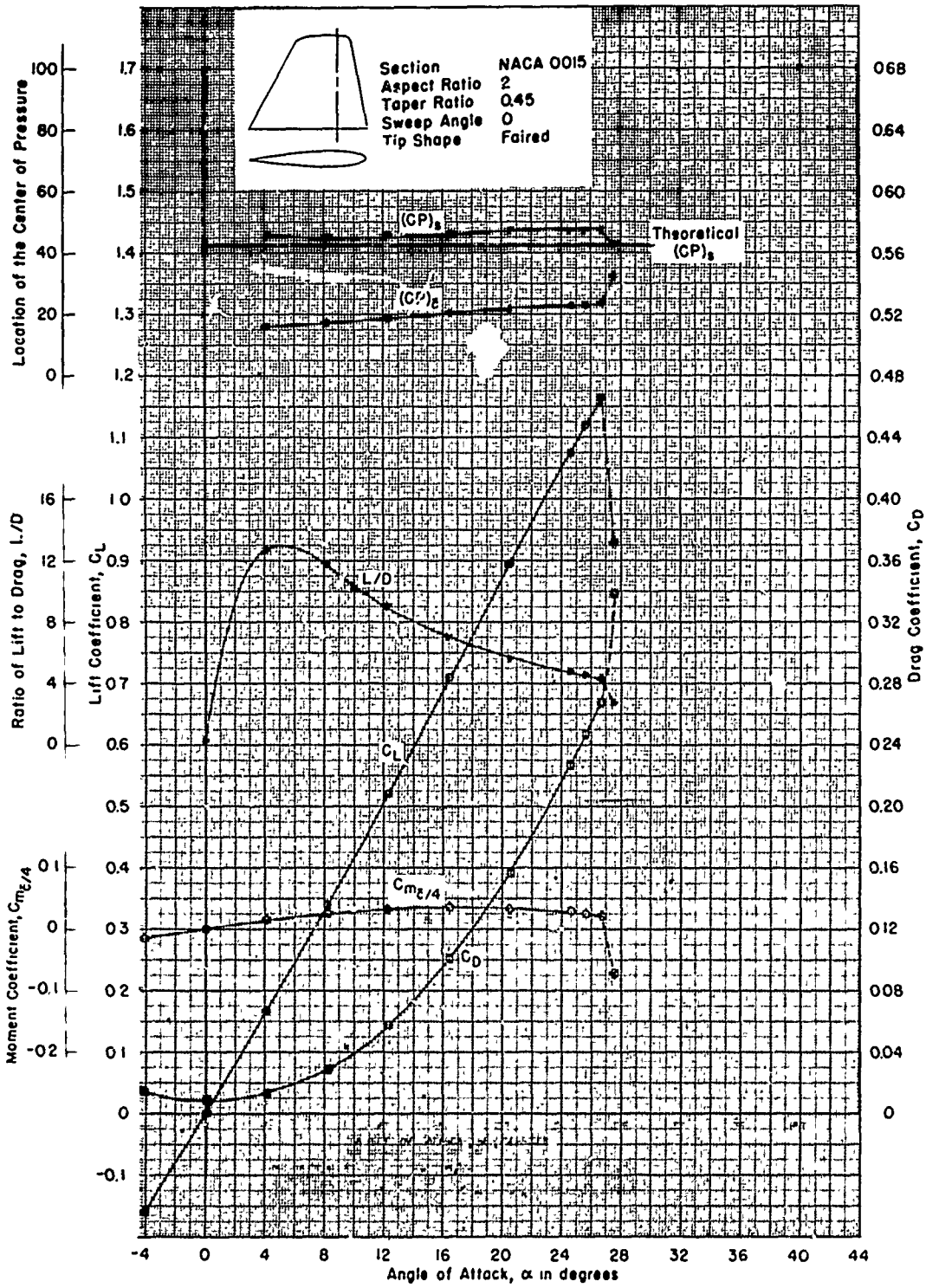

Figure 80 - Reynolds Number of 2.72×10^6

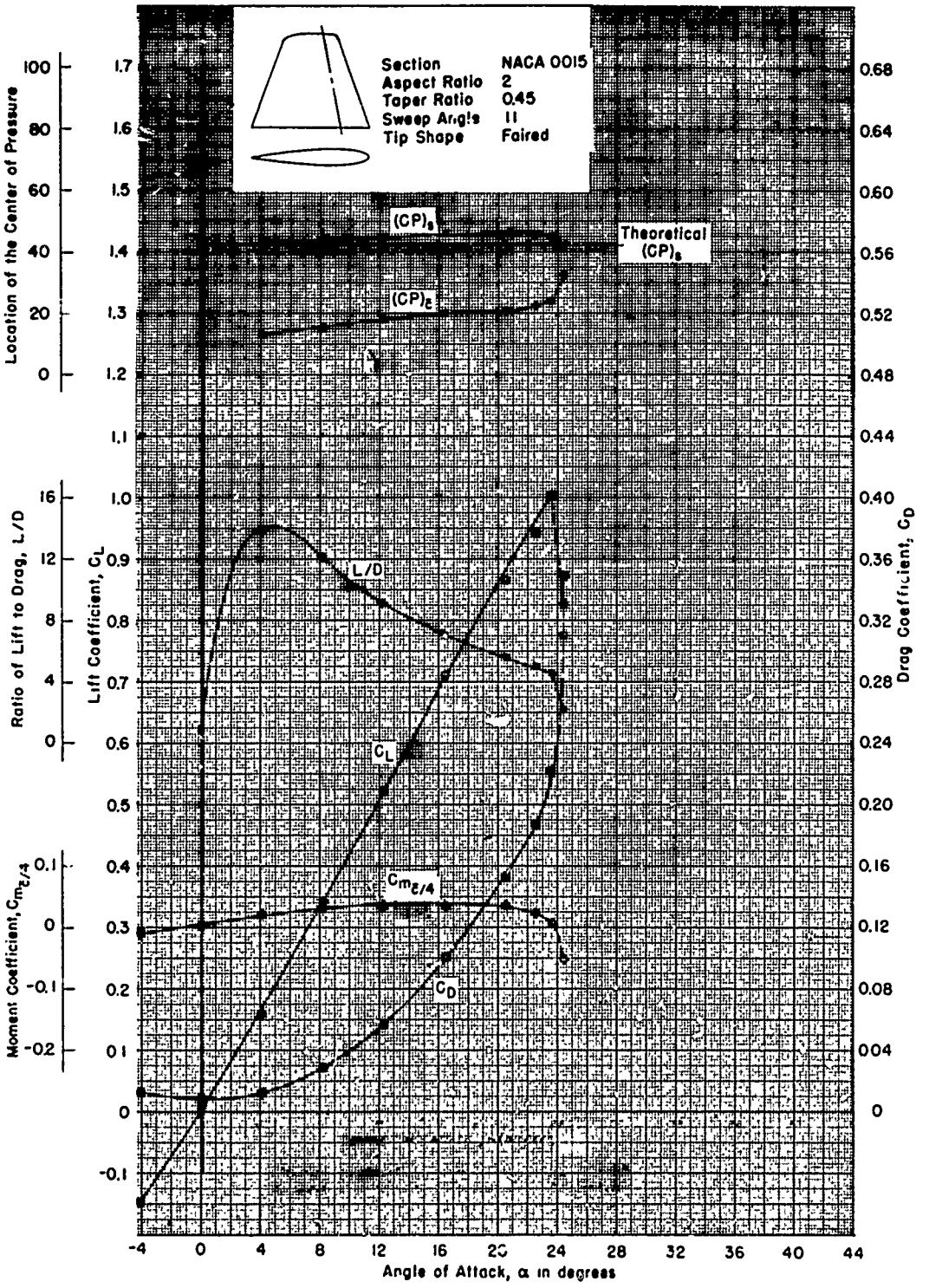

Figure 81 · Reynolds Number of 0.931×10^6

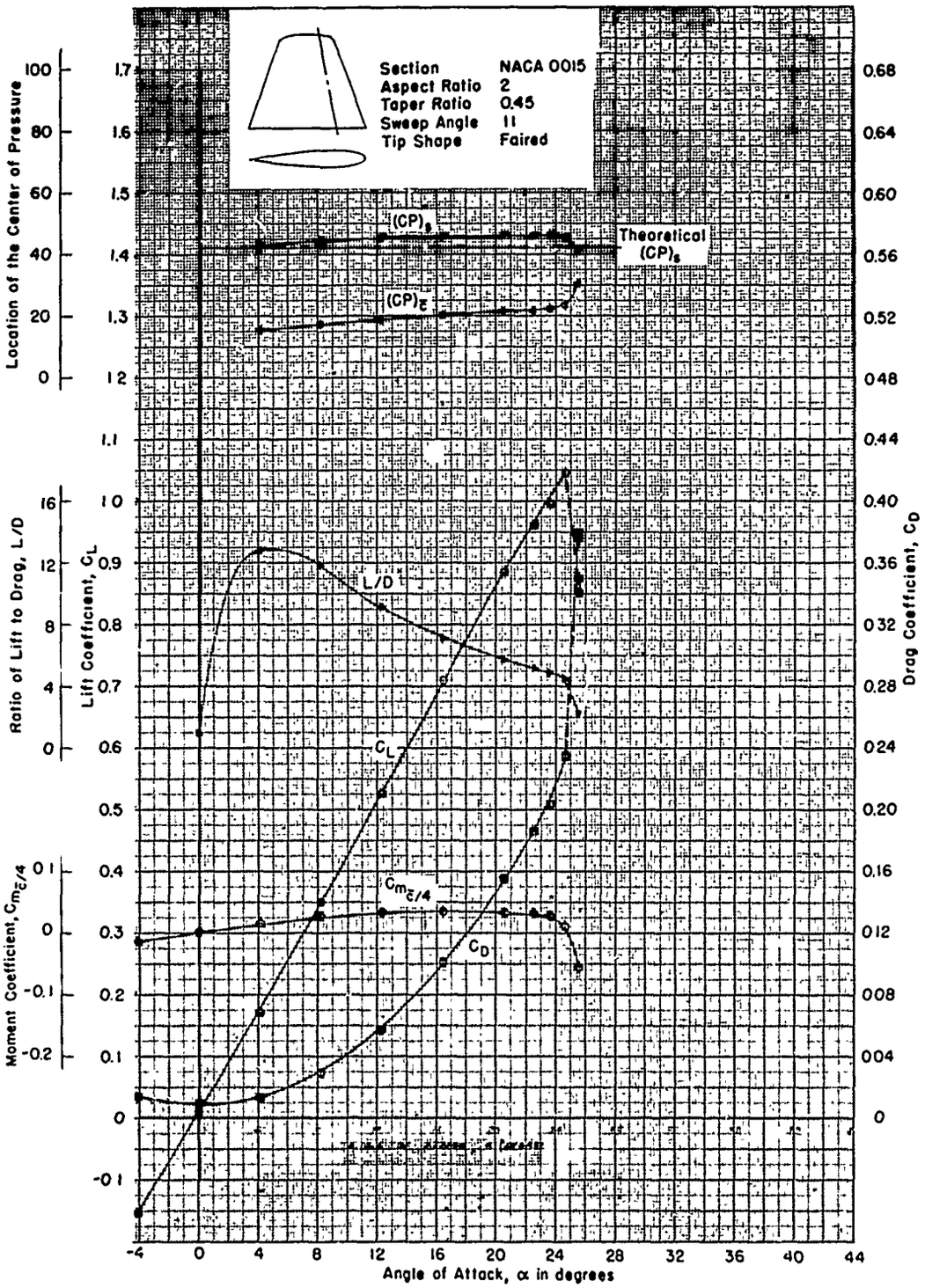

Figure 82 - Reynolds Number of 1.40×10^6

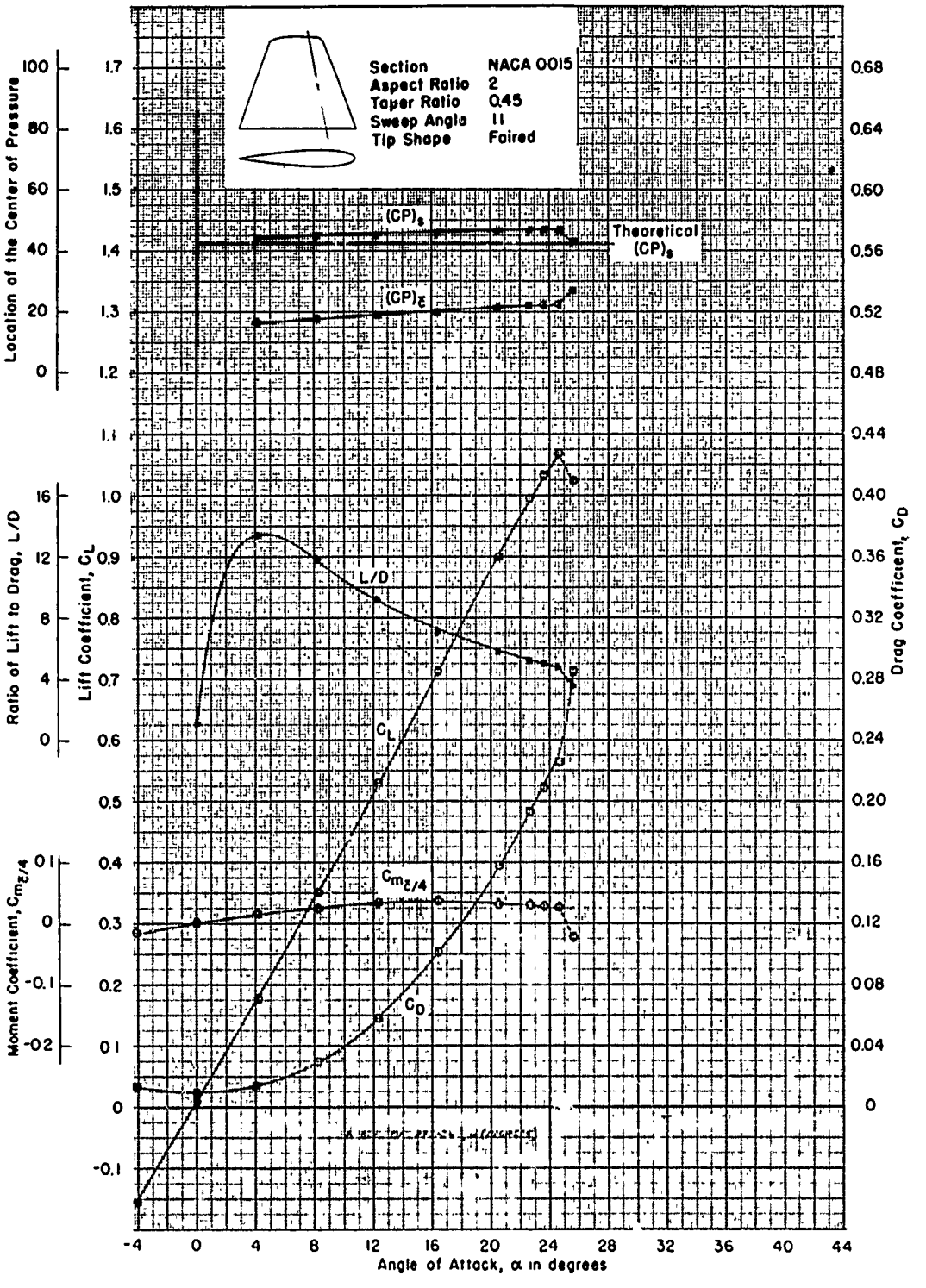

Figure 83 - Reynolds Number of 1.84×10^6

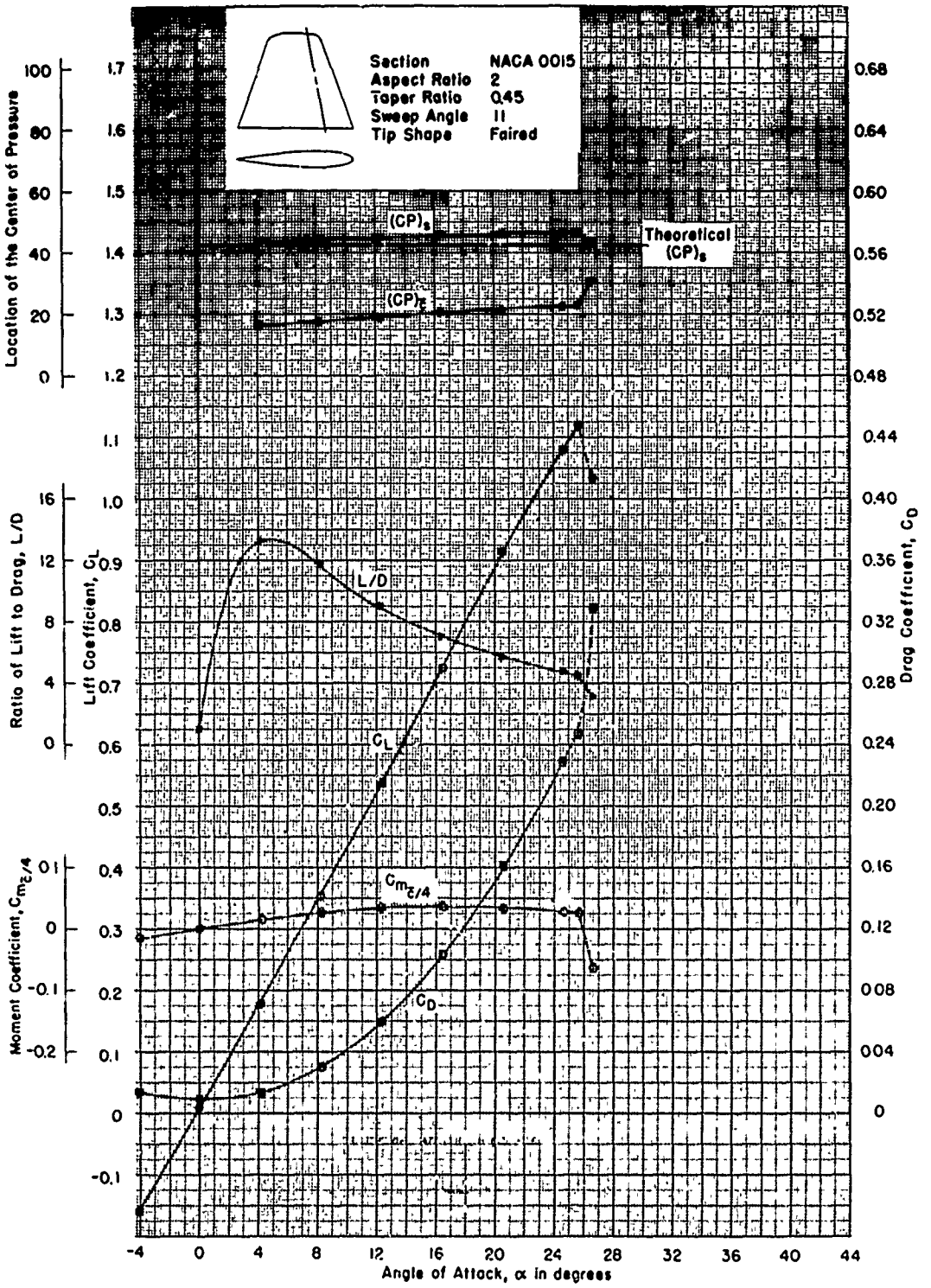

Figure 84 - Reynolds Number of 2.29×10^6

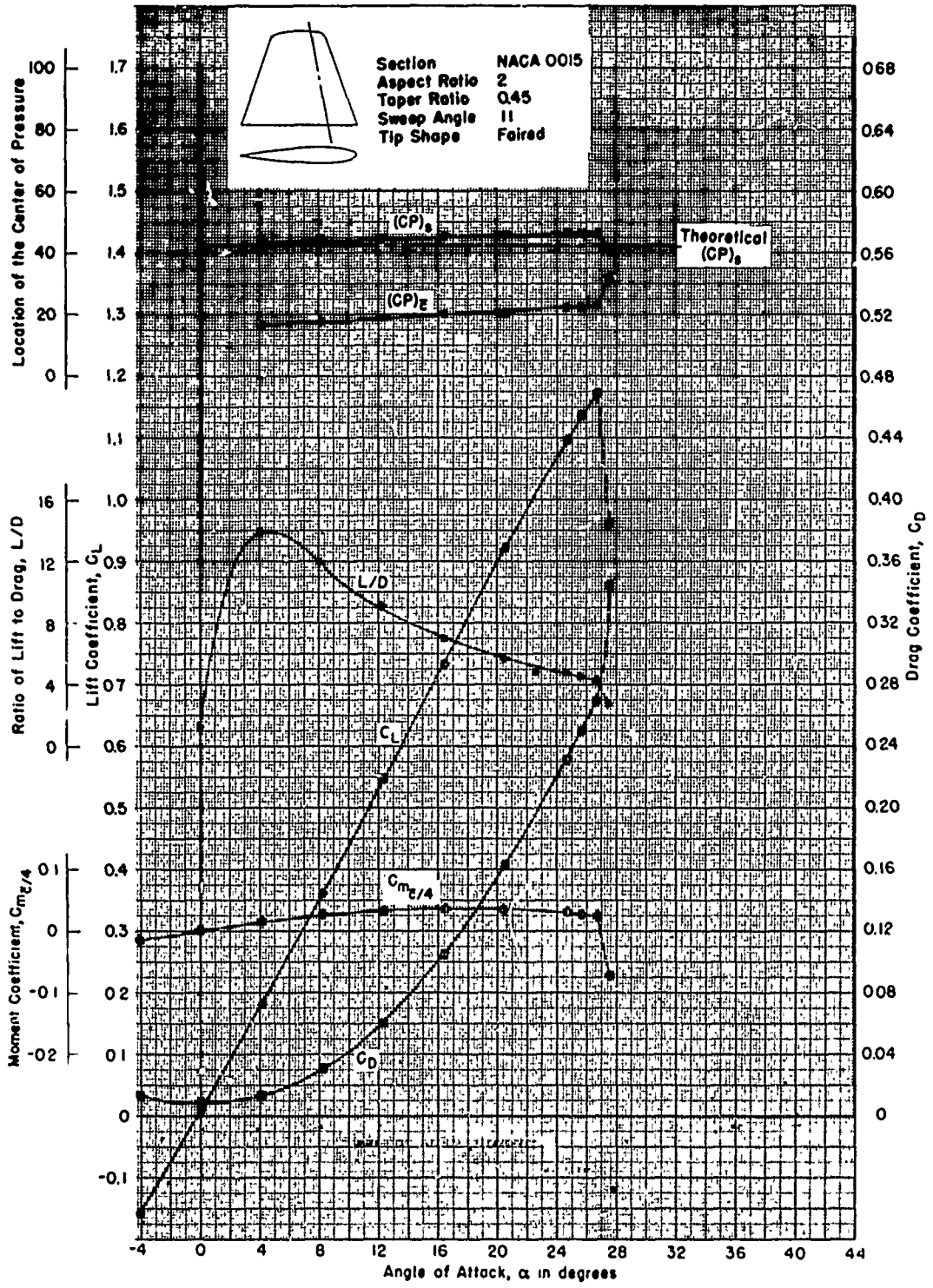

Figure 85 - Reynolds Number of 2.72×10^6

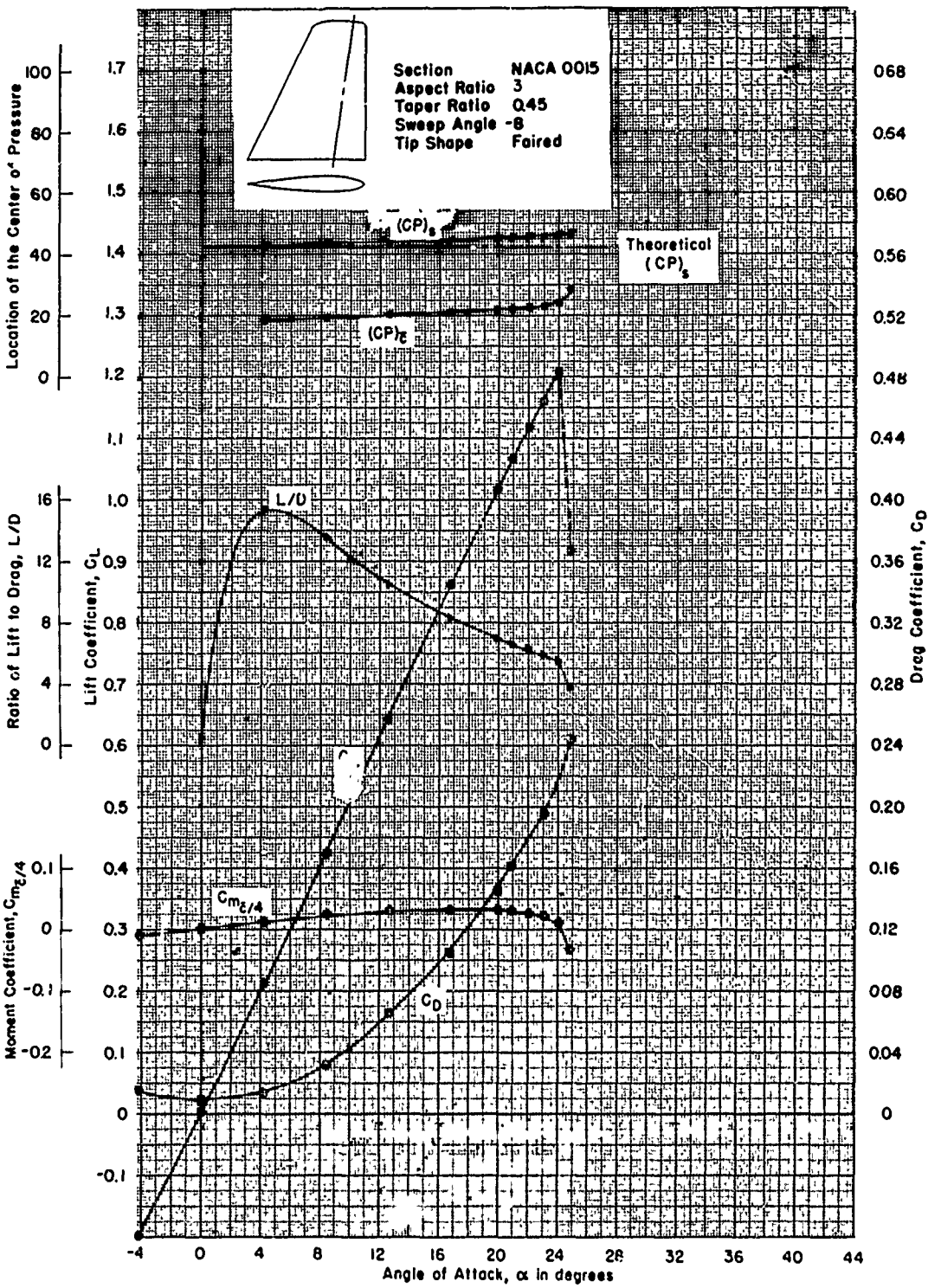

Figure 86 - Reynolds Number of 2.26×10^6

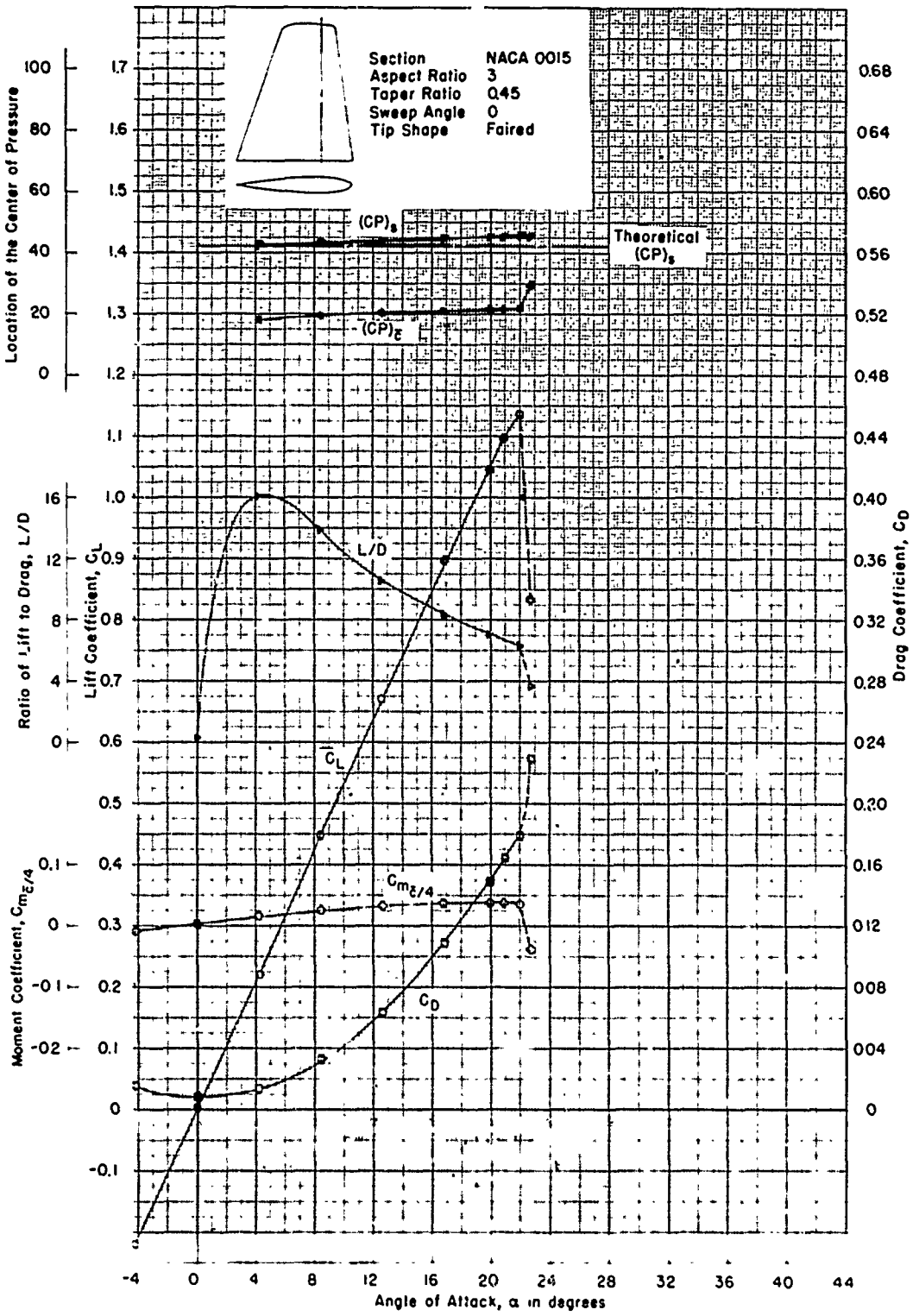

Figure 87 - Reynolds Number of 2.26×10^6

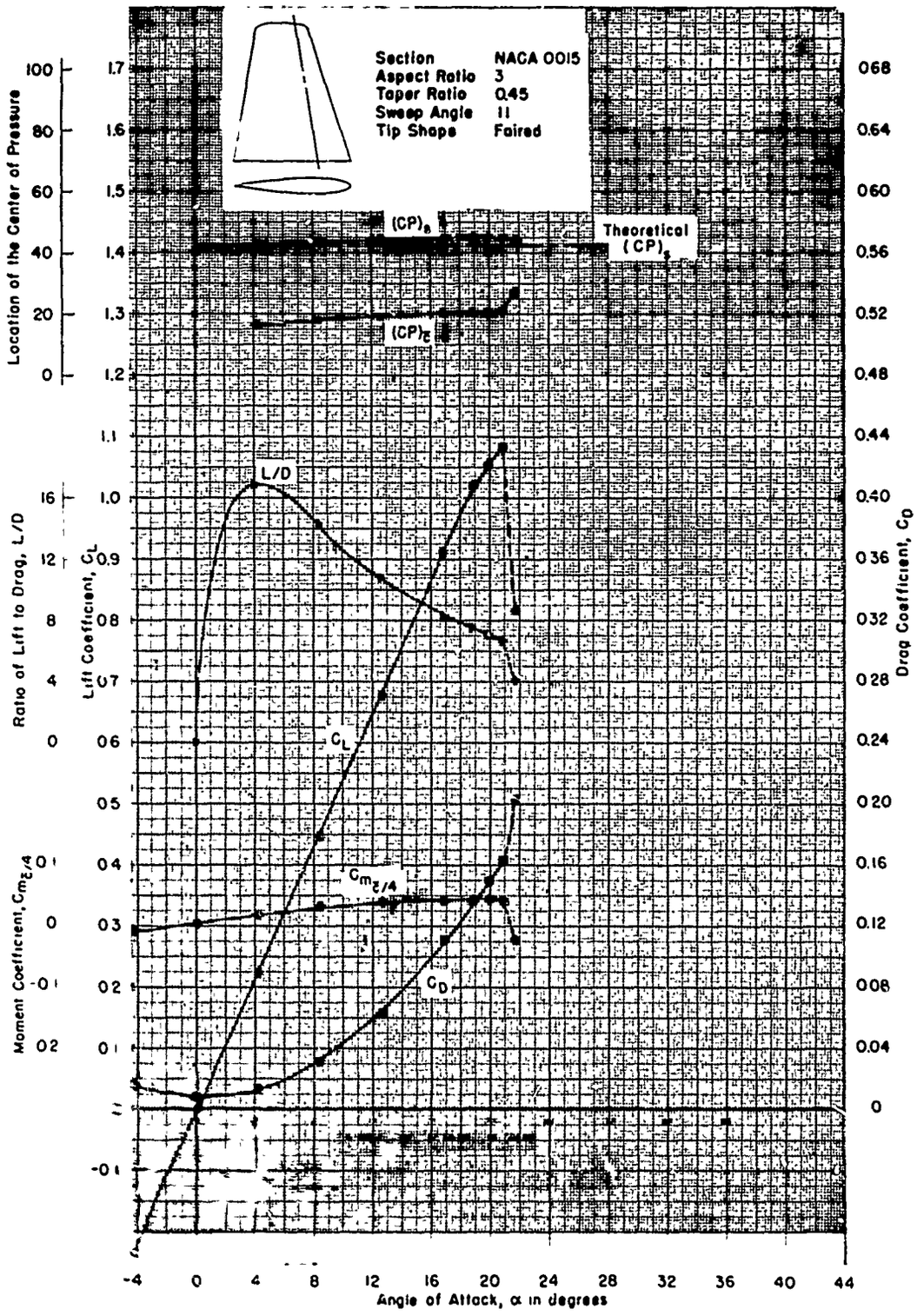

Figure 86 - Reynolds Number of 2.26×10^6

APPENDIX C

FREE-STREAM CHARACTERISTICS OF SQUARE-TIP CONTROL SURFACES WITH AN NACA 0015 SECTION SHAPE IN THE ASTERN CONDITION

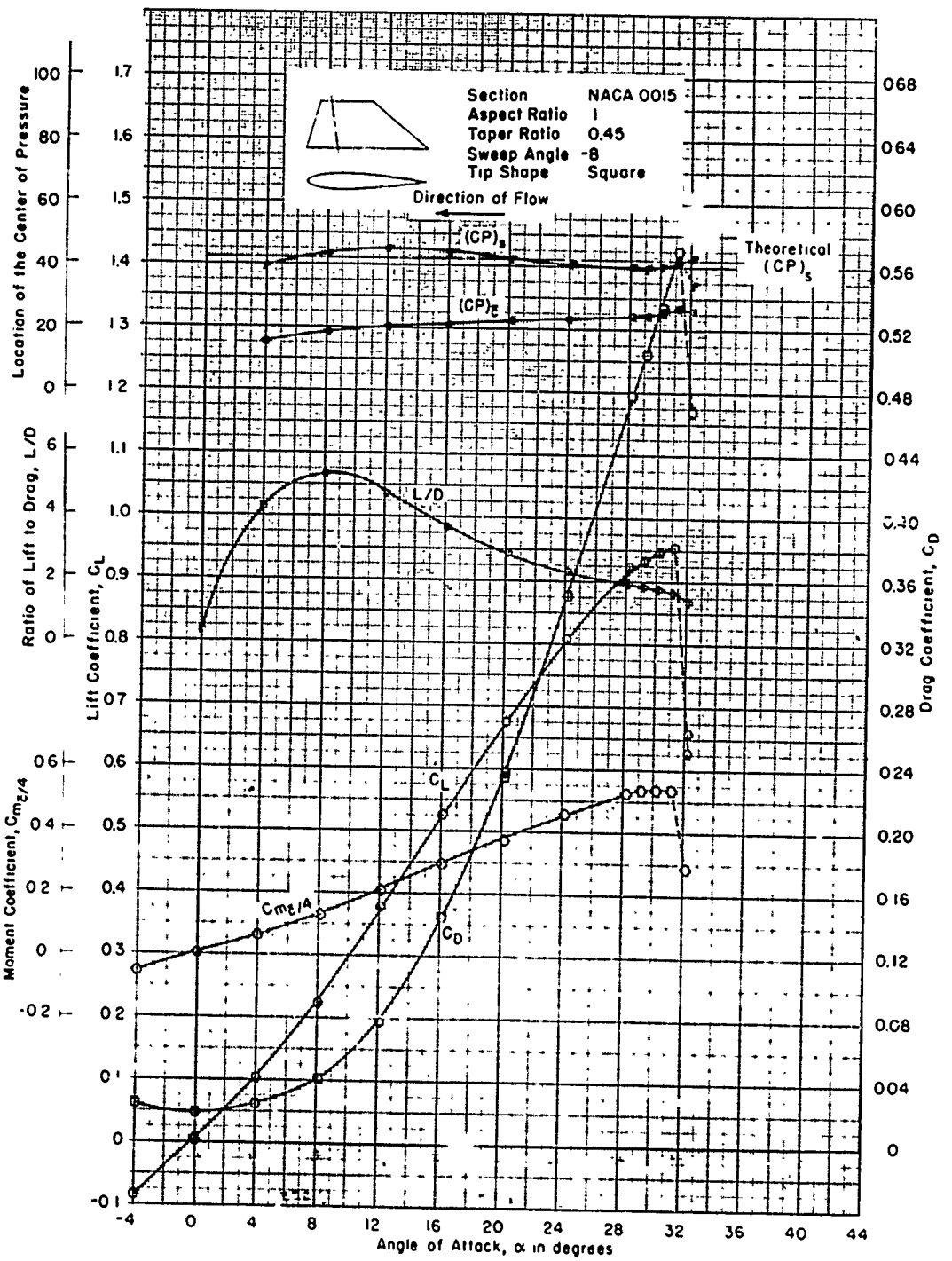

Figure 89 - Reynolds Number of 3.00×10^6

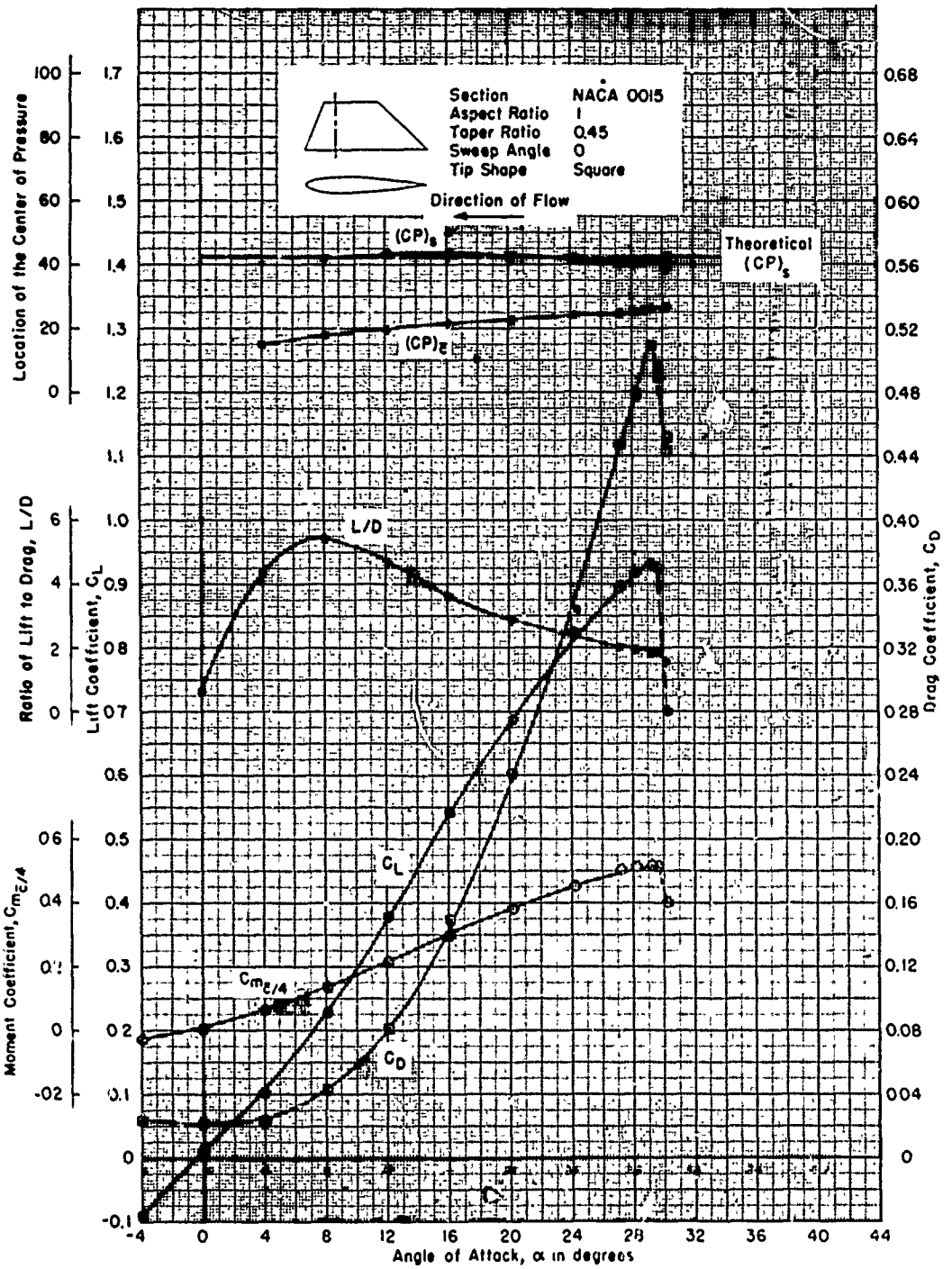

Figure 90 - Reynolds Number of 3.00×10^6

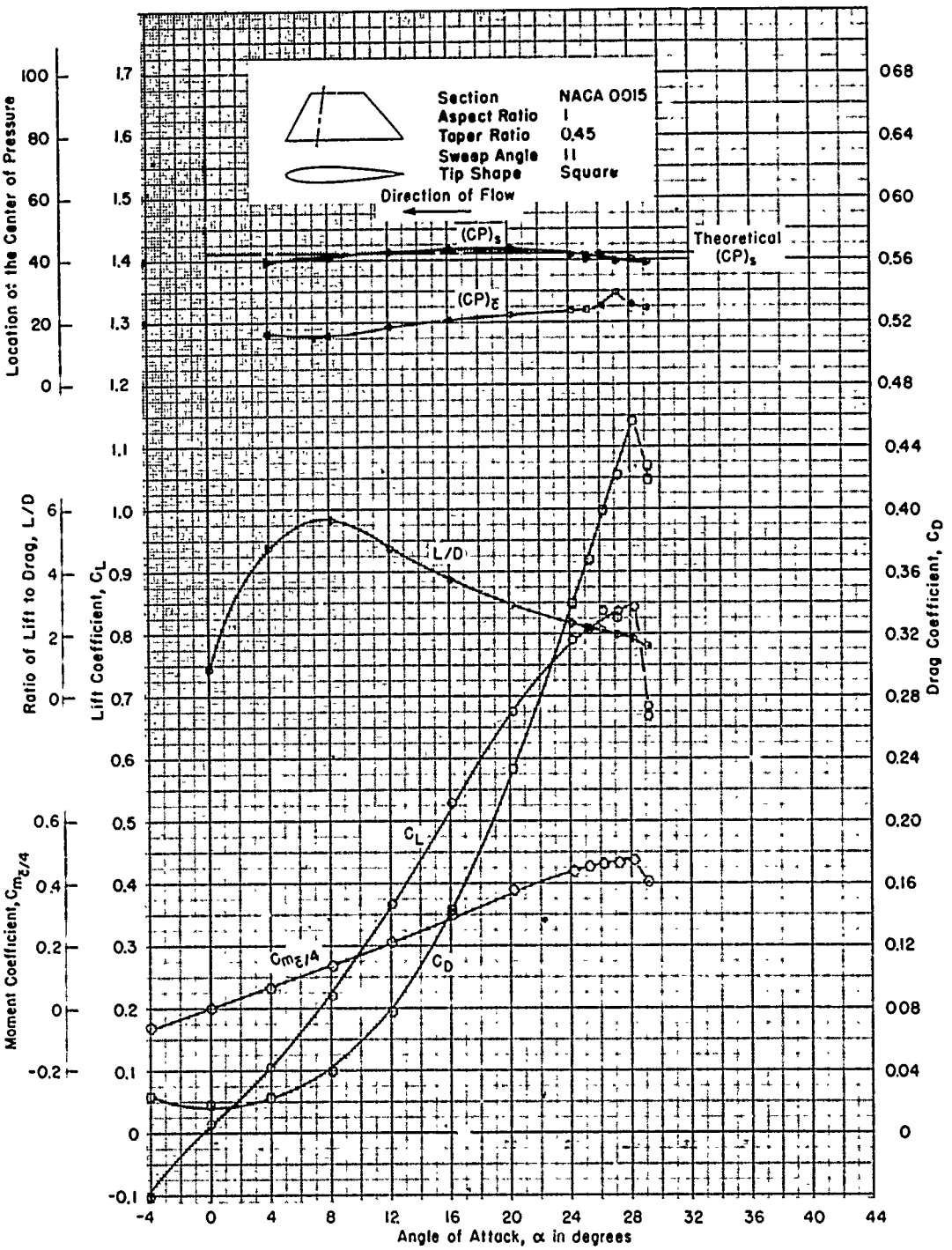

Figure 91 - Reynolds Number of 3.00×10^6

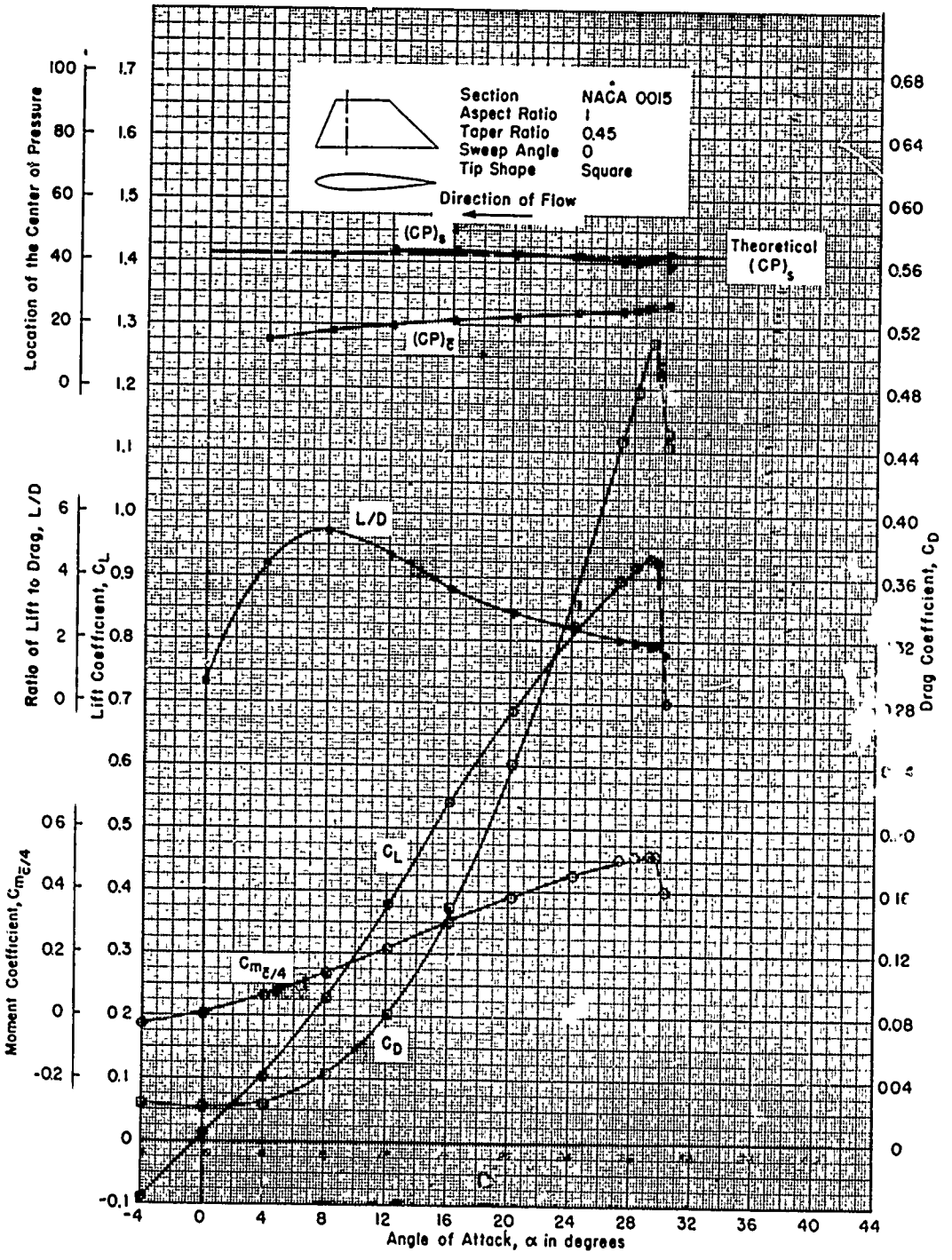

Figure 90 - Reynolds Number of 3.00×10^6

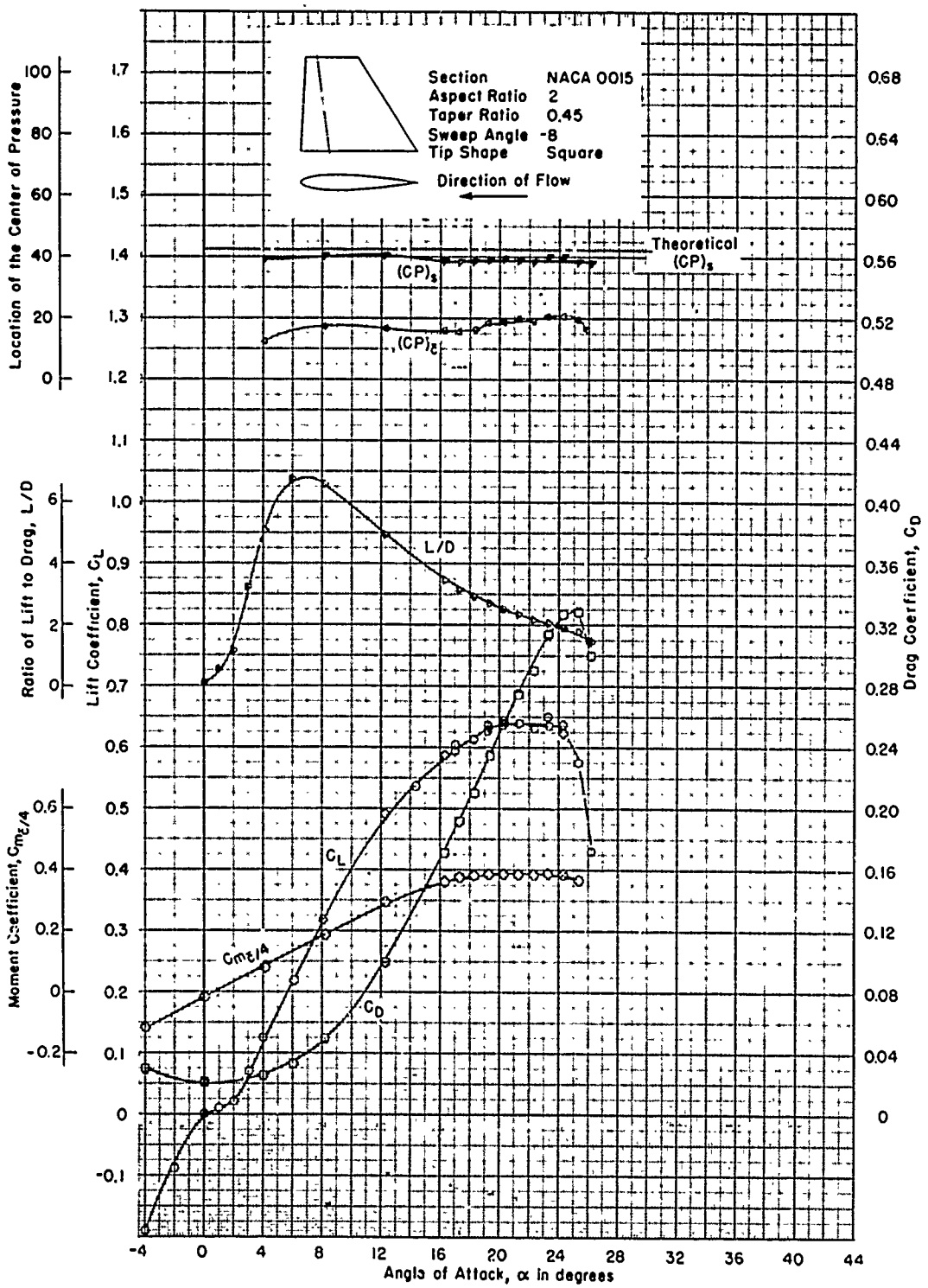

Figure 92 - Reynolds Number of 3.00×10^6

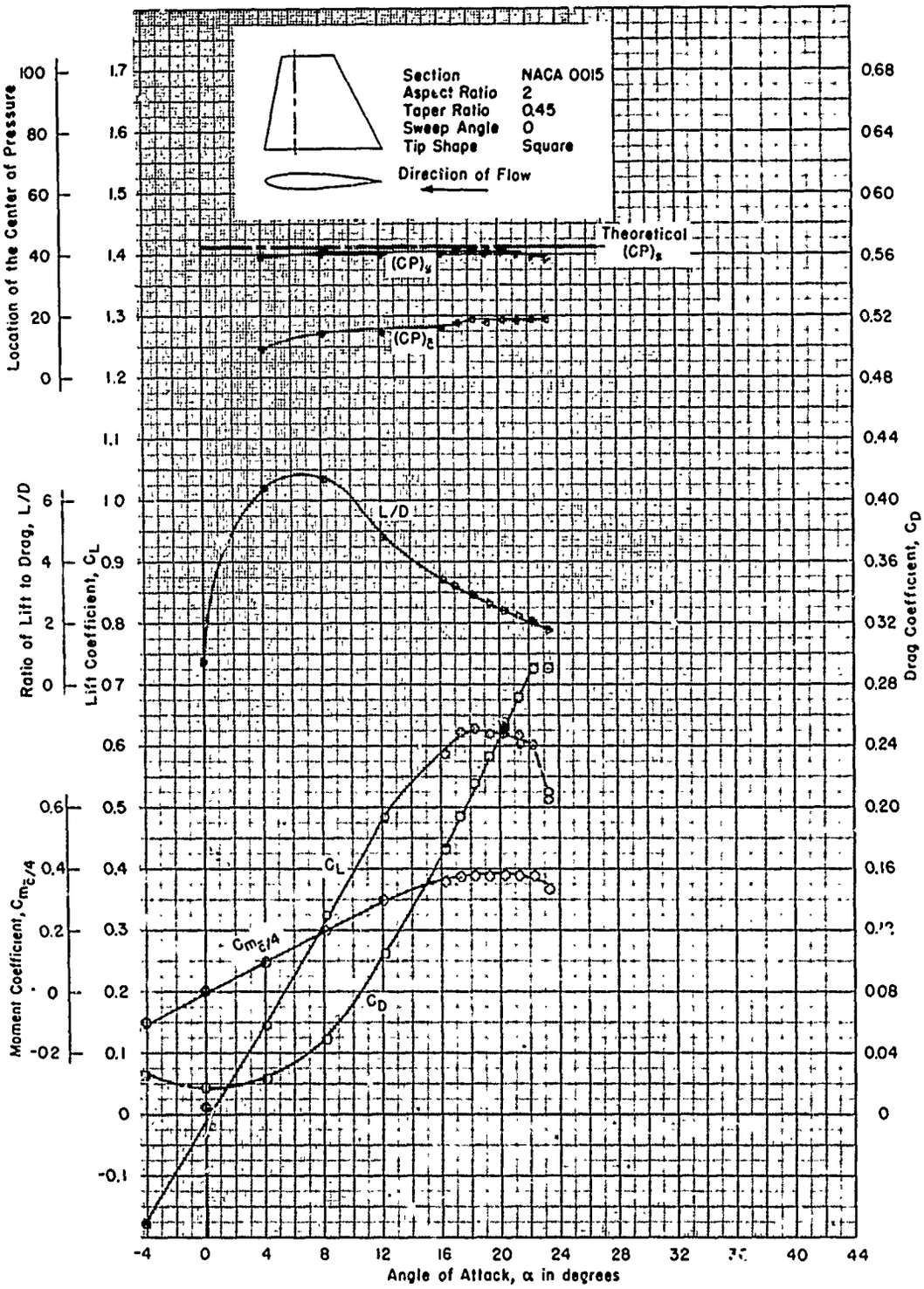

Figure 93 - Reynolds Number of 3.00×10^6

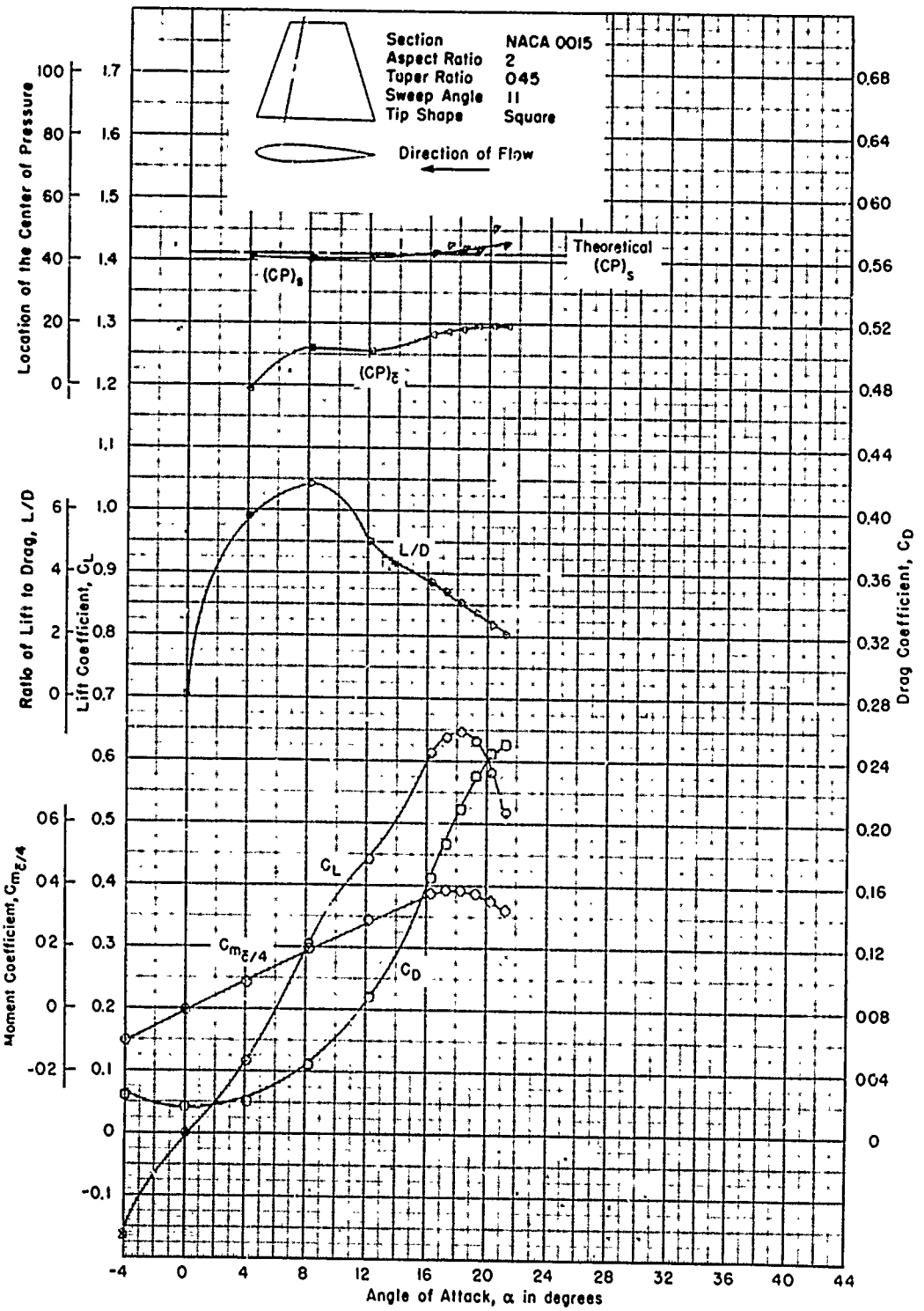

Figure 94 - Reynolds Number of 3.00×10^6

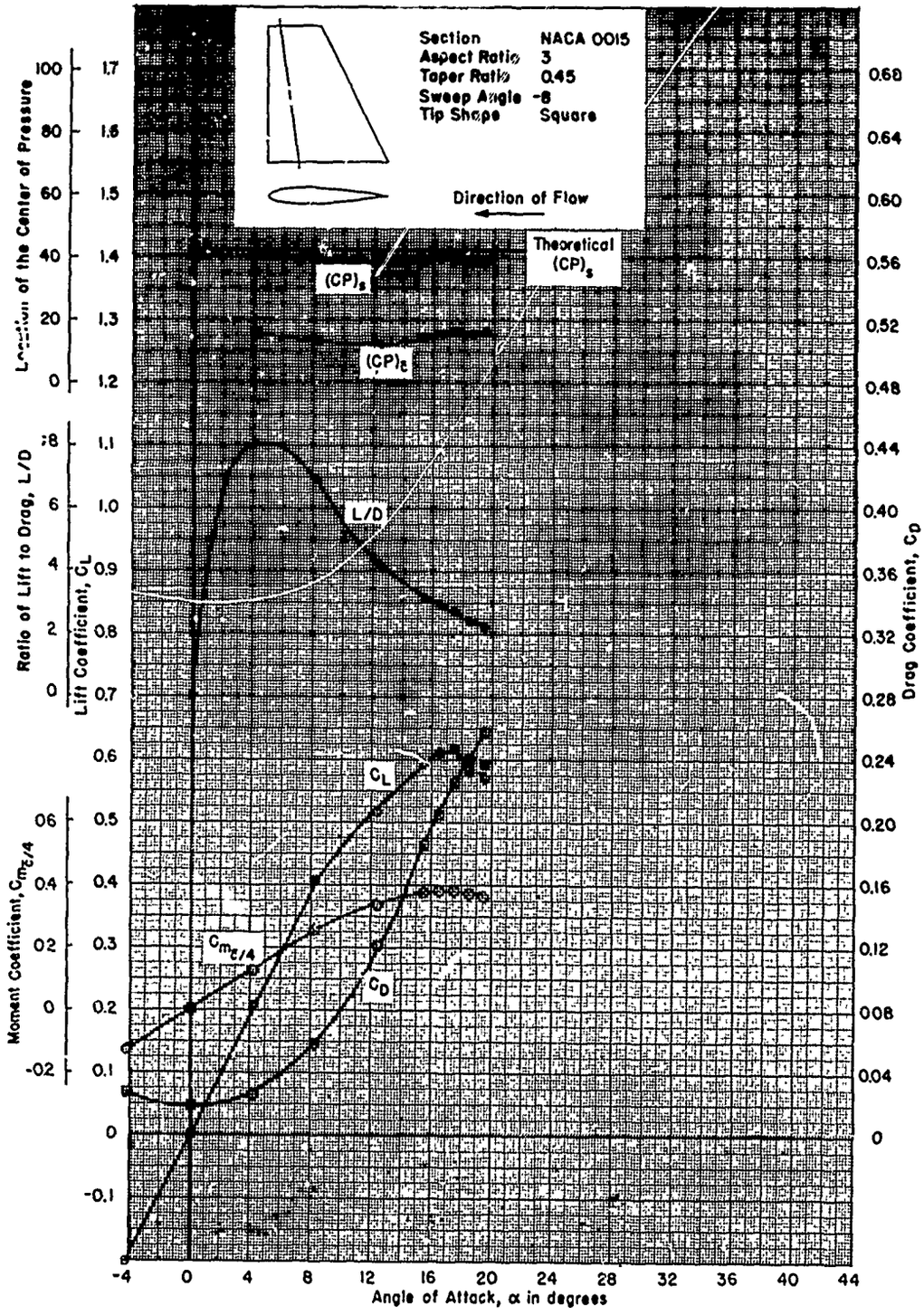

Figure 95 - Reynolds Number of 3.00×10^6

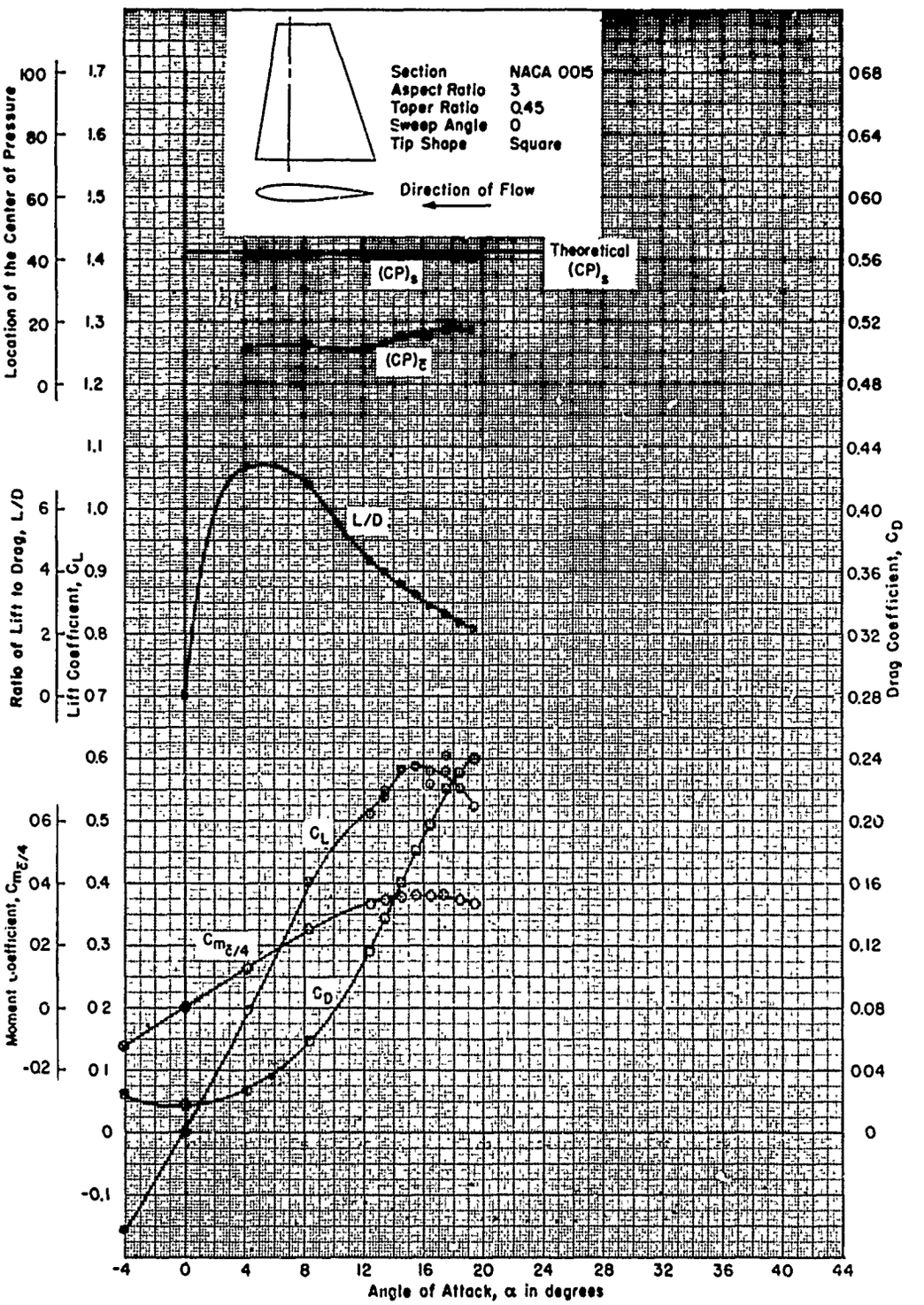

Figure 96 - Reynolds Number of 3.00×10^6

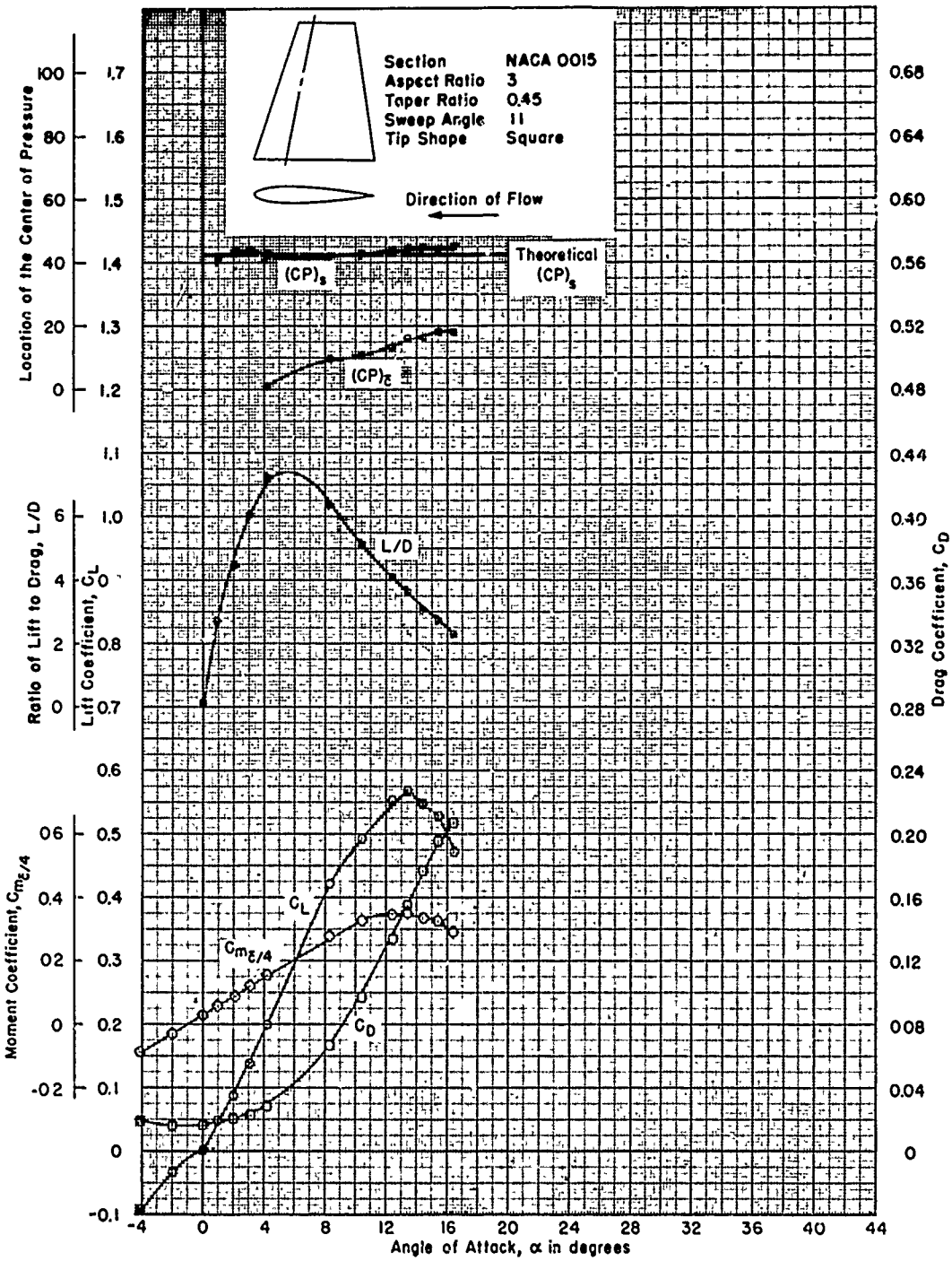

Figure 97 - Reynolds Number of 3.00×10^6

APPENDIX D

FREE-STREAM CHARACTERISTICS OF SQUARE-TIP CONTROL SURFACES WITH TMB-EPH, NSS, TMB 07507515, AND TMB FAIRING NO. 7 SECTION SHAPES IN THE AHEAD AND ASTERN CONDITIONS

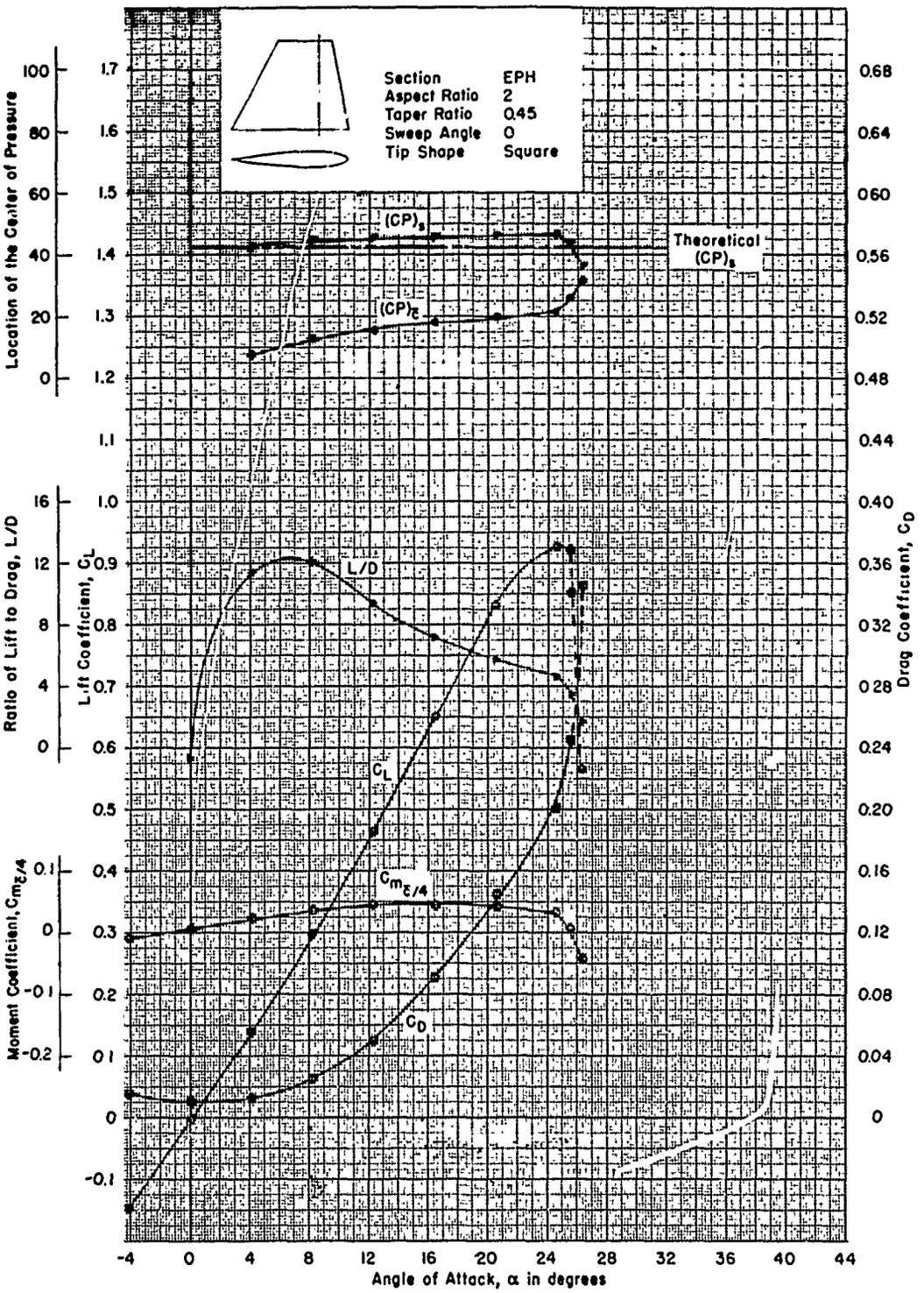

Figure 98 - Reynolds Number of 0.912×10^6

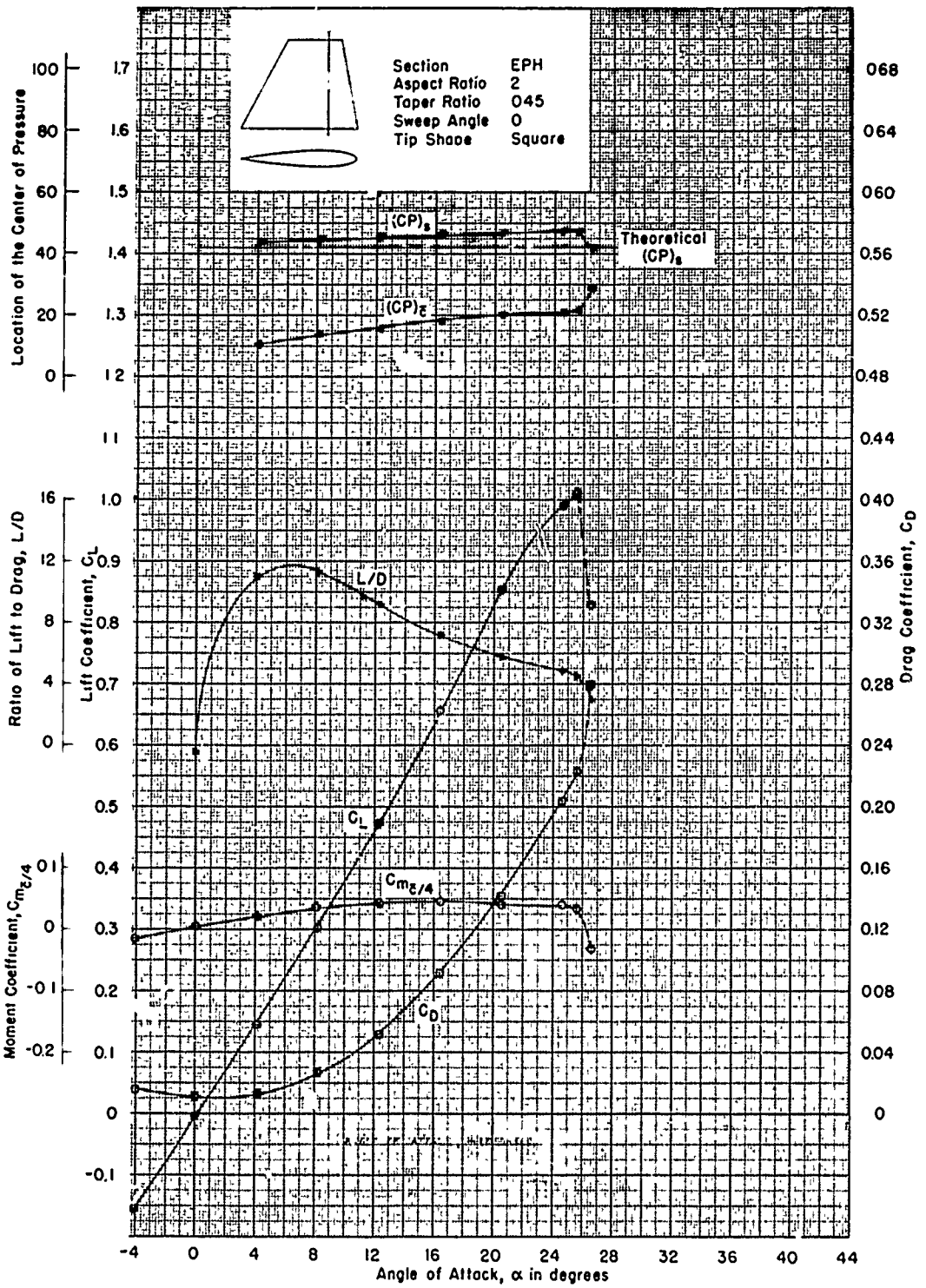

Figure 99 - Reynolds Number of 1.37×10^6

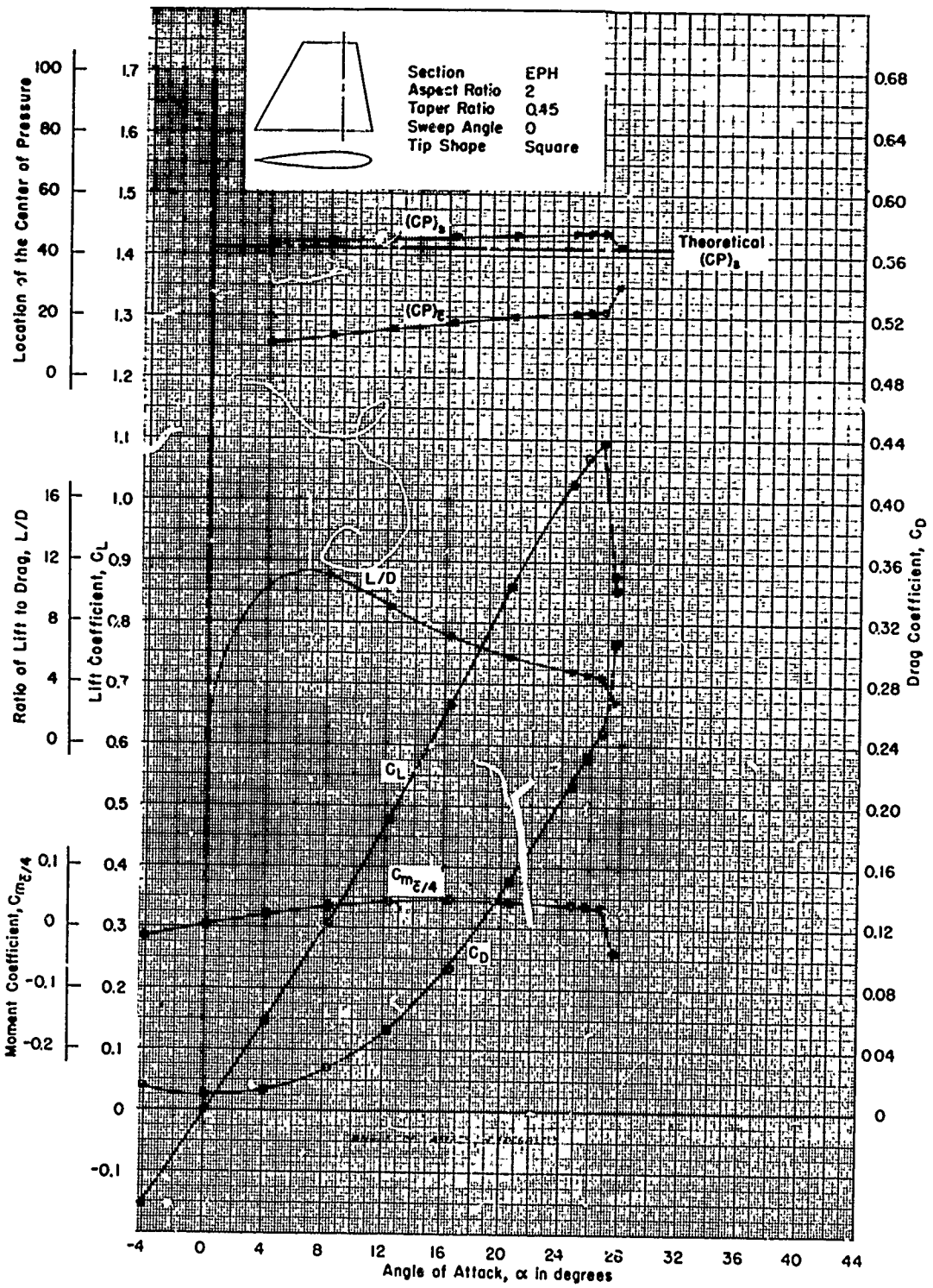

Figure 100 - Reynolds Number of 1.82×10^6

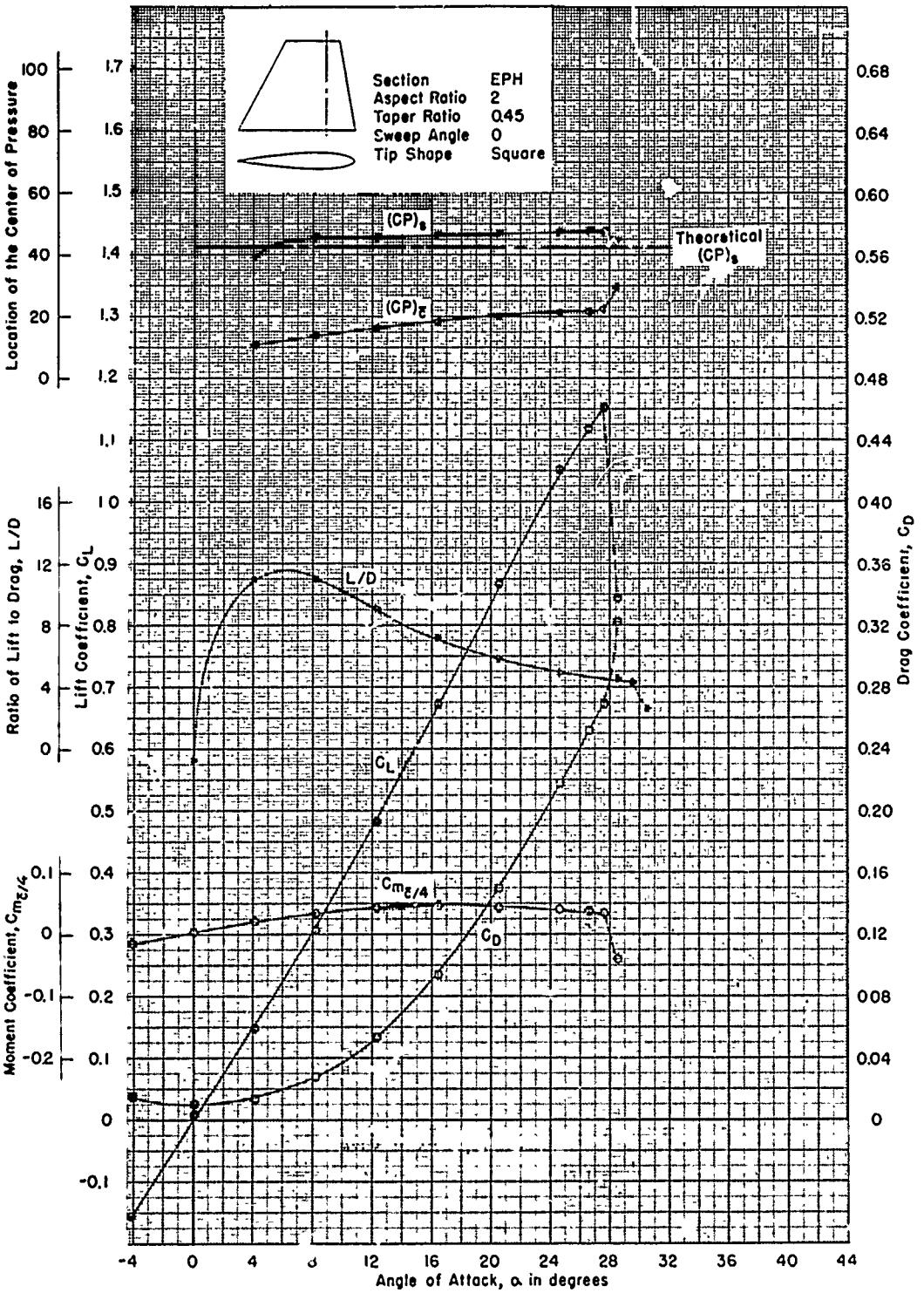

Figure 101 - Reynolds Number of 2.25×10^6

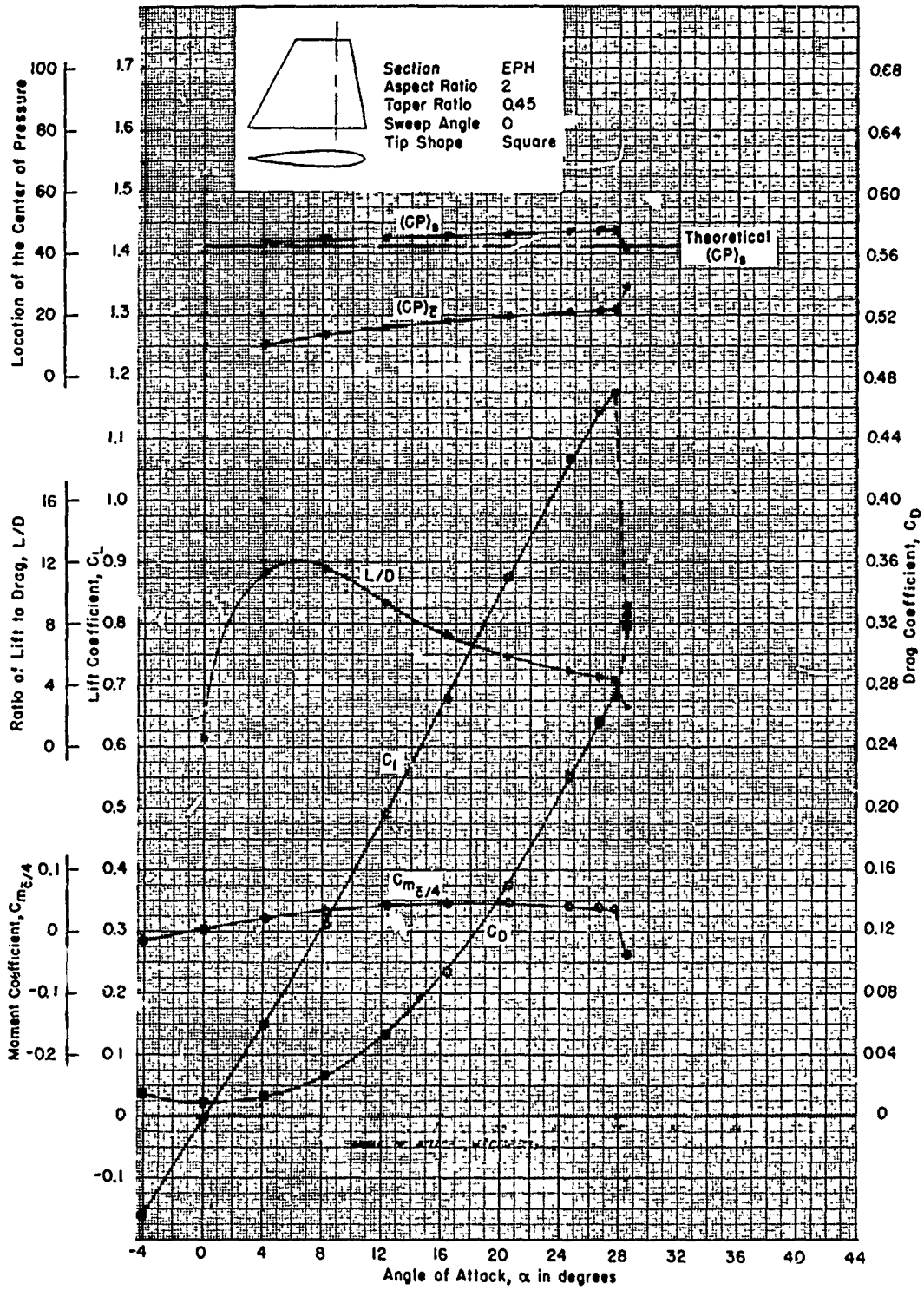

Figure 102 - Reynolds Number of 2.70×10^6

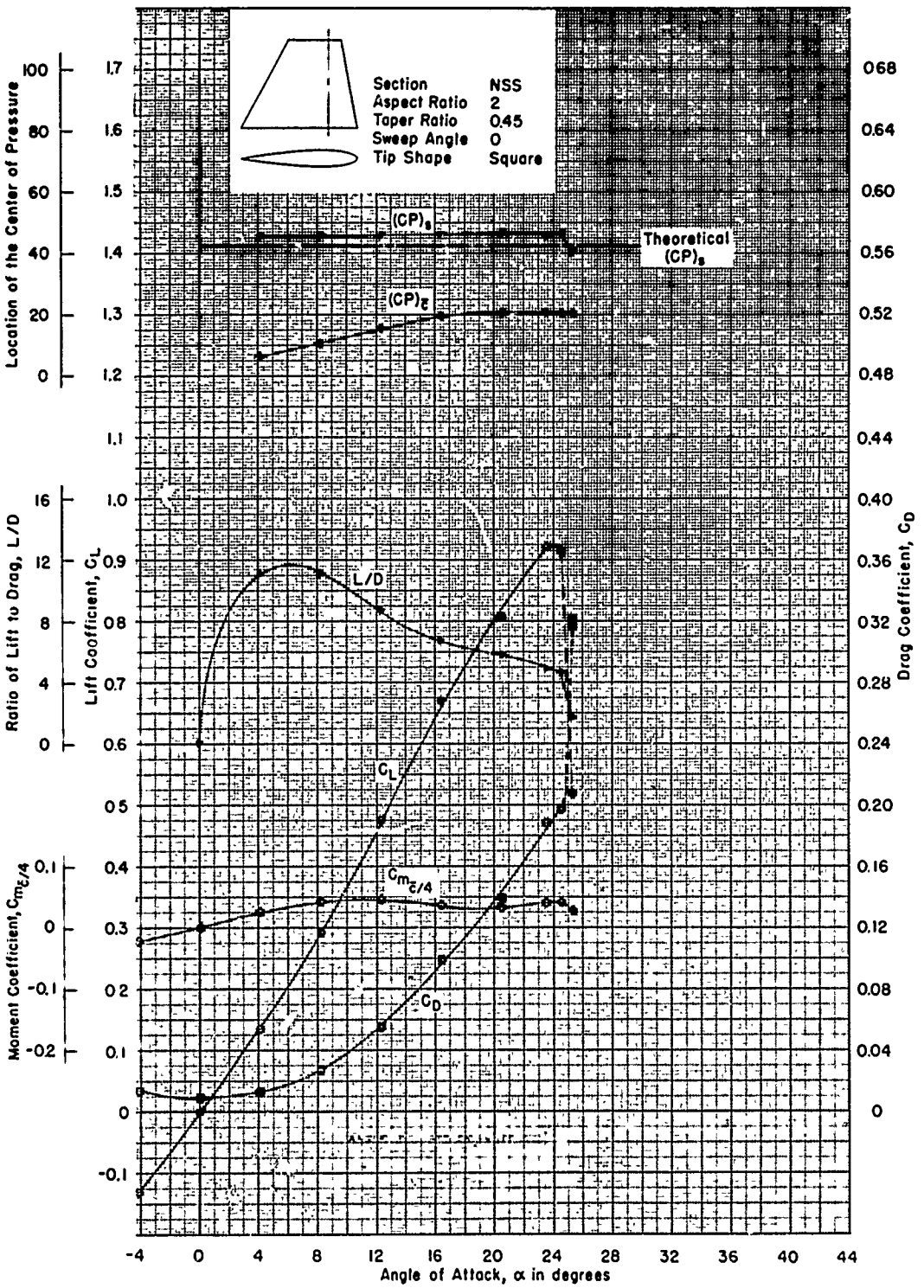

Figure 103 - Reynolds Number of 0.912×10^6

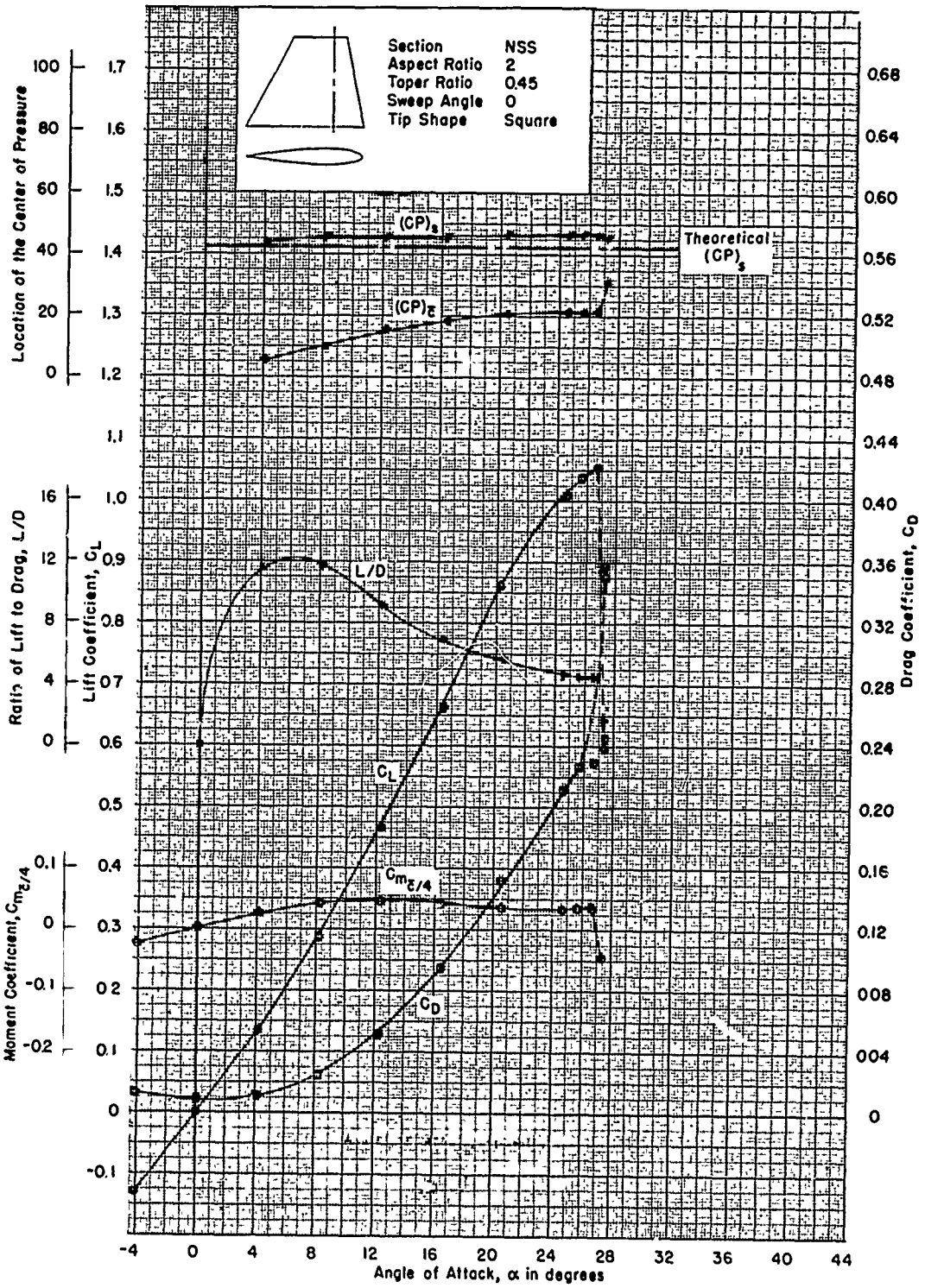

Figure 104 - Reynolds Number of 1.37×10^6

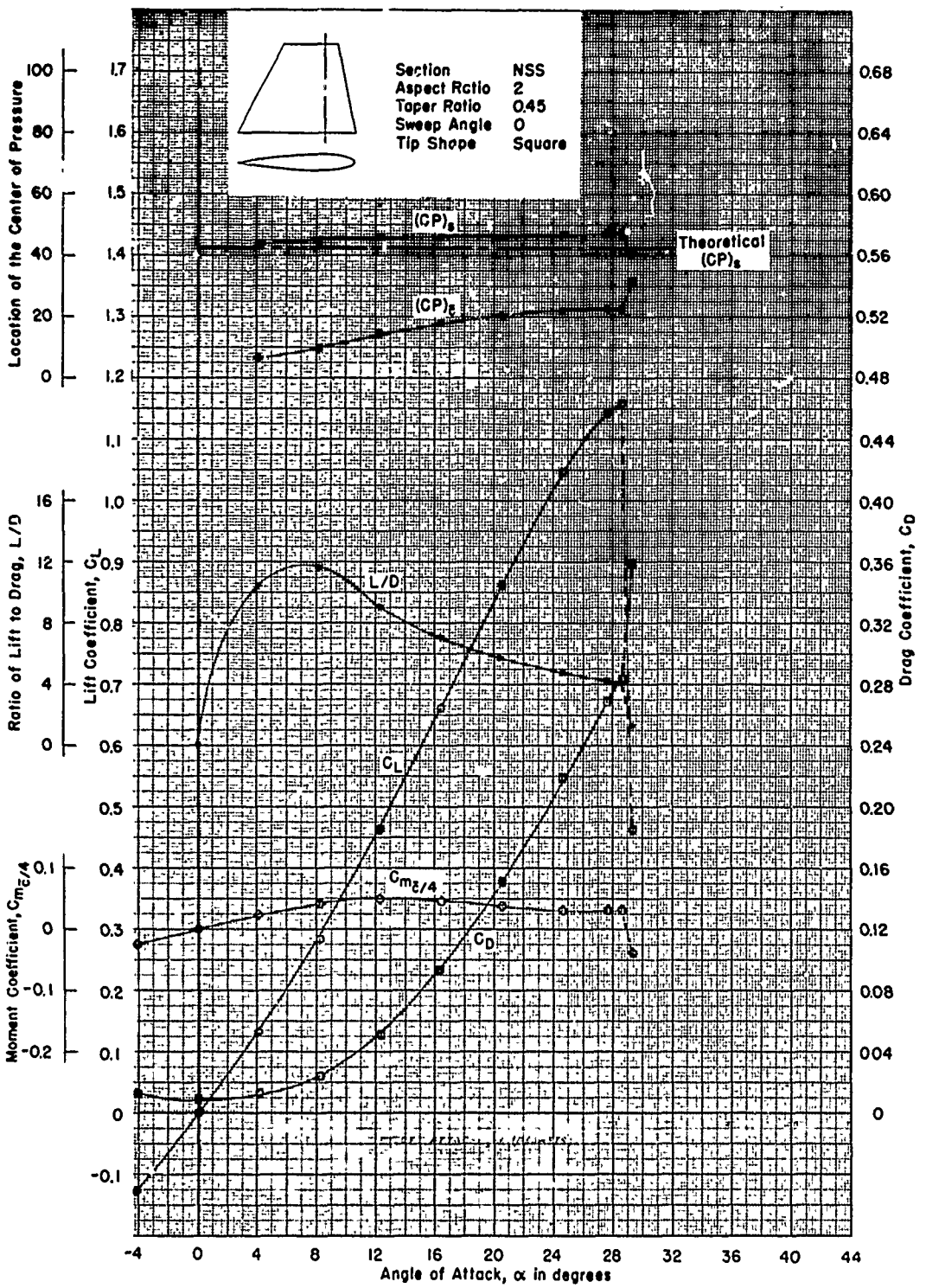

Figure 105 - Reynolds Number of 1.82×10^6

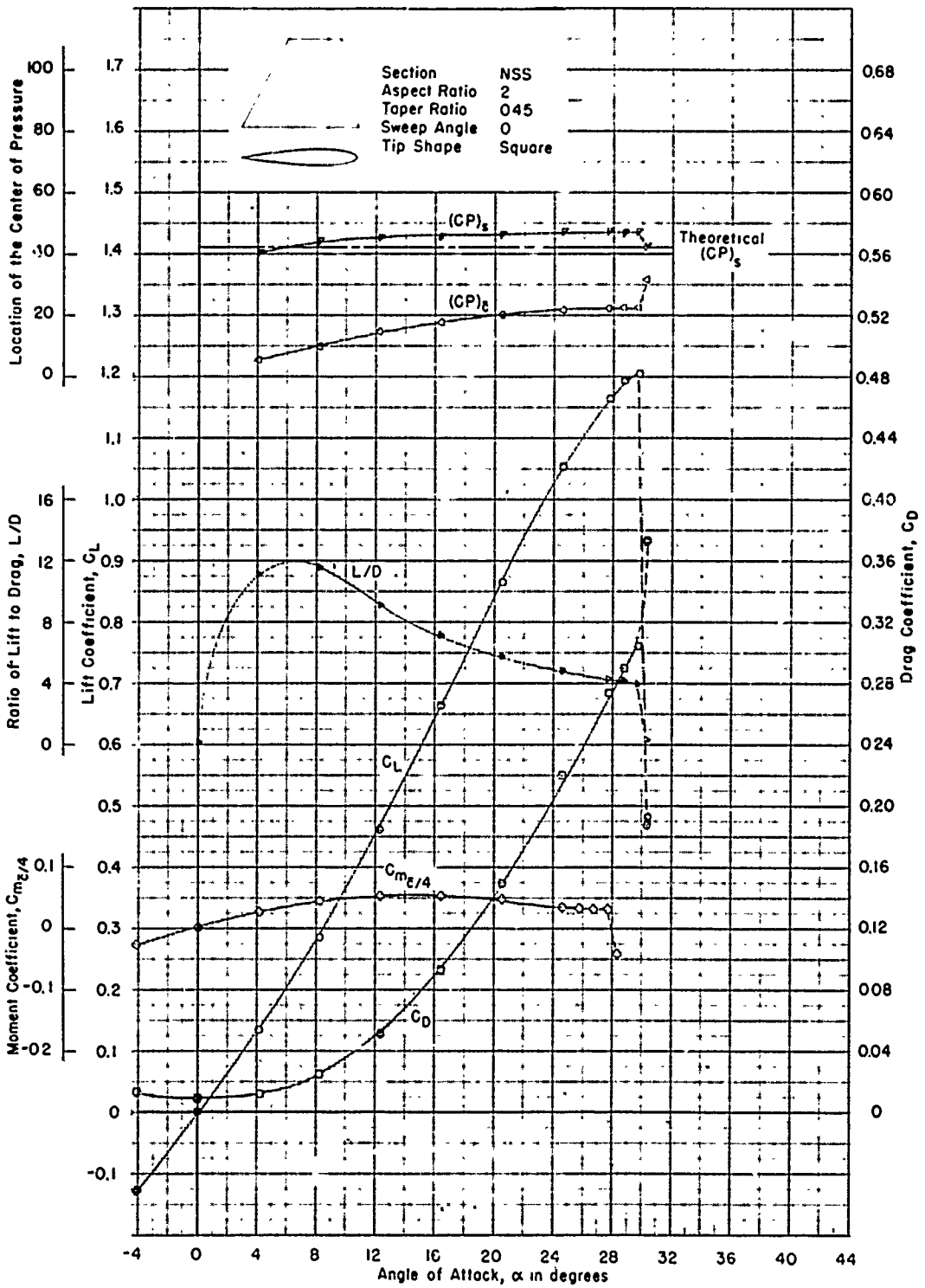

Figure 106 -Reynolds Number of 2.25×10^6

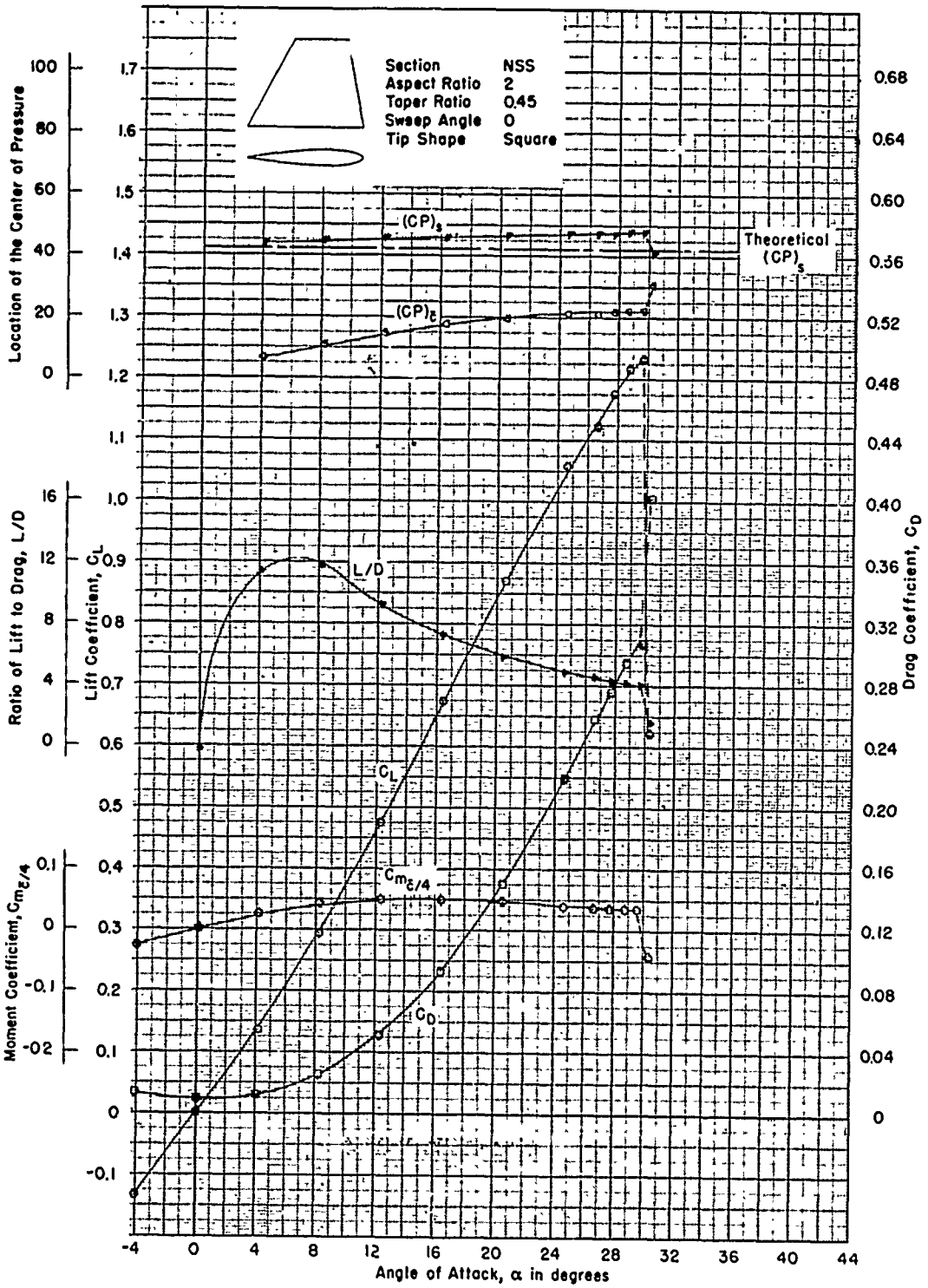

Figure 107 - Reynolds Number of 2.70×10^6

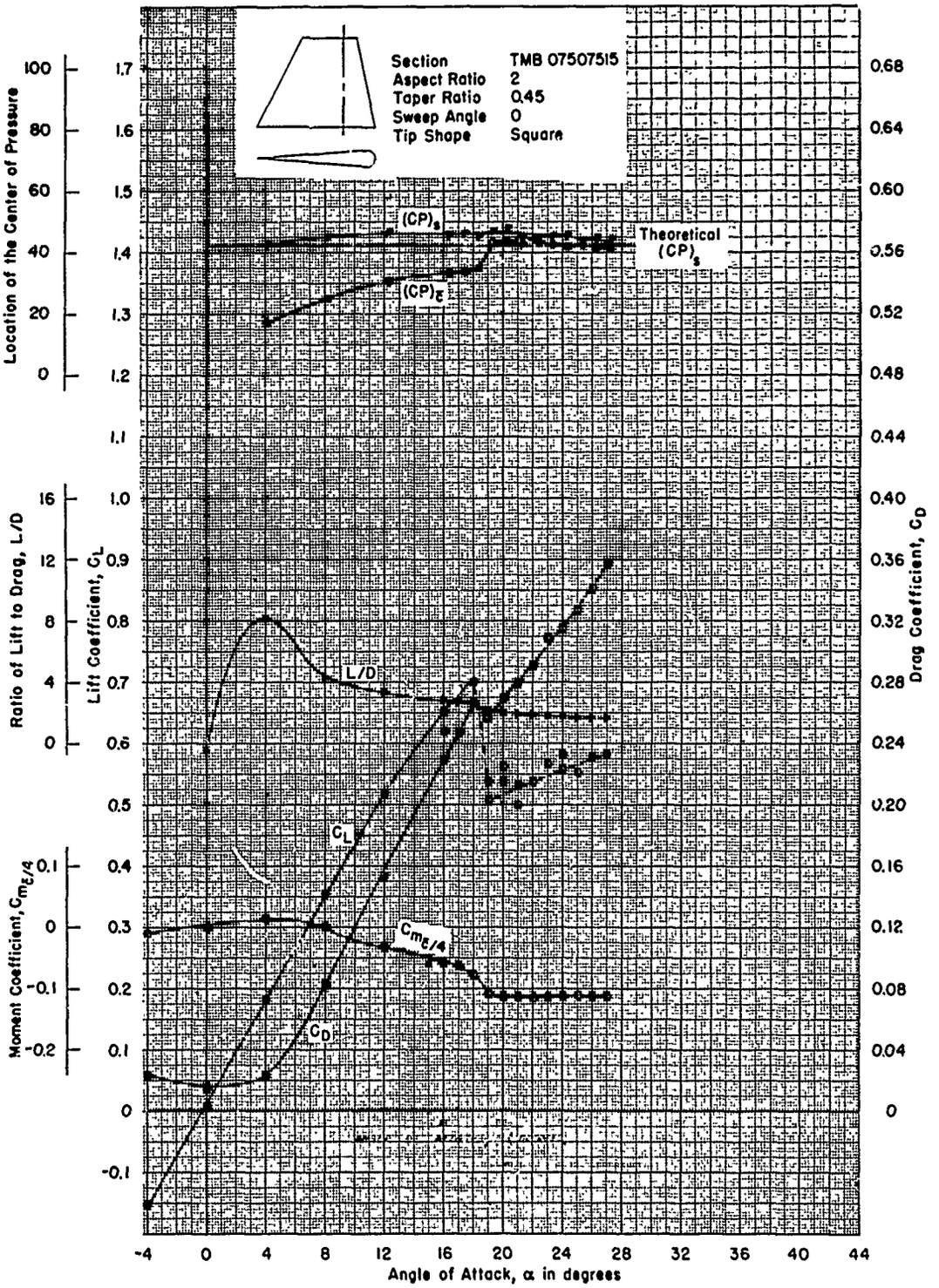

Figure 108 - Reynolds Number of 0.990×10^6

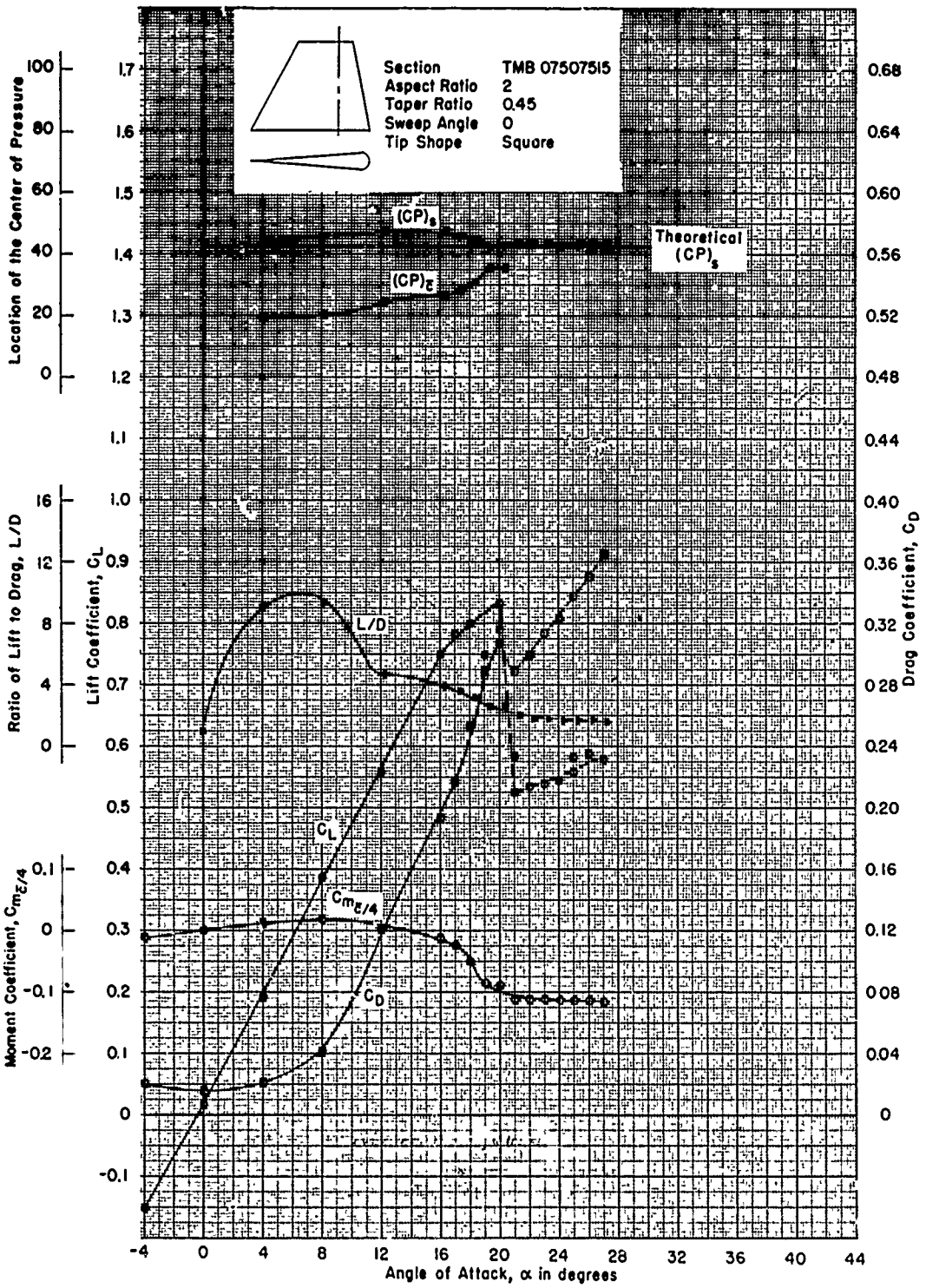

Figure 109 - Reynolds Number of 1.41×10^6

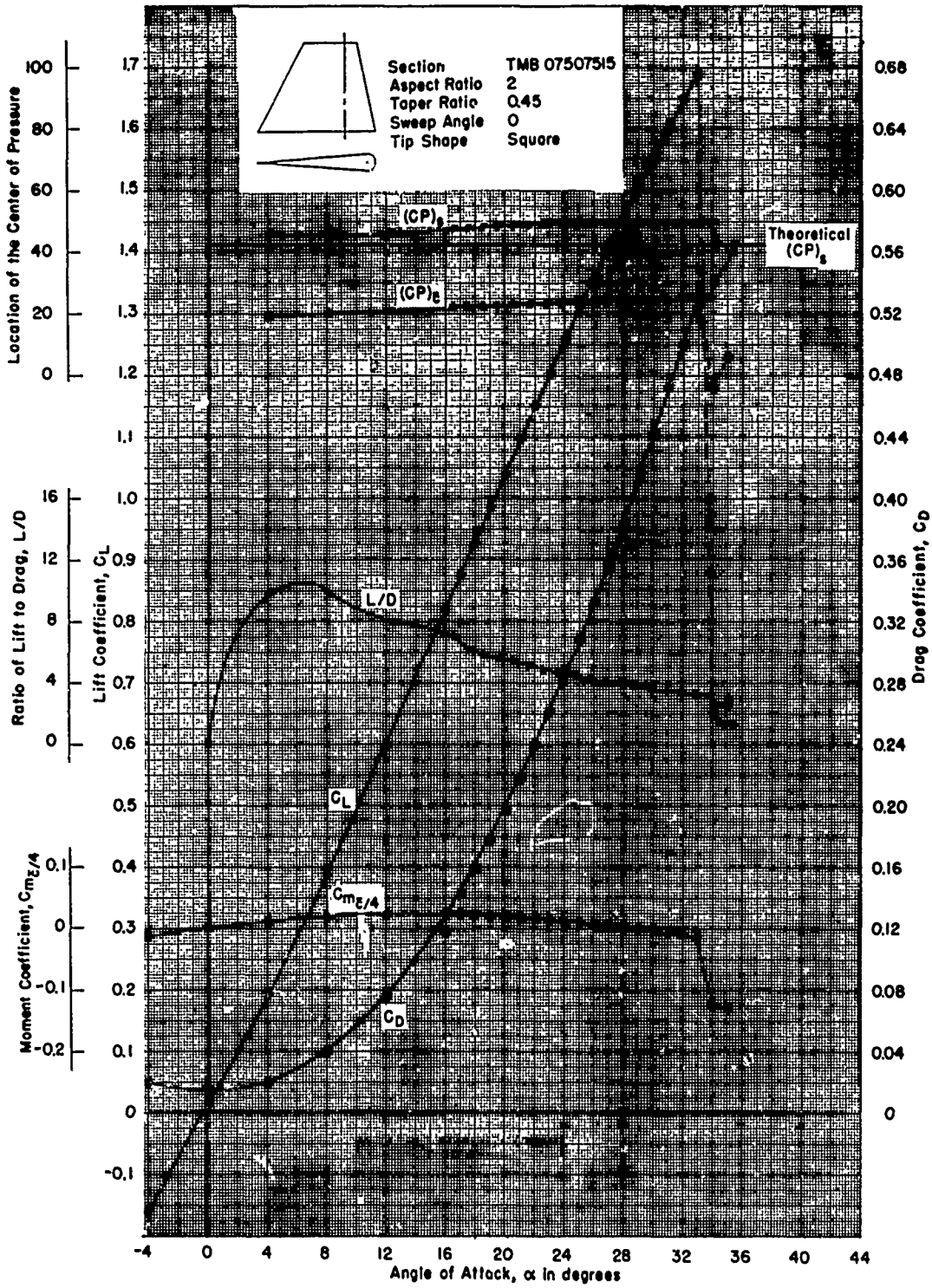

Figure 110 - Reynolds Number of 1.86×10^6

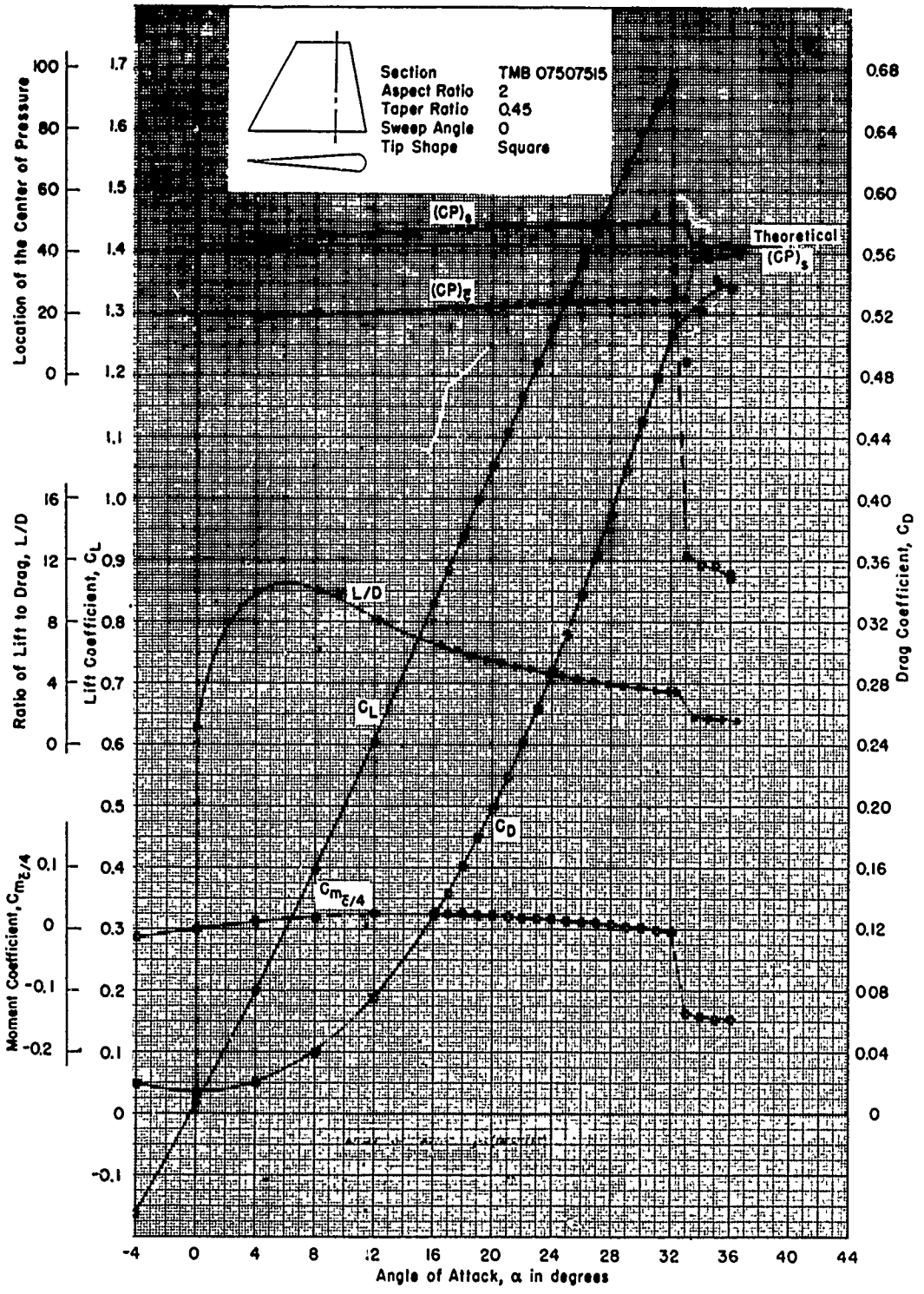

Figure 111 - Reynolds Number of 2.27×10^6

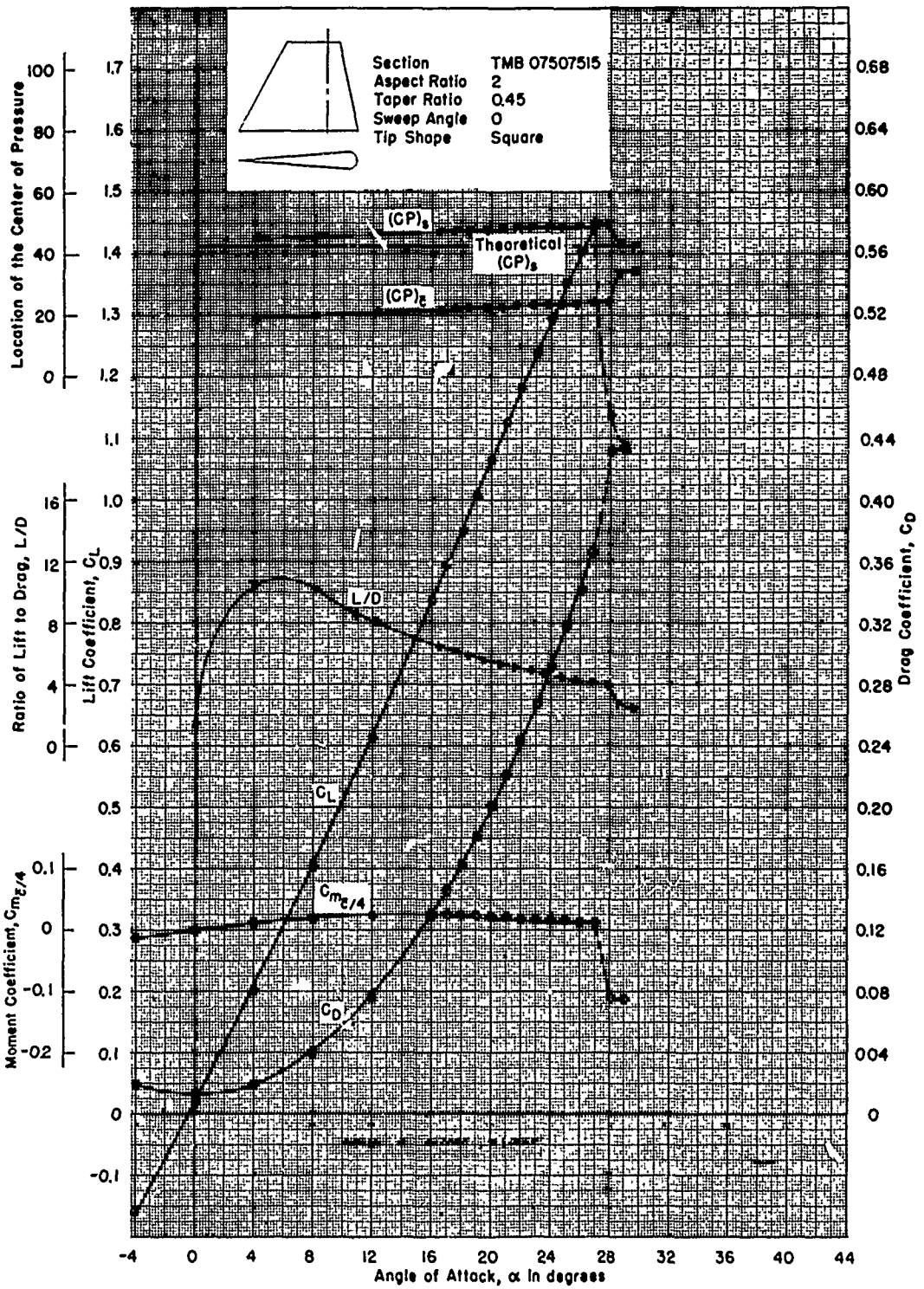

Figure 112 - Reynolds Number of 2.77×10^6

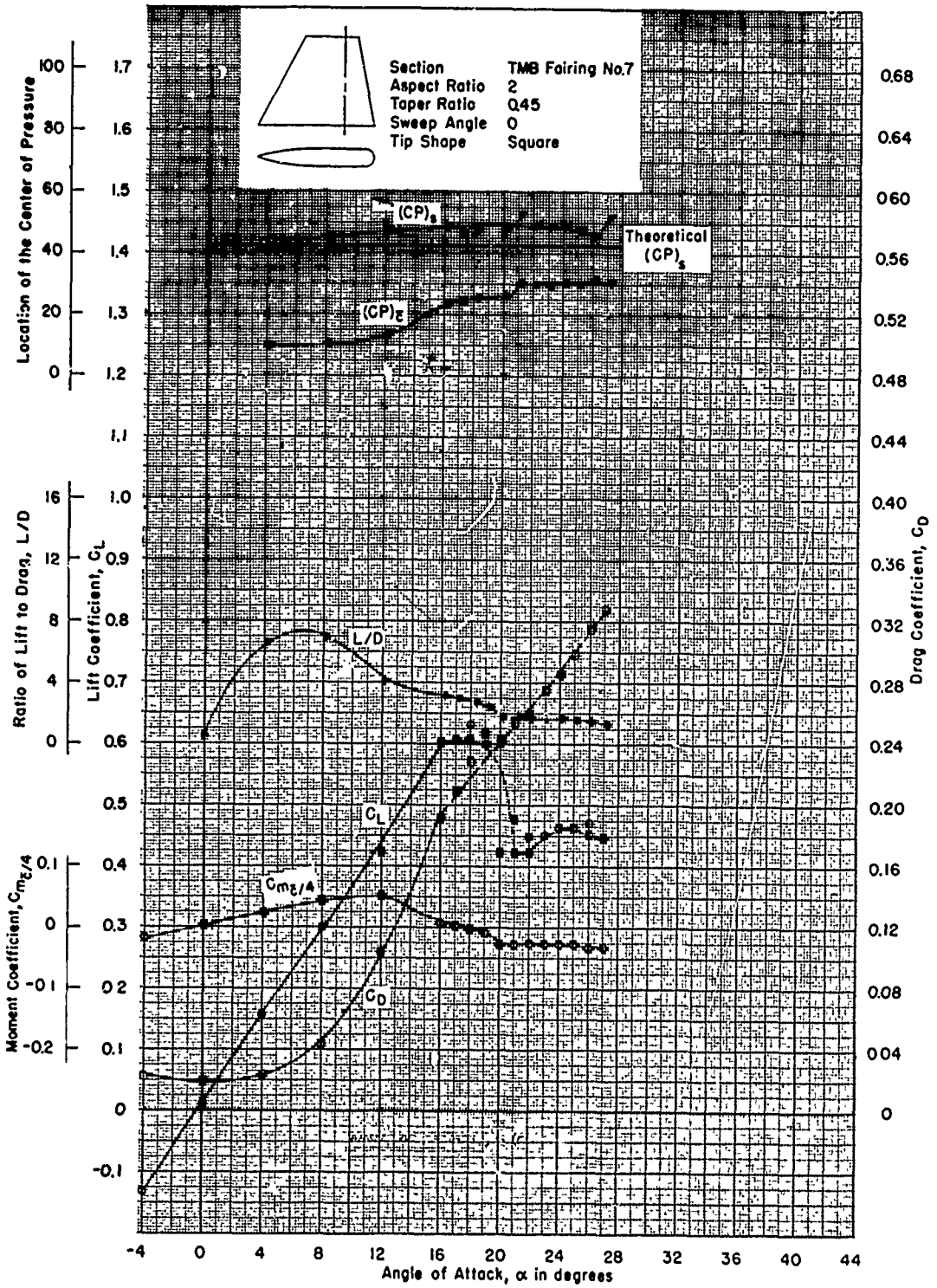

Figure 113 - Reynolds Number of 0.990 x 10^6

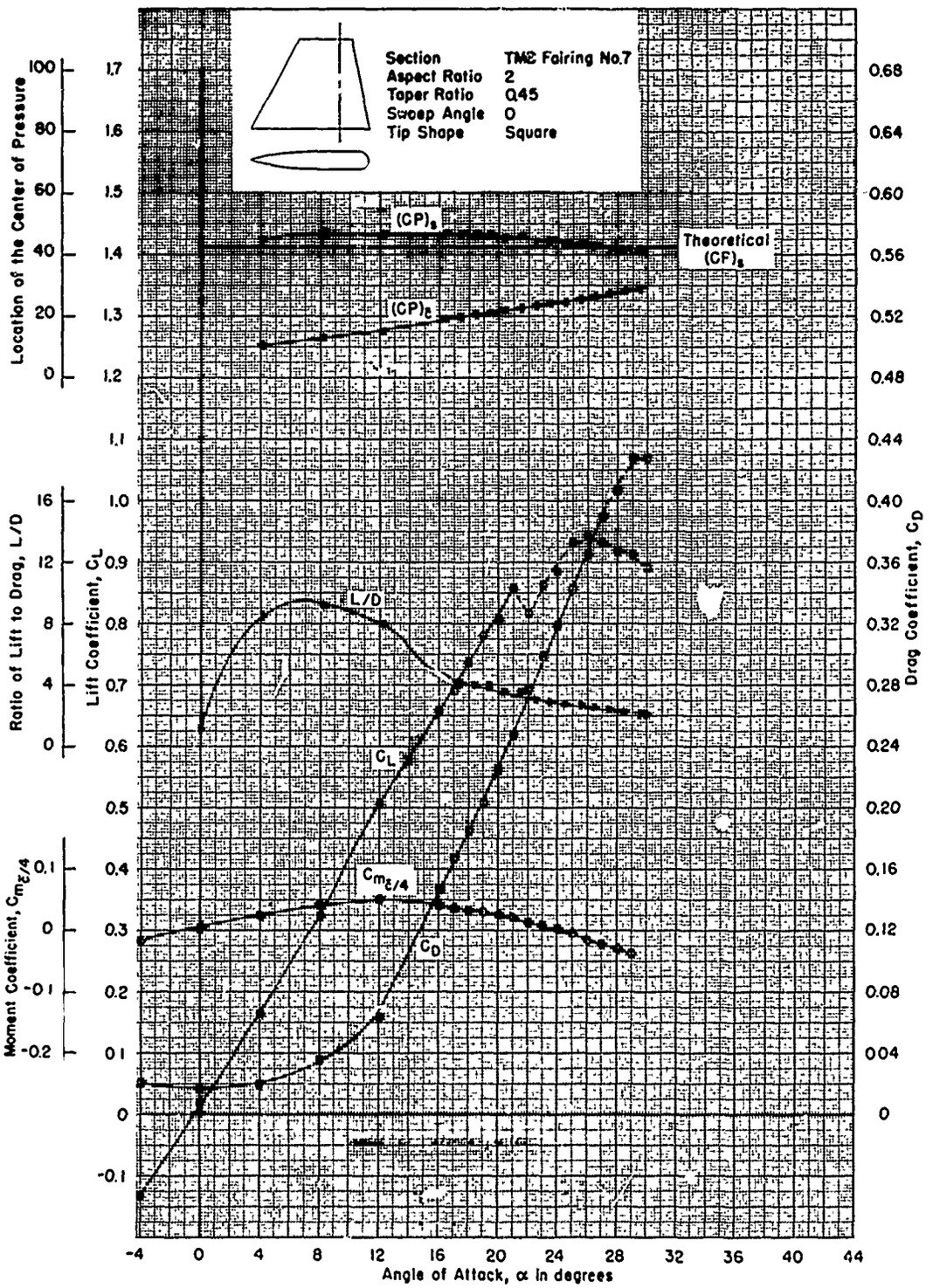

Figure 114 - Reynolds Number of 1.41×10^6

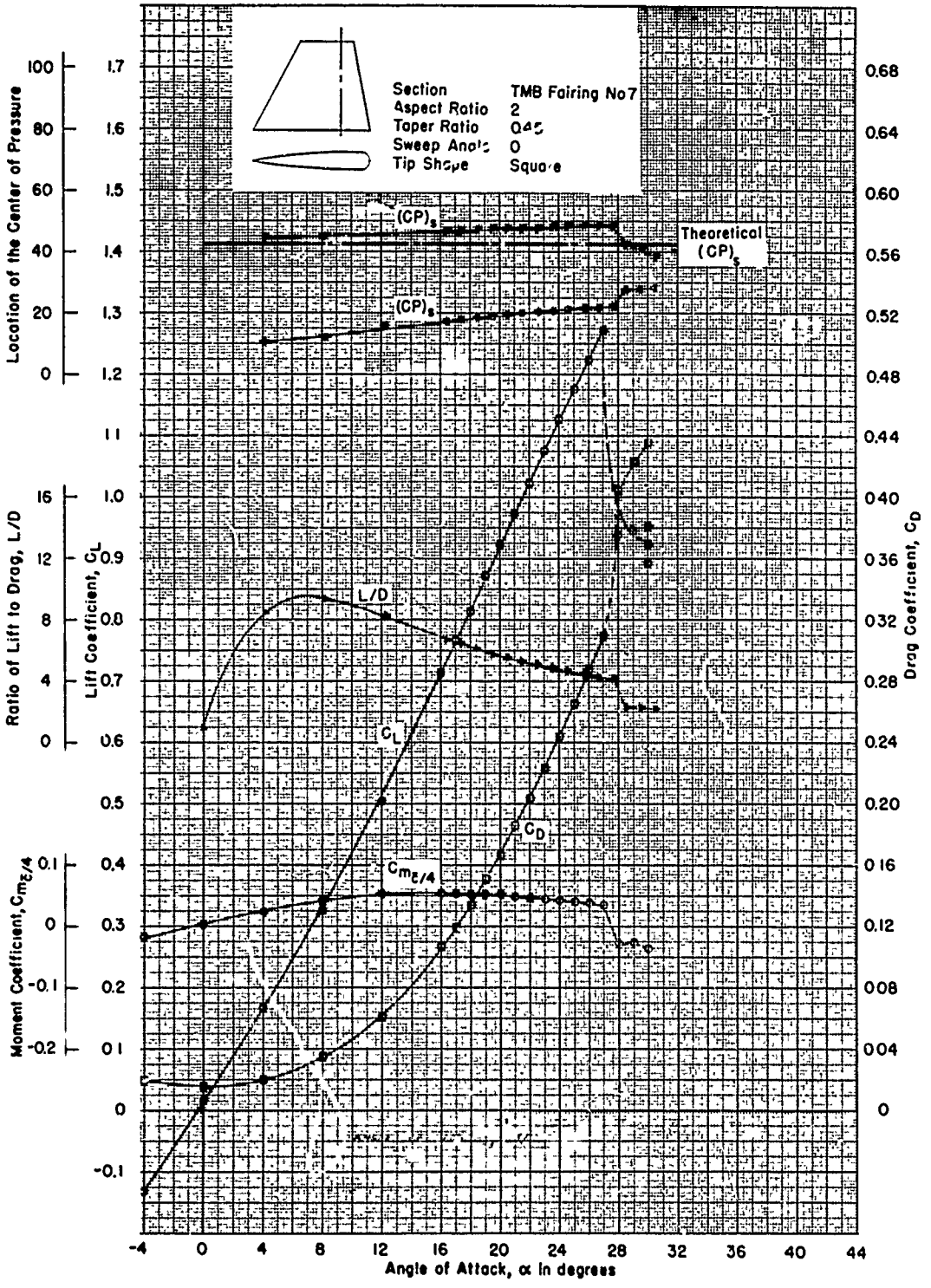

Figure 115 - Reynolds Number of 1.86×10^6

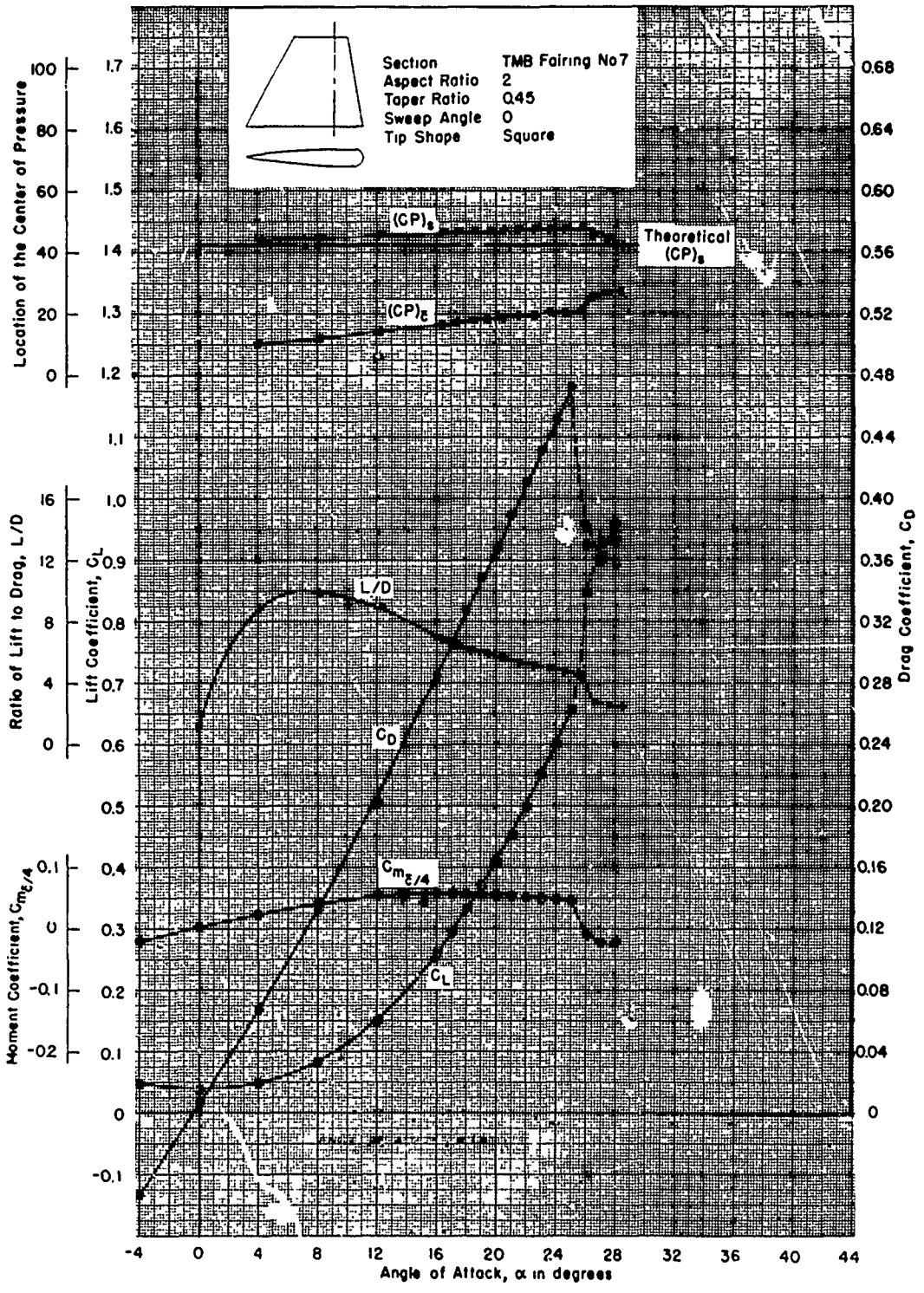

Figure 116 - Reynolds Number of 2.27×10^6

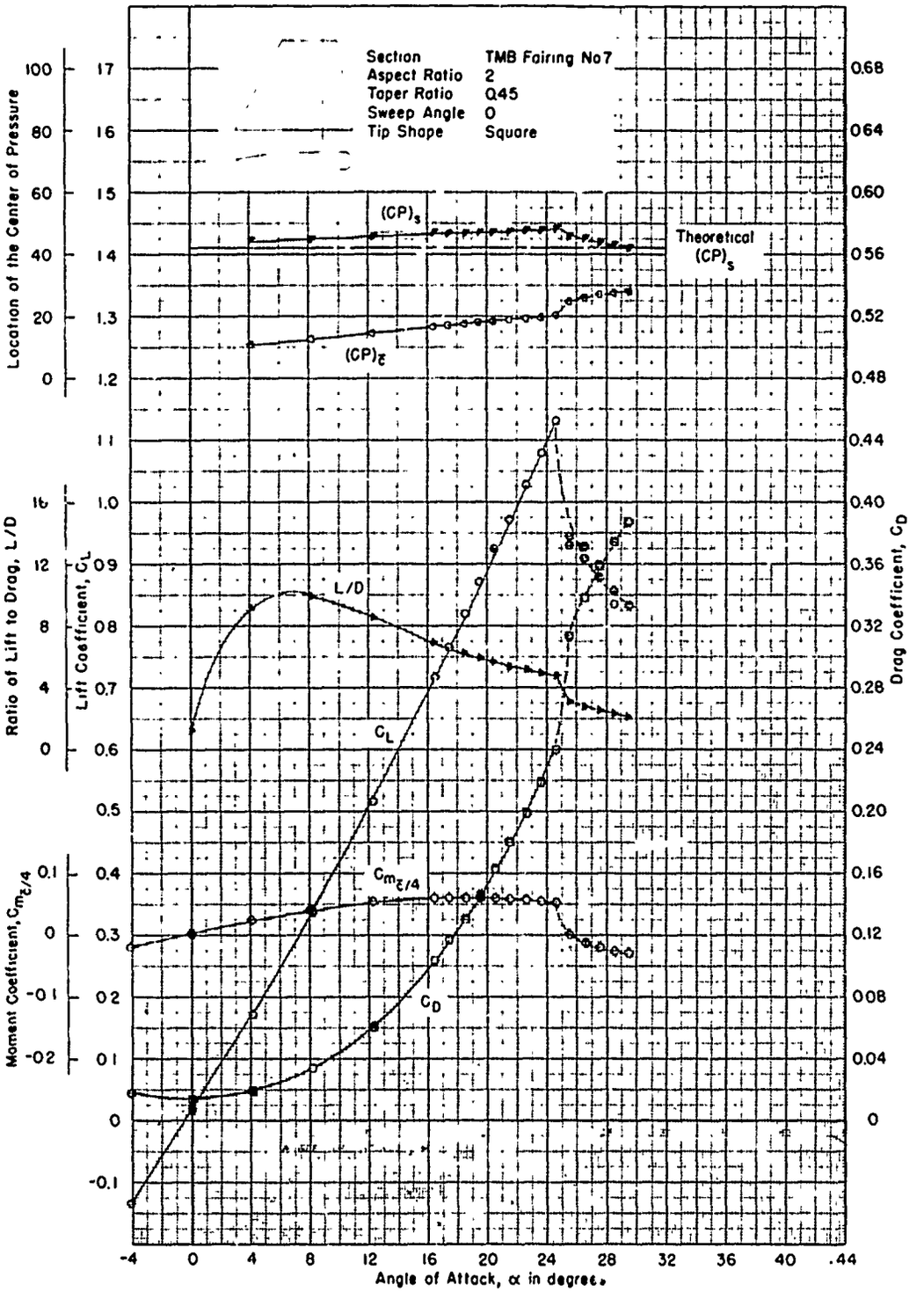

Figure 117 - Reynolds Number of 2.77×10^6

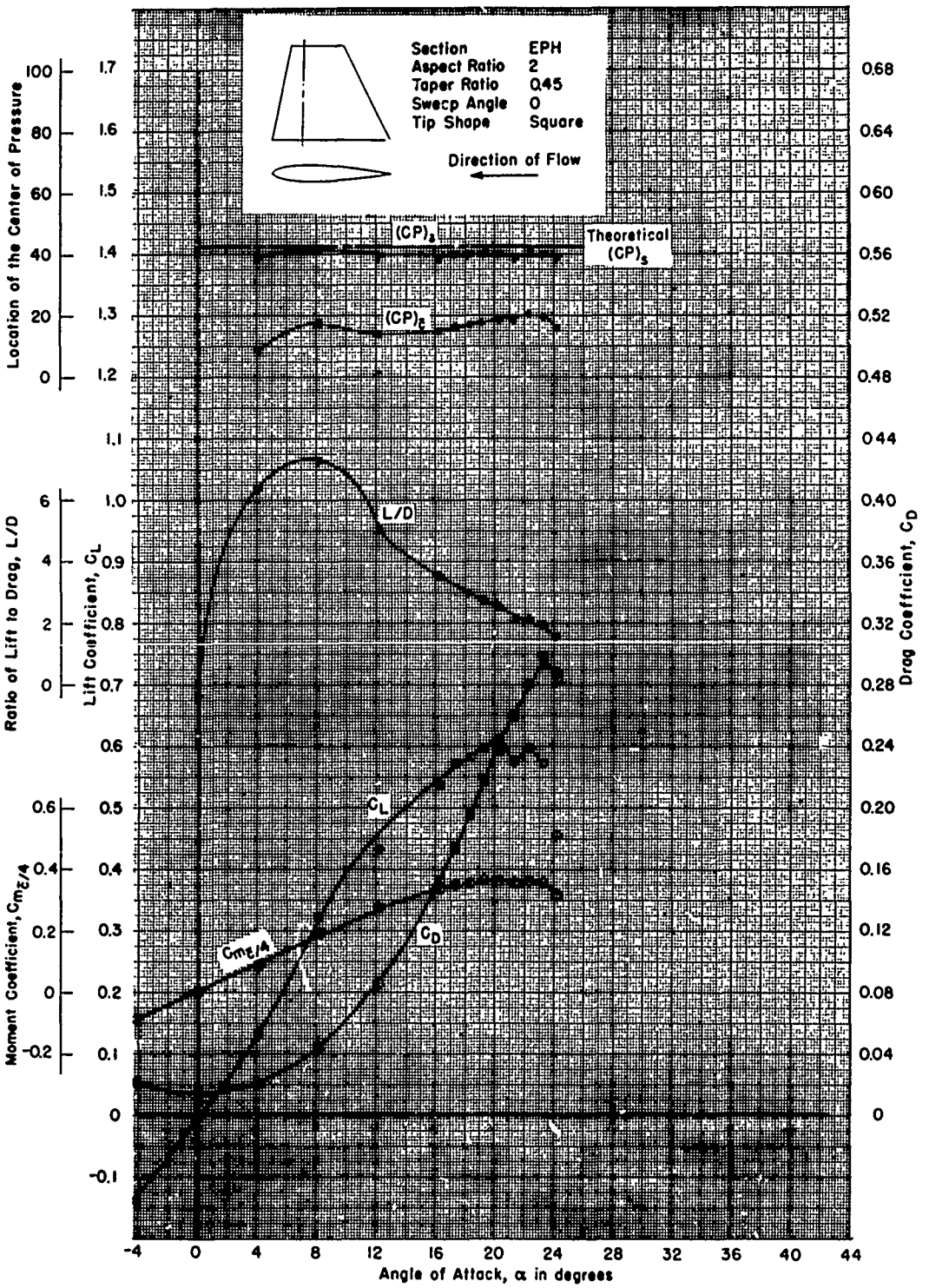

Figure 118 - Reynolds Number of 3.00×10^6

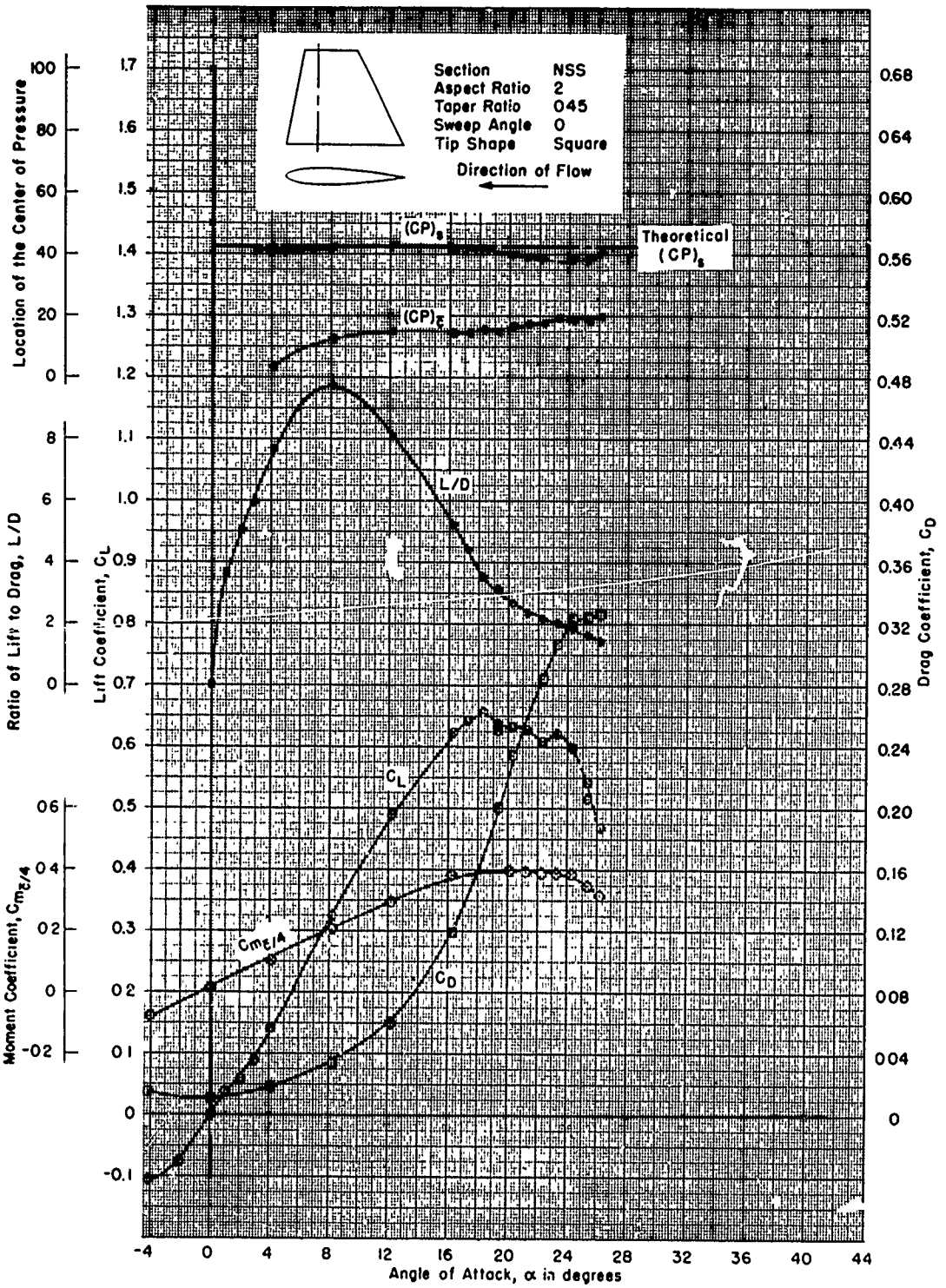

Figure 119 - Reynolds Number of 3.00×10^6

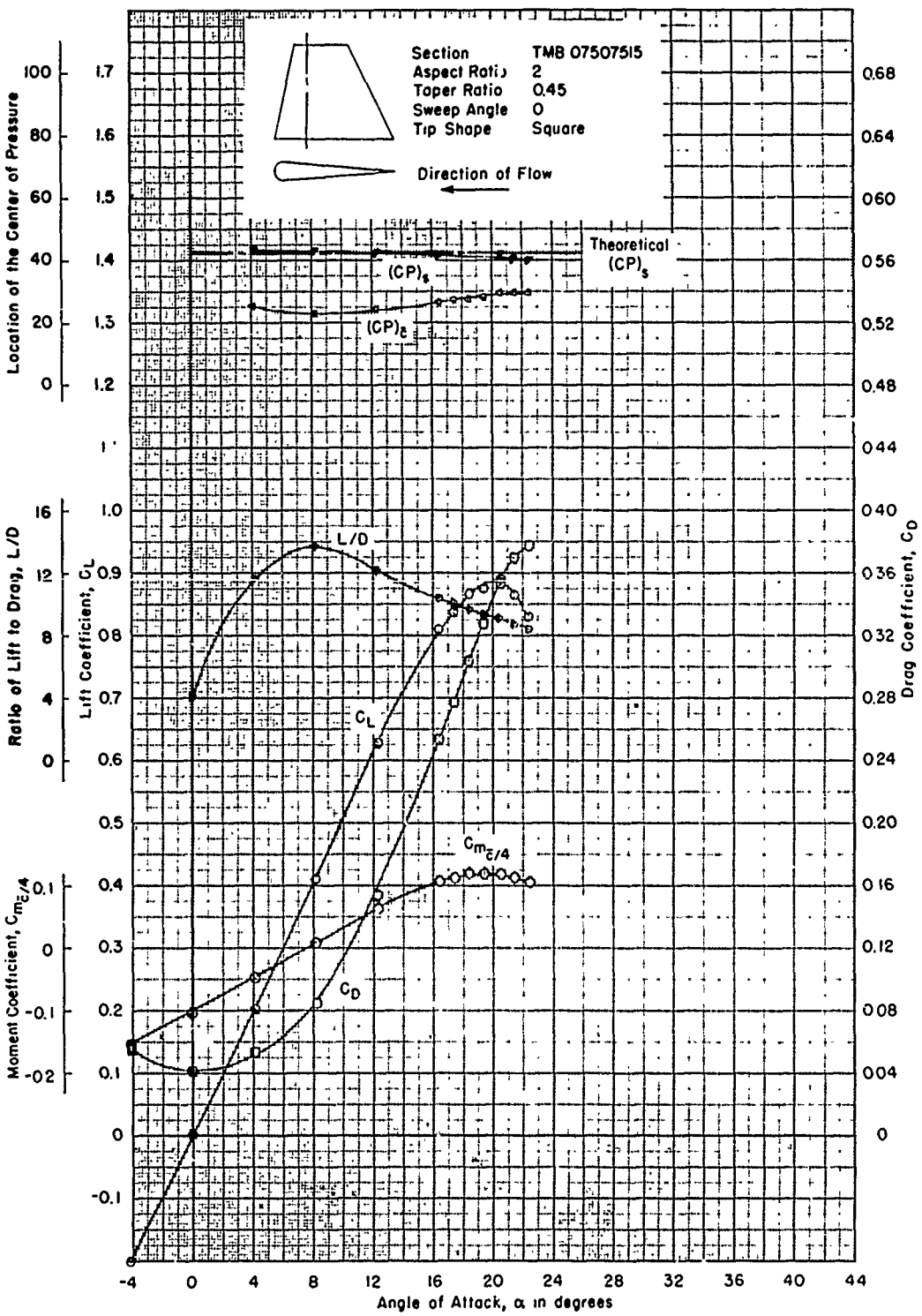

Figure 120 - Reynolds Number of 3.00×10^6

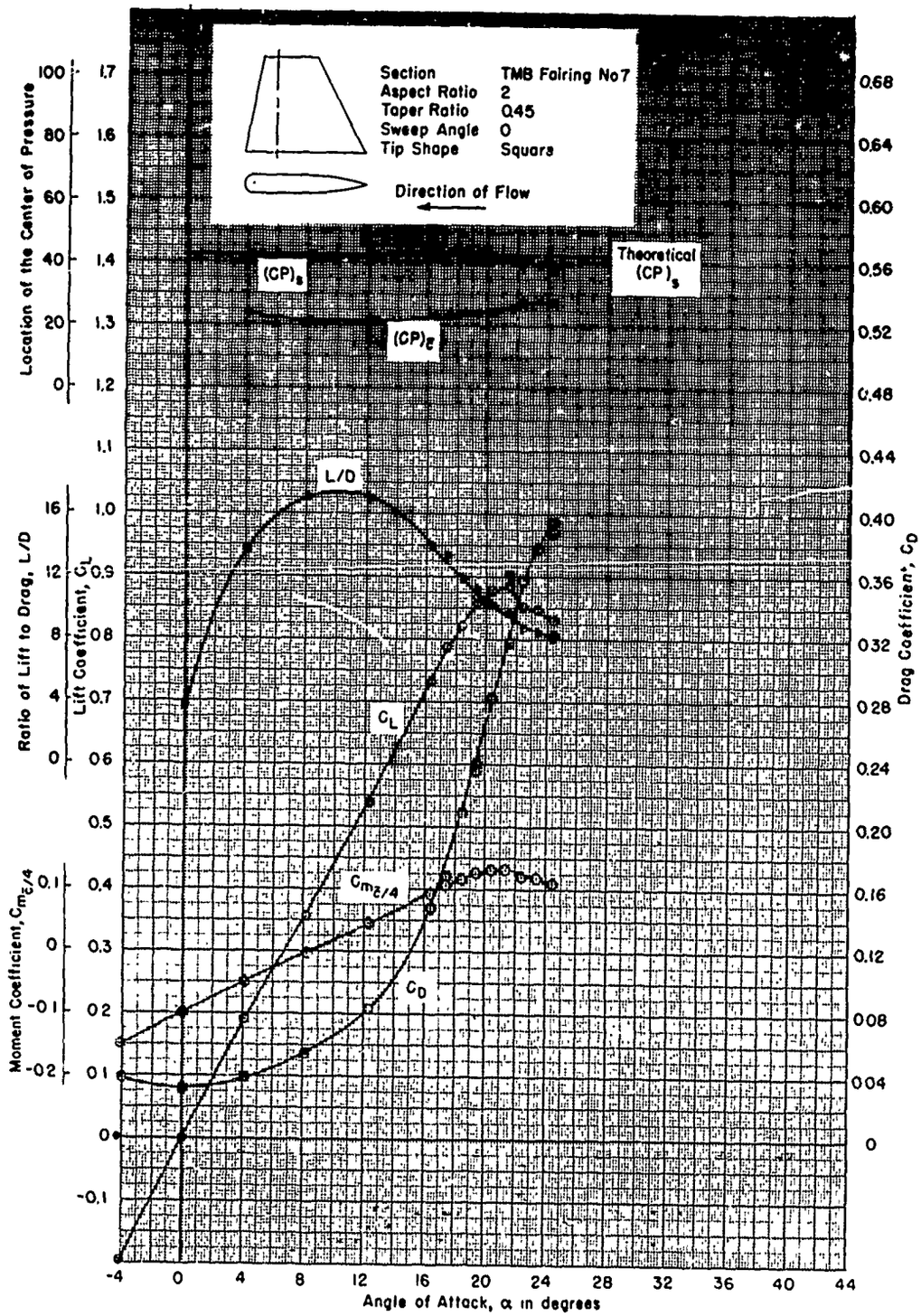

Figure 121 - Reynolds Number of 3.00×10^6

David Taylor Model Basin. Report 933.
FREE-STREAM CHARACTERISTICS OF A FAMILY OF LOW-ASPECT-RATIO, ALL-MOVABLE CONTROL SURFACES FOR APPLICATION TO SHIP DESIGN, by L. Folger Whicker and Leo F. Fehlner. December 1958. Revised Edition. viii, 121p. tables, graphs, diagrs., illus., refs. UNCLASSIFIED

The free-stream characteristics of a family of low-aspect-ratio, all-movable control surfaces are presented. These characteristics —i.e., force and moment coefficients, and chordwise and spanwise center of pressure locations—are plotted as functions of the angle of attack for each surface at various Reynolds numbers in both the ahead and the astern conditions. Investigations were made of the following: three aspect ratios 1, 2, and 3; five section shapes (NACA 0015, Navy Standard Strut, TMB-EPH, TMB Fairing No. 7, and TMB-No. 07507515); two tip shapes, faired and square; and

1. Control surfaces – Design
2. Control surfaces – Hydrodynamic characteristics – Mathematical analysis
3. Control surfaces – Aspect ratio
4. Control surfaces – Applications
I. Whicker, Lester Folger
II. Fehlner, Leo F.

David Taylor Model Basin. Report 933.
FREE-STREAM CHARACTERISTICS OF A FAMILY OF LOW-ASPECT-RATIO, ALL-MOVABLE CONTROL SURFACES FOR APPLICATION TO SHIP DESIGN, by L. Folger Whicker and Leo F. Fehlner. December 1958. Revised Edition. viii, 121p. tables, graphs, diagrs., illus., refs. UNCLASSIFIED

The free-stream characteristics of a family of low-aspect-ratio, all-movable control surfaces are presented. Those characteristics —i.e., force and moment coefficients, and chordwise and spanwise center of pressure locations—are plotted as functions of the angle of attack for each surface at various Reynolds numbers in both the ahead and the astern conditions. Investigations were made of the following: three aspect ratios 1, 2, and 3; five section shapes (NACA 0015, Navy Standard Strut, TMB-EPH, TMB Fairing No. 7, and TMB-No. 07507515); two tip shapes, faired and square; and

1. Control surfaces – Design
2. Control surfaces – Hydrodynamic characteristics – Mathematical analysis
3. Control surfaces – Aspect ratio
4. Control surfaces – Applications
I. Whicker, Lester Folger
II. Fehlner, Leo F.

David Taylor Model Basin. Report 933.
FREE-STREAM CHARACTERISTICS OF A FAMILY OF LOW-ASPECT-RATIO, ALL-MOVABLE CONTROL SURFACES FOR APPLICATION TO SHIP DESIGN, by L. Folger Whicker and Leo F. Fehlner. December 1958. Revised Edition. viii, 121p. tables, graphs, diagrs., illus., refs. UNCLASSIFIED

The free-stream characteristics of a family of low-aspect-ratio, all-movable control surfaces are presented. These characteristics —i.e., force and moment coefficients, and chordwise and spanwise center of pressure locations—are plotted as functions of the angle of attack for each surface at various Reynolds numbers in both the ahead and the astern conditions. Investigations were made of the following: three aspect ratios 1, 2, and 3; five section shapes (NACA 0015, Navy Standard Strut, TMB-EPH, TMB Fairing No. 7, and TMB-No. 07507515); two tip shapes, faired and square; and

1. Control surfaces – Design
2. Control surfaces – Hydrodynamic characteristics – Mathematical analysis
3. Control surfaces – Aspect ratio
4. Control surfaces – Applications
I. Whicker, Lester Folger
II. Fehlner, Leo F.

David Taylor Model Basin. Report 933.
FREE-STREAM CHARACTERISTICS OF A FAMILY OF LOW-ASPECT-RATIO, ALL-MOVABLE CONTROL SURFACES FOR APPLICATION TO SHIP DESIGN, by L. Folger Whicker and Leo F. Fehlner. December 1958. Revised Edition. viii, 121p. tables, graphs, diagrs., illus., refs. UNCLASSIFIED

The free-stream characteristics of a family of low-aspect-ratio, all-movable control surfaces are presented. These characteristics —i.e., force and moment coefficients, and chordwise and spanwise center of pressure locations—are plotted as functions of the angle of attack for each surface at various Reynolds numbers in both the ahead and the astern conditions. Investigations were made of the following: three aspect ratios 1, 2, and 3; five section shapes (NACA 0015, Navy Standard Strut, TMB-EPH, TMB Fairing No. 7, and TMB-No. 07507515); two tip shapes, faired and square; and

1. Control surfaces – Design
2. Control surfaces – Hydrodynamic characteristics – Mathematical analysis
3. Control surfaces – Aspect ratio
4. Control surfaces – Applications
I. Whicker, Lester Folger
II. Fehlner, Leo F.

three sweep angles (−8, 0, 11). Cross-plots were made to assess the effects of these parameters, and semi-empirical equations for the force and moment coefficients suitable for design applications are presented. Also included is a design technique for computing surface shaft torque

three sweep angles (−8, 0, 11). Cross-plots were made to assess the effects of these parameters, and semi-empirical equations for the force and moment coefficients suitable for design applications are presented. Also included is a design technique for computing surface shaft torque.

three sweep angles (−8, 0, 11). Cross-plots were made to assess the effects of these parameters, and semi-empirical equations for the force and moment coefficients suitable for design applications are presented. Also included is a design technique for computing surface shaft torque.

three sweep angles (−8, 0, 11). Cross-plots were made to assess the effects of these parameters, and semi-empirical equations for the force and moment coefficients suitable for design applications are presented. Also included is a design technique for computing surface shaft torque.